Characterisation and Implementation of Synthetic Diamond as a Raman Laser Material

By

Sean Reilly

A thesis presented in fulfilment of the requirements for the degree of Doctor of Philosophy.

Institute of Photonics, Department of Physics, University of Strathclyde

2015

Declaration of authenticity and author's rights

Signed:

Date:

Acknowledgments

First and foremost, I would like to thank Professor Alan Kemp for giving me this opportunity and for supporting me throughout my PhD. I couldn't have asked for a better supervisor! Secondly, thanks to Dr Vasili Savitski, for the patience you had showing me the ropes in the lab, and for your continued guidance with problems big and small.

Thanks are also due to the laser engineering team as a whole, who deserve a special mention: Rolf, Elisabeth, Gerald, Peter, Danny(pedia), and Ewan – along with Alan and Vasili, I truly enjoyed working in such a genial group. Furthermore, although I didn't get to work with you for nearly long enough, thanks to David Burns and John-Mark Hopkins.

Although too many to name individually, I would like to thank my fellow PhD students and researchers in the IoP. Thanks to Paul Hynd, for building me mounts etc. and making me the things I didn't quite have the time to make myself (being too busy "twiddling knobs" in the lab). Thanks also to Ewan "Metro" Mulhern, for your "turn it off and on again" IT support. Thanks to Sharon Kelly, Grace Tedman and Lorraine Annand for everything, along with Lisa Flanagan and Lynda Mclaughlin.

Lastly, I would like to thank my mum, dad, Caitlin, Grandparents and girlfriend Donna. I couldn't have done this without you.

Abstract

Diamond's unrivalled thermo-mechanical and optical properties make the material an attractive material for use in laser systems. Improvements in growth techniques over the past decade have led to a surge of research employing diamond in optical systems. This thesis presents the characterisation of diamond and its implementation in Raman lasers, utilising the materials high Raman gain as well as its impressive thermal properties. Diamond's potential as both an extremely compact and robust method for frequency conversion, allowing access to relevant but otherwise hard to reach wavelengths, and also as a means to convert low brightness sources to near diffraction limited beams will also be discussed.

A pump-probe measurement is used to conduct the first systematic study of the Raman gain in diamond over a wide range of wavelengths, from 355nm to 1450nm, with a $\frac{1}{\lambda}$ dependence observed.

Using the high Raman gain measured, both CW and pulsed Raman systems were designed and characterised. An 11-fold brightness enhancement was achieved in an Nd:YAG pumped intra-cavity diamond Raman laser, while record powers of 7.6W are presented using an Yb:LuAG pumped diamond Raman laser. Two monolithic diamond Raman lasers are discussed, achieving near quantum limited conversion efficiencies.

An investigation of the laser induced damage threshold of diamond surfaces is conducted, with attempts made to improve the measured value of 25Jcm^{-2} discussed.

Contents

Chapter 1 – Introduction

Natural diamond has, for centuries, been a sparkling symbol of status. In 1954, however, the first commercially viable process to synthesise diamond was demonstrated [1]. With this breakthrough came the question, is diamond wasted on jewellery? In the years that followed, diamond gradually became an economically feasible option in applications varying from brute force drilling to more niche scientific processes.

This thesis will present the use of diamond in laser technology. An initial comparison between the thermo-mechanical requirements of a laser gain material and the properties of diamond suggests an excellent match; unfortunately obtaining laser gain in diamond is not trivial. Several methods have previously been explored to exploit diamonds unrivalled properties, including: "hybrid" approaches, diamond colour centre lasers, and diamond Raman lasers. Hybrid systems consist of more conventional laser materials such as neodymium and ytterbium based crystals "sandwiched" with diamond. This approach ameliorates thermal issues in the laser material [2], [3], and has proven to be particularly effective when implemented in semiconductor disk lasers, allowing significant power scaling [4], [5] . Introducing laser gain directly into diamond, however, allows the full exploitation of the materials properties. To date, this has been achieved using two methods. Firstly, taking advantage of diamond's large Raman gain and using the stimulated Raman scattering (SRS) effect, many Raman lasers have been developed at a variety of wavelengths, operating in both pulsed and continuous wave (CW) regimes [6]–[15]. Secondly, a diamond colour centre laser has been presented in [16], using colour centres in diamond to provide optical gain. This demonstration was all the more impressive due to the very low finesse of the laser resonator used.

This thesis will focus on using diamond as the gain material in Raman lasers whilst also presenting characterisation of the material, including a study of the dependence of the Raman gain in diamond on wavelength and an investigation into the laser induced damage threshold (LIDT) of diamond surfaces. Such values

are crucial when designing optical systems implementing diamond, providing an insight into the pump intensities required to reach threshold and the maximum intensity permitted before catastrophic damage occurs.

In this chapter, stimulated Raman scattering (SRS) will be discussed, as well as the design of Raman lasers. An overview of the progress in diamond Raman lasers will also be presented, with the limitations of the material also addressed.

1.1 Stimulated Raman Scattering

Raman scattering is an inelastic process in which a photon with a given frequency ω_L interacts with a material's vibrational modes [17] and is converted into a photon with frequency ω_S and a phonon of frequency ω_R (intrinsic to the material), which is described in equation 1.1.

$$\omega_S = \omega_L - \omega_R \tag{1.1}$$

At low pump intensities, Raman conversion is a purely spontaneous process, meaning the Raman shifted photon is emitted in a random direction, represented schematically in Figure 1.1.

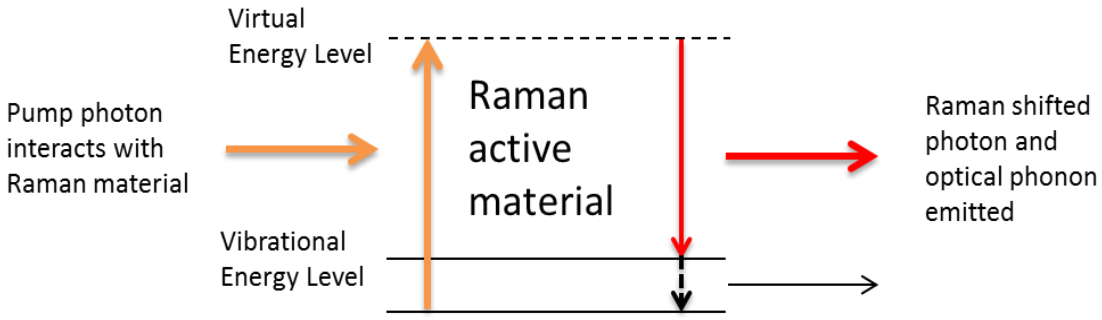

Figure 1.1. Spontaneous Raman scattering process. An incident photon interacts with the vibrational modes of a material resulting in the generation of a lower energy photon and a phonon.

If the intensity of the incident pump is high enough, SRS can occur [18]. A photon of frequency ω_S interacts with the material, which has been excited by an incident pump photon, stimulating the material to relax to a lower vibrational energy level, while in the process emitting a second photon identical to the original in wavelength, phase and direction. This interaction is represented schematically in Figure 1.2.

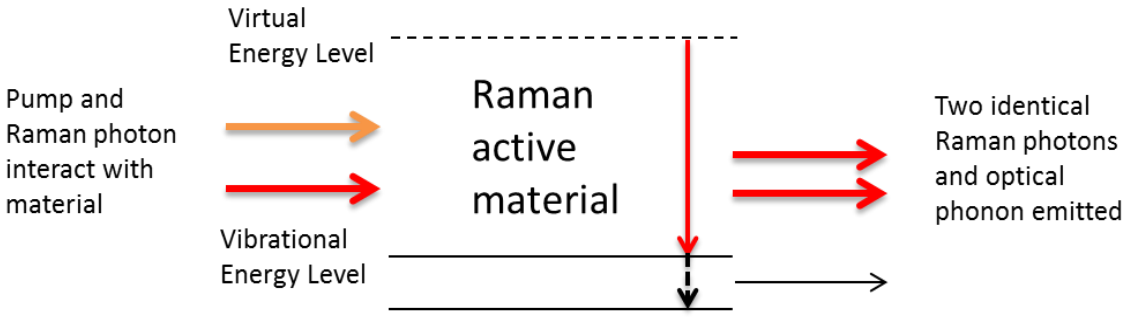

Figure 1.2. Stimulated Raman scattering process. Incident pump and Raman photons interact with the vibrational energy levels in a material resulting in the generation of an additional Raman photon and an optical phonon.

Should the intensity of the Raman shifted beam be large enough, further Raman shifts are possible, also known as cascaded Raman [19]–[24]. This allows further access to otherwise hard to reach wavelengths such as the "eye safe" spectral region above 1.5μm [23], [24], using 2nd, and in some cases 3rd, Raman shifted beams.

SRS is described quantum mechanically by Penzkofer in [17]. We can consider the rate at which Raman photons are generated in a single Stokes mode. The rate of growth of the population of Raman photons, n_s, in the Stokes mode can then be described by equation 1.2 [17].

$$\frac{dn_s}{dt} = N\left(\frac{\partial\alpha}{\partial q}\right)^2 \frac{4\pi^3}{\mu_L\mu_s mc}\frac{\omega_s}{\omega_R}[1+n(k_s)]I_L\rho(\omega_s-\omega_L+\omega_R) \qquad 1.2$$

where N is the number per unit volume of Raman active molecules in the material, $\frac{\partial \alpha}{\partial q}$ is the normal mode derivative of the molecular polarizability tensor (α) [17], [25], with its square being proportional to the imaginary part of χ^3, the third order nonlinear susceptibility of the material. The refractive indices of the material at the pump and Raman wavelengths are represented by μ_L and μ_S respectively. The term $\rho(\omega_s - \omega_L + \omega_R)$ represents the spectral distribution of the interaction [17]. For a spectrally narrow pump laser field (significantly narrower than the Raman transition) and a homogeneously broadened Raman transition, the spectral distribution of the Raman interaction can be described by equation 1.3 [17]

$$\rho(\omega_s - \omega_L + \omega_R) = \frac{\frac{\Gamma}{2\pi}}{(\omega_s - \omega_L + \omega_R)^2 + \left(\frac{\Gamma}{2}\right)^2} \qquad 1.3$$

Where Γ is the linewidth (FWHM) of the Raman peak, which is related to the dephasing time of the phonon field, T_2, by the relationship $\Gamma/2 = 1/T_2$ [17][18].

Now, we can consider the case when stimulated Raman scattering, into a single Stokes mode is the primary process. The population of the Stokes photons, n_S, is found to grow exponentially [18], shown in equation 1.4.

$$n_S \propto \exp(g_R I_L l) \qquad 1.4$$

Where I_L is the intensity of the pump laser, l is the interaction length in the Raman material and g_R is the Raman gain coefficient, described in equation 1.5.

$$g_R = N\left(\frac{\partial \alpha}{\partial q}\right)^2 \frac{4\pi^2 \omega_s}{\mu_L \mu_S c^2 m \omega_R} \frac{\frac{\Gamma}{2}}{(\omega_s - \omega_L + \omega_R)^2 + \left(\frac{\Gamma}{2}\right)^2} \qquad 1.5$$

The presence of frequency terms in this equation highlights the wavelength dependence of the Raman gain coefficient, with a $\frac{1}{\lambda_L}$ dependence discussed in Chapter 2.

Now, as the intensity of the Stokes field is proportional to the number of Stokes photons, we can rewrite equation 1.4 as follows [26].

$$I_S(x) = I_S(0)\exp(g_R I_L x) \quad 1.6$$

This is analogous to the equation describing stimulated emission in a laser material. This fact, in combination with SRS producing "cloned" photons (similar to stimulated emission) highlights the potential to pump a Raman active material with an intense laser and achieve Raman laser oscillation. It should be noted, however, that unlike in a "conventional" laser system, a Raman laser has no population inversion. This means, due to the absence of energy storage, that a Raman laser cannot by directly q-switched or mode locked; however, as will be discussed in Section 1.3 and Chapter 4, pump sources can be q-switched and mode-locked to achieve pulsed Raman output.

1.2 Raman laser designs

The three common methods of obtaining Raman laser action are presented in Figure 1.3. An external Raman laser cavity (shown in Figure 1.3(a)), implements a cavity in which only the Raman field oscillates, and is pumped with the output of, most commonly, a solid state laser with good beam quality. The intensity of the pump spot required to reach the threshold for Raman laser action is of the order of a few tens to hundreds of $MWcm^{-2}$. By double passing the pump laser through the Raman gain material, the threshold of the Raman laser can be reduced [18], [27]; however, it will still be in the region of a few tens to hundreds of $MWcm^{-2}$. Laser oscillation is present when the conditions shown in equation 1.7 are met [18].

$$R_1 R_2 \exp(2 g_R I_L l) \geq 1 \quad 1.7$$

Where R_1 and R_2 are the reflectivities of the 2 mirrors (normally an input coupler and an output coupler), I_L is the pump intensity and l is the length of the Raman crystal. Assuming an output coupler of 80% reflectivity, an input coupler with reflectivity of 99.9% (both at the Raman wavelength), and perfect transmission of

the pump, the intensity required to reach threshold in a 6mm long diamond Raman laser is of the order of 200MWcm^{-2}. Due to the large intensities required, these systems are most commonly pumped by q-switched laser sources; however, CW operation has been achieved by Kitzler et al [13], reaching a maximum Raman output power of 10.1W, discussed in more detail in section 1.3.

An intra-cavity Raman laser is illustrated in Figure 1.3(b). The Raman active material is placed inside the "conventional" laser cavity, capitalising on the high oscillating field (potentially killowatts), as well as having the added benefit of being more compact than its external cavity alternative. Several solid state lasers have been used to pump intra-cavity Raman systems [6], [10], [15], [28]–[30], while tunable vertical external cavity semiconductor lasers (VECSEL's) have been used to demonstrate tuneable intra-cavity Raman lasers [31]–[33]. Although relatively low thresholds have been demonstrated in external Raman laser systems [27], indicating that it may be possible to externally pump a Raman laser with a VECSEL, an intra-cavity approach has proven to be the preferred route to date. Prior to the submission of this thesis, the highest power intra-cavity Raman laser was achieved by Savitski et al. [6], with 6.1W output reached using potassium gadolinium tungstate (KGW) as the Raman gain material. This will be discussed in more detail in section 3.1.

To avoid confusion, before discussing intra cavity lasers further, terminology will be established. The diode pump will hereafter be referred to as the "pump", while the conventional laser, which pumps the intra-cavity Raman laser, will be referred to as the "fundamental".

The drawbacks of an intra-cavity approach include the necessity for a more complex cavity design, with the requirement of specific mode sizes at two points in the resonator, namely in the conventional laser gain material and the Raman gain material. The presence of two thermal lenses further complicates matters; with a lens present in both the Raman and laser gain materials, the resulting thermal lenses in the cavity can become highly dynamic [18], meaning power scaling can be complicated. This fact is highlighted by analysis of equation 1.8

[18], defining the focal length, f, of the thermo-optic contribution to the thermal lens in a Raman crystal.

$$\frac{1}{f} = \left(\frac{dn}{dT}\right)\frac{1}{K}\frac{P_s}{\pi\omega_s^2}\left(\frac{\lambda_s}{\lambda_p} - 1\right) \qquad 1.8$$

Where K is the thermal conductivity of the Raman material, P_s is the average Raman output power, dn/dT is the material's thermal expansion coefficient, ω_s is the Raman beam radius in the material, λ_s is the Raman wavelength, and λ_p is the pump wavelength (external cavity case) or fundamental wavelength (intra-cavity case). The focal length of the thermal lens is dependent on the both the Raman power and the cavity mode radius; however these are dependent on the thermal lens itself. This, as discussed, can result in a highly dynamic thermal lens. The intrinsic quantities presented in equation 1.8 will be further discussed in section 1.4.

With this being said, the thermal conductivity of diamond allows for efficient heat extraction and minimises the thermal lens, often to almost negligible values, even for the highest power systems presented to date. To give a very rough quantitative comparison, a 5W CW Raman laser pumped with a 1064nm beam with mode radius 30μm would have a thermal lens of around 750mm in diamond, and 2mm in KGW. In order to reduce the effect this dynamic lens has on the fundamental cavity, coupled cavity Raman lasers have often been employed [6], [10], [34], [35]. Using a dichroic mirror to separate the Raman field from the fundamental field, the thermal lens in the conventional gain material is removed from the Raman cavity. This also allows for further mode control in the Raman cavity, potentially advantageous while operating a multimode fundamental laser.

The conditions required to reach threshold in an intra-cavity Raman laser are presented in equation 1.9 [36]. It should be noted that the assumption is made that there is efficient diode to fundamental conversion, i.e. the intensity of the fundamental field is greater than the saturation intensity of the laser gain material.

$$P_P = \frac{A_R}{g_R l}\frac{\lambda_F}{\lambda_P}\frac{(T_s + L_s)(T_F + L_F)}{4} \quad 1.9$$

where P_P is the diode pump power, A_R is the Raman mode area, λ_F and λ_p are the fundamental and pump wavelengths, respectively, and T_F, T_S, L_F and L_S are the corresponding output coupling transmissivity and residual round-trip losses at the fundamental and Raman wavelengths, respectively.

We can now investigate the performance of the Raman laser above threshold, with an output power P_s. Assuming the fundamental power clamps as Raman oscillation reaches threshold, the diode to Stokes efficiency, P_S/P_P, is calculated using the relationship shown in equation 1.10 [36].

$$\frac{P_S}{P_P} = \frac{T_S}{(T_S + L_S)}\frac{\lambda_S}{\lambda_P} - \frac{T_S(T_F + L_F)}{4}\frac{A_R}{P_P g_R l} \quad 1.10$$

We can see from equations 1.9 and 1.10 that the round-trip residual loss (arising from scatter, unwanted mirror leakage, and unwanted absorption in gain media) has a significant effect on both the threshold and efficiency of the Raman laser. Spence et al [36] demonstrated theoretically that, for a CW intra-cavity Raman laser with a spot radius in the Raman gain material of 125μm and an output coupling of 2%, reducing the round trip residual losses from 1% to 0.5% saw an increase in the Raman conversion efficiency from 18% to 39%. It is clear to see that, when designing a Raman laser resonator, careful consideration should be taken to minimize loss. It should also be highlighted that, although decreasing the cavity mode radius in the Raman gain material will, in principle, increase the efficiency of the laser; a balance must be met due to potential laser induced damage.

Similarly to an intra-cavity Raman laser, a self-Raman laser, shown in Figure 1.3(c) has both the Raman field and fundamental field resonant [20], [37]–[39]. In a self-Raman laser, however, both the fundamental and Raman photons are generated in the same laser crystal. This is done by utilising the Raman shift

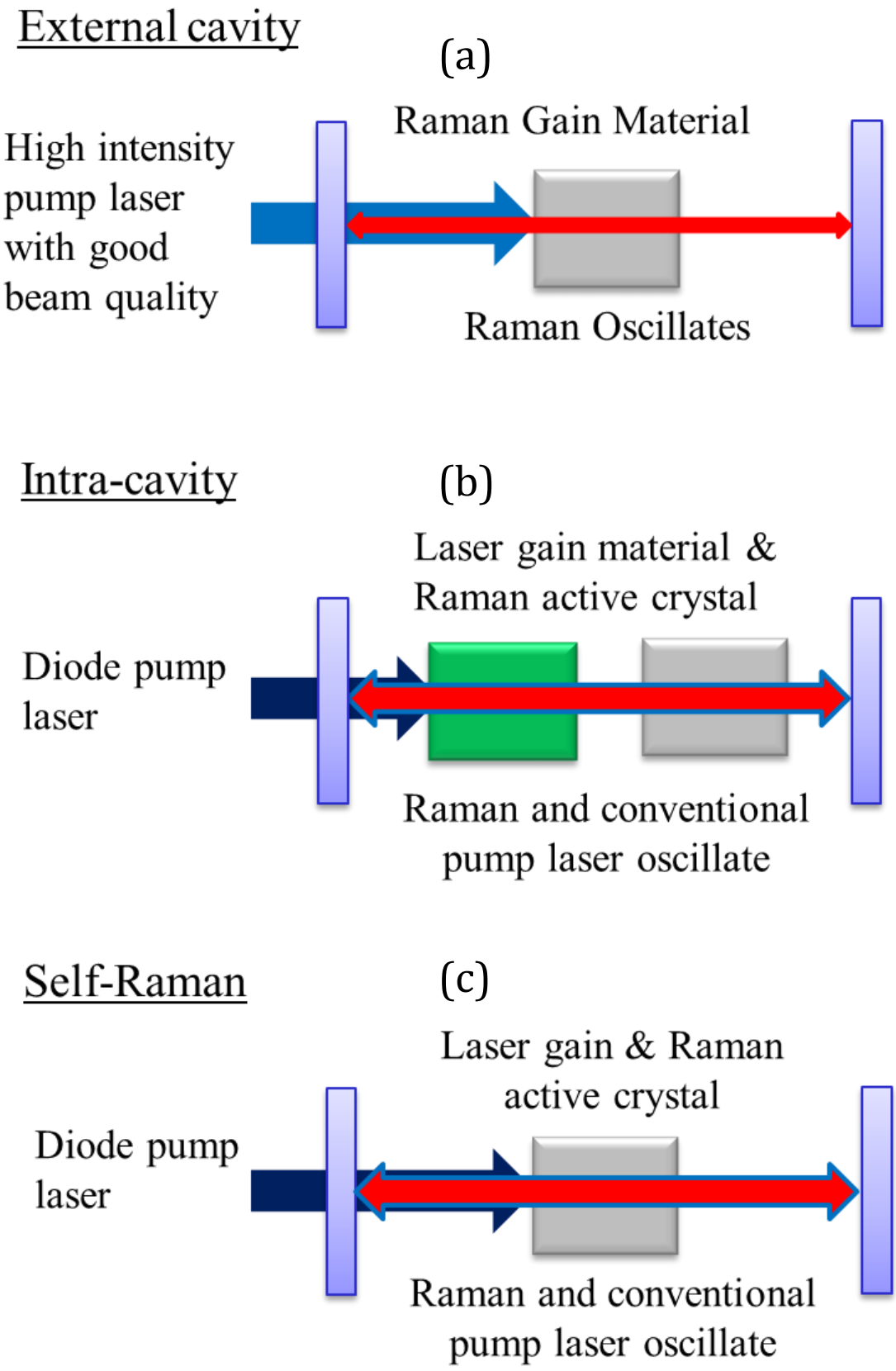

Figure 1.3. Cavity design for external and intra-cavity Raman lasers

present in the laser crystal itself. Host materials such as YVO_4, $GdVO_4$, and various tungstate materials, all of which are easily doped with neodymium and ytterbium, are most commonly used in this type of design [21], [38]–[41]. These types of Raman laser also offer the chance to greatly reduce the overall size of the system, which may be commercially favourable.

As in an intra-cavity system, this approach exploits the high intra-cavity field of the resonating fundamental laser; however, by combining the fundamental and Raman generation into one laser crystal, the heat load deposited in the material significantly increases. This can lead to a strong thermal lens in the laser crystal affecting cavity stability [28].

1.3. Overview of crystalline Raman lasers

As this thesis presents work on solid state Raman lasers, a general review of crystalline Raman lasers will be presented. It should, however, be noted that Raman lasers with fibres and gases acting as the Raman gain materials are also very common [42]–[44].

In crystalline Raman lasers, the high intensities required to achieve efficient Raman conversion mean that they are most commonly pumped with a q-switched laser. The first Raman laser was developed, accidentally, by Woodbury and Ng in 1962 [45]. Using a ruby laser, 30 to 40 millijoules of Raman emission was observed at a wavelength of 767nm, approximately 20% of the output observed at the 694nm laser line in ruby.

Practical, efficient and compact solid state Raman lasers were not developed until years later, when, in 1995, Murray et al [46] demonstrated an “eye safe” laser at 1.5μm with a 48% energy conversion efficiency resulting in 12mJ Raman pulses . A flurry of research into the topic resulted in demonstrations of both highly efficient [47] and high average power [9] Raman lasers pumped by q-switched solid state lasers.

To the best of our knowledge, the first demonstration of an all solid state CW Raman laser didn't come until 2004 [48]. Demidovic et al presented a barium nitrate Raman laser pumped with the 514nm emission of an Argon ion laser, capable of up to 10W output power. A maximum of 164mW of Raman emission at a wavelength of 543nm was achieved. H.M Pask [28] then achieved a Raman output of 800mW; however, unlike Demidovic et al, an intra-cavity approach was preferred, diode pumping an Nd:YAG crystal to produce fundamental oscillation at 1064nm with a KGW crystal used to generate Raman emission at 1176nm.

Although SRS had previously been observed in natural diamond as early as 1963 [49], [50] , SRS was not observed in synthetic diamond until 2004. Kaminskii at al [51] demonstrated the phenomena in a 350μm thick polycrystalline diamond film; pumped with nanosecond and picosecond IR laser sources, both Stokes and anti-Stokes shifts were observed. The authors concluded that, due to the continual progress in growth technology, along with the materials excellent thermo-mechanical properties, diamond could soon "hold a leading position among all known Raman laser materials".

Within a year, Demidovich et al reported, to the best of the authors knowledge, the first Raman laser using diamond as the active Raman material [52]. This was achieved via passive q-switching of a microchip laser to generate picosecond Raman output.

In 2008, Mildren et al [53] demonstrated an external cavity diamond Raman laser to convert q-switched 532nm pump pulses to 573nm and 620nm Raman pulses, the first and second Stokes respectively. Although Mildren et al were, in this case, limited by laser induced damage of the diamond surfaces and forced to work close to threshold of the Raman laser, limiting conversion efficiencies, this was a significant milestone in the development of diamond's role in laser engineering; with a flurry of pulsed diamond Raman lasers subsequently reported [8], [12], [54]. A variety of different wavelengths were investigated, while efficiencies were also improved upon. Sabella et al achieved near quantum defect limited efficiencies of 84% [54], generating 2W of Raman output power at 1240nm,

pumping with 3.4W using a Q-switched Nd:YAG laser generating 10ns pulses at 1064nm.

The first CW diamond Raman laser was reported by Lubeigt et al [15] in 2010, which used an intra-cavity approach to take advantage of the high power oscillating fundamental field. An output power of 200mW was achieved, which was limited, not by the diamond, but by the thermal lens in the fundamental gain medium ($Nd:YVO_4$). Under quasi-CW operation, an on time Raman output power of 1.75W was achieved, highlighting the potential for a multi-watt CW diamond Raman laser. Lubeigt et al [10] further demonstrated this by designing a 1.6W diamond Raman laser with true CW Raman output.

Feve et al [9] then demonstrated an impressive 24.5W average Raman output power at a wavelength of 1193nm. To the best of our knowledge, this is the highest average output power produced by a pulsed diamond Raman laser, which was pumped with a very sophisticated, cryogenically cooled, Q-switched Yb:YAG laser, delivering up to 340W into the external diamond Raman laser cavity. Furthermore, the output power was limited only by damage to anti-reflection optical coatings deposited on the diamond, meaning there is still scope to further improve output powers.

Several Watts of CW output power have also recently been achieved using diamond Raman lasers. The first of which was demonstrated by Savitski et al [6] using an intra-cavity approach. An output power of 5.1W was obtained; however, arguably the more impressive characteristic of the laser was the 43 fold brightness enhancement observed from the fundamental to the Raman output. This diamond Raman laser was compared to a KGW Raman laser in an almost identical cavity design, and although power of 6.1W was achieved, a substantially smaller 2.5 fold brightness enhancement was seen. It is thought that the improved thermal management in diamond is at least in some part responsible for this considerable improvement in brightness. It is also worth noting that there was no thermal rollover observed in this system, meaning the Raman output was pump power limited. To the best of the author's knowledge, the 6.1W is, prior to

the results presented in this thesis, yet to be surpassed using an intra-cavity approach

To the best of our knowledge, the highest true CW crystalline Raman power achieved to date was demonstrated by Kitzler et al, using an external cavity diamond laser [13]. With a maximum available pump power of 31W, 10.1W of Raman power was achieved. It is worth noting, however, that a high brightness pump beam was used, therefore a brightness decrement was observed.

High power CW Raman fibre lasers have been demonstrated.Over 150W of Raman output power achieved in a single mode silica fibre [55], where an Yb fibre laser operating at 1070nm was used to obtain output at the Raman shifted wavelength of 1120nm. This relatively short Raman shift is typical in the materials used for fibre Raman lasers [55]–[61], potentially limiting a large spectral coverage; however, this can be overcome by implementing "nested Bragg reflectors" in the Raman active fibre to achieve cascaded Raman lasers [56]. This technique was implemented to demonstrate a Raman fibre laser, pumped by an ytterbium fibre laser at 1170nm, operating at 1480nm with over 300W of Raman output power [57]. To the best of the author's knowledge, this is the highest output power achieved from a cascaded Raman fibre laser to date. Although impressive, this system has drawbacks. Firstly, 6 Stokes shifts are required to reach the "eye safe" wavelength reported, with losses at each wavelength reducing the diode to desired Stokes conversion efficiency. Secondly, all 6 Stokes wavelengths resonant in the cavity are seeded, adding complexity to the pumping system. Furthermore, the single mode nature of such Raman fibres means that a pump source with very good beam quality is required. Cladding pumped fibre Raman lasers may provide a route to ameliorate some of these issues; however, to date, output powers have been limited to a few 10's of Watts [60].

1.4 Diamond as a Raman material

1.4.1 Thermal-mechanical properties

The principle of operation of a conventional laser leads to a large amount of heat being deposited in the laser gain material. This is also true for Raman lasers [18]. This heating can lead to several problems in the laser cavity such as thermal lensing in the gain material, with the magnitude of such a lens shown in equation 1.8. Furthermore, large heat loads can lead to deformation of the crystal, and eventually fracture. Caused by a transverse refractive index gradient in the laser gain material, a thermal lens can affect cavity stability which can often lead to "thermal rollover", limiting the achievable output power [62]. Temperature gradients can also cause mechanical stress in the gain material, which lead to thermally induced birefringence, swelling of the crystal and, eventually, fracture [62]. Thermally induced birefringence can introduce problems in the laser resonator if it contains an element which has a polarisation dependent loss, for example, a Brewster surface. Swelling surfaces have a similar effect to the thermal lens, while the problems incurred when a laser material fractures are self-explanatory.

It is clear to see from the above that efficient extraction of the unavoidable heat load deposited in a laser gain material is essential. With a thermal conductivity of 2000$Wm^{-1}K^{-1}$ [63](c.f. Nd:YVO_4 of 10.5$Wm^{-1}K^{-1}$ [64] or KGW of 3.5$Wm^{-1}K^{-1}$ [65]), diamond has an unrivalled ability to deal with heat loads well in excess of other common laser host materials and Raman materials, with some examples shown in Figure 1.4.

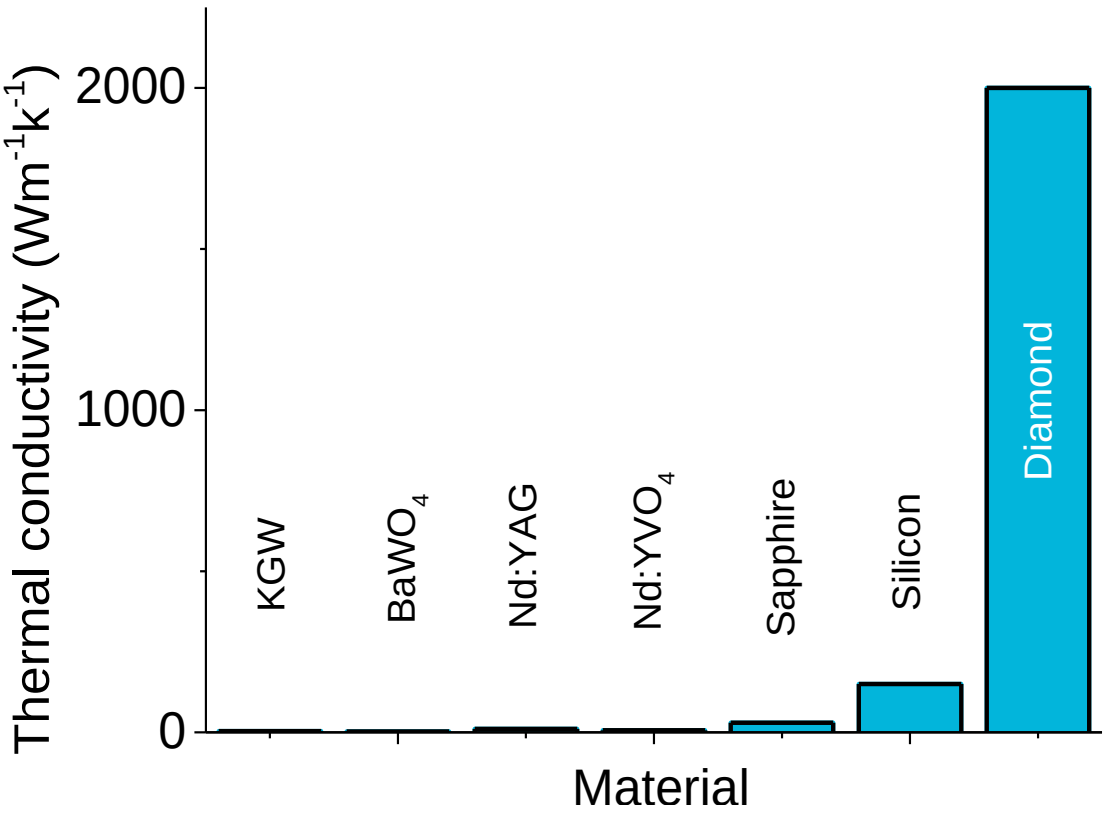

Figure 1.4. A comparison of diamond's thermal conductivity with some typical laser host materials. Values taken from [63]–[66]

As well as having an unrivalled thermal conductivity, diamond has a change in refractive index per Kelvin $\left(\frac{dn}{dT}\right)$ of $9.6\text{x}10^{-6}\text{K}^{-1}$ [63], which is comparable to most oxide crystals which are of the order of a few 10^{-6}K^{-1}. Diamond also has a comparatively low thermal expansion coefficient ($1\text{x}10^{-6}$ K^{-1} c.f. $Nd:YVO_4$ with a value of $11.4\text{x}10^{-6}$ K^{-1} and KGW with quoted values as large as $17\text{x}10^{-6}$ K^{-1}), which, along with a large Young's modulus, minimises any lensing effects caused by bulging surfaces.

1.4.2 Optical properties

Diamond has a broad range of transparency, stretching from its band gap in the ultraviolet (226nm) through the visible range up to 2.5μm where multi-phonon absorption occurs [63]. As seen in Figure 1.5, this absorption band spans from 2.5μm to 6μm, with the material then being transparent into the THz region [67]

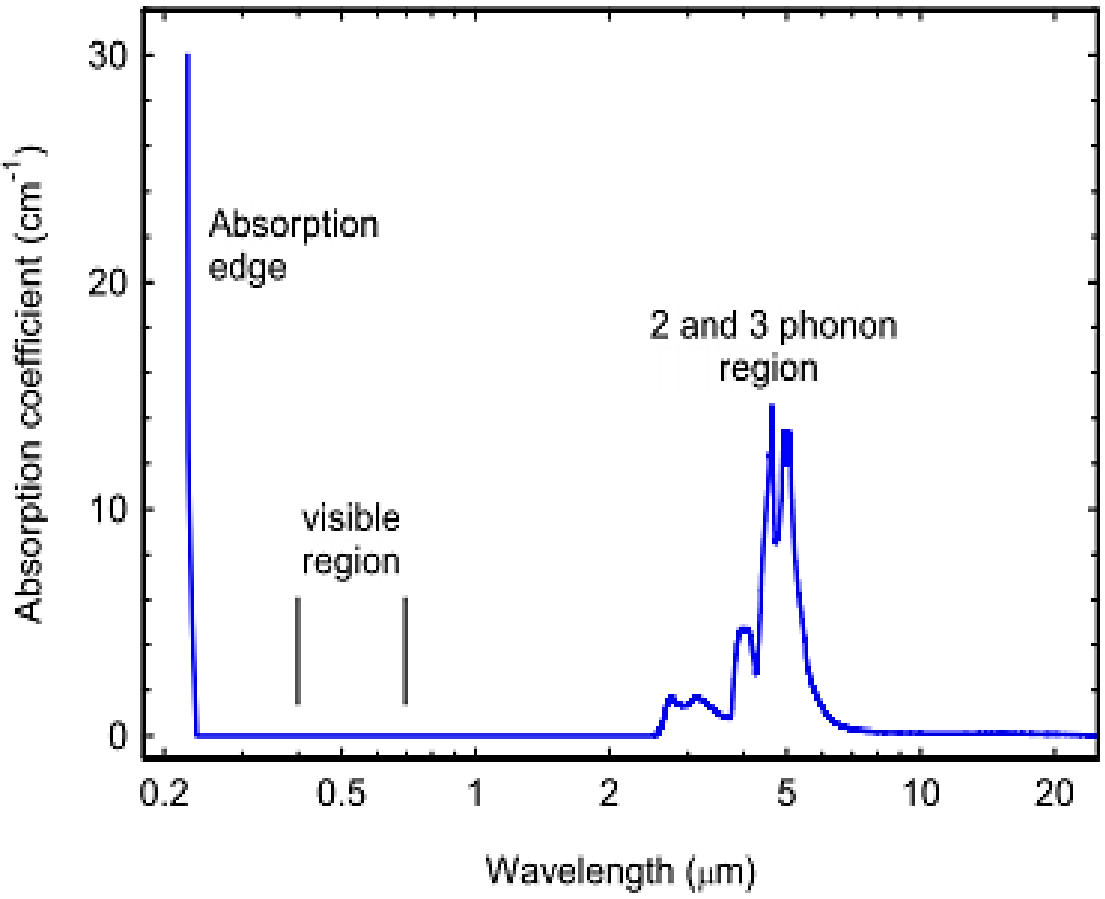

Figure 1.5. Absorption spectrum of high purity diamond from ultra-violet to far infra-red [68]

The main source of optical loss in single crystal CVD diamond arises from single substitutional nitrogen, where a nitrogen atom replaces a carbon atom in the diamond lattice [63]. These nitrogen impurities cause loss via absorption, with any nitrogen impurities causing both broad band absorption throughout the materials transparency range (see section 2.2) and narrower absorption peaks [69].

A second potential source of loss arises when the diamond has stress induced birefringence, which, as discussed previously, can lead to polarisation dependent loss in a laser cavity when there is an element in the cavity, such as a Brewster surface, which has polarisation dependent loss. This effect is discussed in more detail in Chapter 3. Whilst absorption losses are caused by substitutional nitrogen, birefringence is caused by dislocations in the diamond lattice [63].

These dislocations cause strain and distortion in the lattice which lead to complex localised changes in the refractive index. Figure 1.6 compares metripol maps [70] of two diamond samples with different birefringence. It highlights that there can be a large variation in the birefringence on a single diamond sample, which, when implementing diamond in Raman lasers, may result in optimal performance only when the laser field passes through specific sections of the diamond. The sample on the right of Figure 1.6 was grown specifically for low dislocation density.

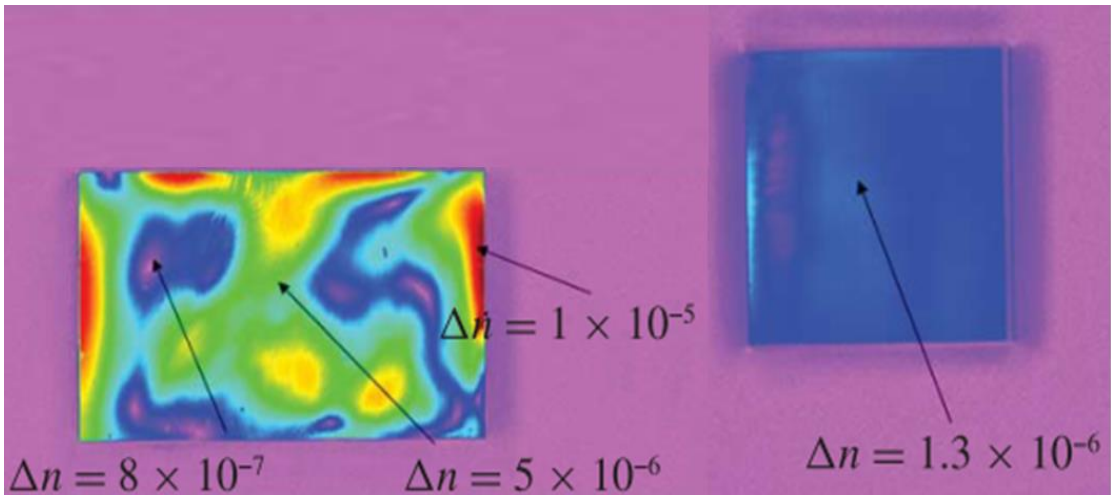

Figure 1.6. Metripol map of birefringence in 2 different diamond samples. The sample on the left has a high birefringence, while the sample on the right was grown specifically for low birefringence. The associated values of Δn are represented for specific locations. Data courtesy of Element 6 Ltd.

In the past 5 to 10 years, advances in the growth technique used to produce single crystal CVD synthetic diamond have resulted in a marked improvement in the available material. Where before, samples with 100 parts per billion (pbb) nitrogen content was considered state of the art, it is now possible to achieve 10's of ppb, resulting in absorption coefficients $<0.005 cm^{-1}$ whilst a reduction in dislocation density allows a reduced birefringence of $<1x10^{-6}$ [6], [13], [23].

1.4.3 Diamond as a Raman laser material

In order to highlight the advantages diamond has as a Raman laser gain material, and approximately quantify the power scaling ability, Lubeigt et al [15] derived a "figure of merit", represented in equation 1.11. This figure, taking into consideration the thermal conductivity, κ, the wavelength shift Δλ, and the rate of change in refractive index with temperature, $\frac{dn}{dT}$, essentially gives a comparison of the strength of the thermal lens generated in the Raman active material, while also considering the desire for a low threshold; including the Raman gain coefficient, g_R, and the typically available length, l, of the material. The higher the FoM, the weaker the thermal lens for a given output power.

$$FoM = \left| \frac{\kappa . g_R . l}{\left(\frac{dn}{dT}\right) . \Delta\lambda} \right| \qquad 1.11$$

Lubeigt et al [15] quote a figure of merit of 430 for diamond, however with the recent developments allowing longer samples (>6mm), along with the authors' slight underestimation of the Raman gain in diamond, a value of 1200 is quoted in this thesis. Compared with other commonly used Raman materials including YVO_4, KGW and silicon (FoM of 20, 3, and 70, respectively), diamond has a FoM almost 20 times higher, when it is noted that much longer crystal lengths (>25mm) are available for the non-diamond materials. Table 1.1 shows a comparison of the mechanical and Raman properties of some common Raman materials and their corresponding figure of merit.

Table 1.1. Comparison of mechanical and Raman properties of selected Raman gain materials

	Material			
	YVO_4	KGW	Silicon	Diamond
Raman gain at 1064nm, g_R (cm/GW)	~5	~4	15	17
Raman shift, Δλ (cm^{-1})	892	901	521	1332
Thermal conductivity, κ ($Wm^{-1}\ K^{-1}$)	~5.2	~3	150	2000
dn/dT ($x10^{-6}\ K^{-1}$)	3	~ –10	215	9.6
Typical available length l (mm)	25	25	40	6
Figure of Merit (defined from Eq.1.9)	20	3	70	1200

1.4.4 Limitations of diamond as a laser gain material

Although diamond has many favourable properties, it is important to highlight the problems faced when using the material as a laser gain material. Ideally, diamond would be used as a host material to laser active ions; however, although doping of diamond has been achieved with transition metals [71], [72], an area of the periodic table rich in laser active ions, the doping was conducted with applications in quantum information processing [73] in mind. This meant that a concentrated thin layer was doped in the diamond surface, rather than the necessary uniform doping throughout the material. To the best of the authors'

knowledge, no studies have yet been conducted on the optical properties of these centres with laser applications in mind.

As an alternative means to introduce laser gain into diamond, and as will be extensively discussed throughout this thesis, SRS can be used. Such a system is, however, highly susceptible to loss, particularly when attempting CW conversion [36]. Minimising the cavity round trip loss is therefore paramount in obtaining optimal conversion efficiencies, however obtaining effective anti-reflection coatings on diamond has proven difficult. Several attempts at depositing coatings have resulted in de-lamination, with an example of this shown in Figure 1.7. It should be emphasised that, in some instances, purchased coatings adhered well to the surface and laser action was achieved, however the coatings at these wavelengths have yet to achieve the quality and reliability of the coatings deposited on diamond for work at the CO_2 laser wavelength of 10.6μm. Recent results reported by Williams et al [74] have, however, highlighted that it is possible to obtain high quality AR coatings on diamond, with over 100W on-time Raman output power achieved from a diamond Raman laser.

As well as unpredictable coating quality, experience has proved single crystal CVD diamond has varying values of optical loss; with the growth of ultra-low nitrogen content samples presumed far from trivial. Samples with a loss coefficient as high as $0.07cm^{-1}$ at 1064nm have been measured, while the best samples purchased have had a loss coefficient of $0.003cm^{-1}$ at 1064nm. For a typical 6mm long diamond sample, these two loss coefficients would result in an inhibitive 8% round trip loss and a 0.35% round trip loss, respectively.

Further limitations are introduced by the (relatively low for pulsed systems) surface laser induced damage threshold of diamond surfaces [75], which will be discussed in more detail in Chapter 5.

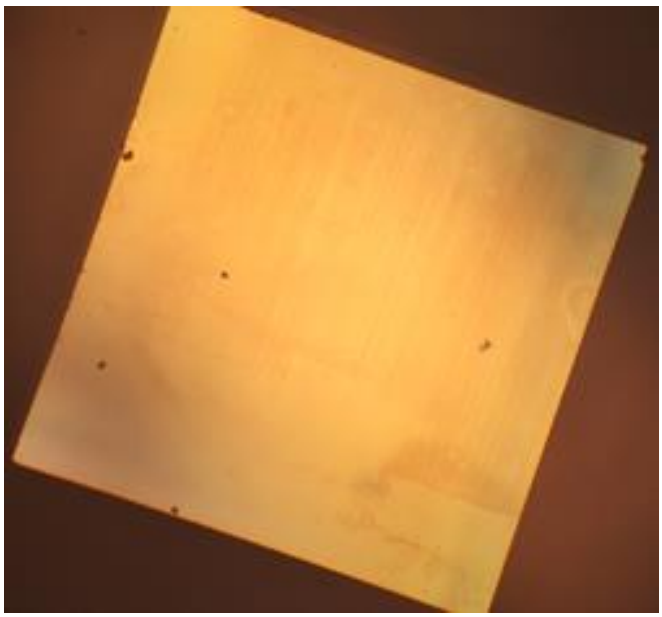

Figure 1.7. De-lamination of deposited diamond coatings. Coatings were designed for a zero degree angle of incidence, AR at 1064nm and 1240nm.

1.5 Thesis outline

In Chapter 2, a systematic study of the wavelength dependence of the Raman gain in diamond is presented. An absolute measurement of the Raman gain at a variety of wavelengths ranging from 355nm to 1450nm, is accompanied by an investigation into the wavelength dependence on the threshold of SRS. Results confirmed the $\frac{1}{\lambda}$ dependence predicted theoretically [17].

In Chapter 3, continuous wave intra-cavity diamond Raman lasers are discussed, with two systems presented. The first is pumped with an unpolarized Nd:YAG laser module, while the second is pumped with an Yb:KLuW thin disk. To the best of the author's knowledge, the highest power intra-cavity CW Raman lasers are realised, with a maximum output power of 7.6W achieved.

In Chapter 4, compact pulsed diamond Raman lasers are investigated. Nanosecond q-switch pulses from a commercially available 532nm laser are converted using a monolithic diamond Raman laser, with a maximum 84% conversion efficiency from pump to the combined 1st, 2nd and 3rd Stokes. Both a

plane-plane sample and a sample with microlens structures etched into the front surface were utilised; with the structured sample achieving slightly higher conversion efficiencies. Further work was conducted to achieve shorter pulses in the picosecond regime, using intra-cavity Raman laser pumped with a passively mode-locked Nd:YVO_4 laser. Problems arising from competing nonlinearities in the fundamental laser cavity hindered stable oscillation; however 15ps pulses at the 1st Stokes wavelength of 1240nm were achieved.

In Chapter 5, the laser induced damage threshold of diamond will be studied, with a variety of different surface finishes investigated for nanosecond pulse durations. Attempts to improve the surface damage threshold via surface etching are presented.

Chapter 6 will contain a summary of the work presented in this thesis, with further discussion on the conclusions and the prospects for continuing this work.

Bibliography

[1] F. P. Bundy, H. T. Hall, H. M. Strong, and R. H. Wentorf, "Man-made diamonds," *Nature*, vol. 176, no. 4471, 1955.

[2] R. B. Birch, P. Millar, A. J. Kemp, and D. Burns, "Multi Watt operation of a Nd:YVO4 Microchip Laser Incorporating a Synthetic Diamond Heat Spreader," in *Conference on Lasers and Electro-Optics Europe*, 2010, p. CTuU7.

[3] W. Z. Zhuang, Y. Chen, K. W. Su, K. F. Huang, and Y. F. Chen, "Performance enhancement of sub-nanosecond diode-pumped passively Q-switched Yb : YAG microchip laser with diamond surface cooling," *Opt. Express*, vol. 20, no. 20, pp. 22602–22608, 2012.

[4] N. Laurand, C. Lee, E. Gu, J. E. Hastie, A. J. Kemp, S. Calvez, and M. D. Dawson, "Array-Format Microchip Semiconductor Disk Lasers," *IEEE J. Quantum Electron.*, vol. 44, no. 11, pp. 1096–1103, 2008.

[5] J. Kim, S. Cho, S. Lee, G. B. Kim, J. Lee, J. Yoo, K. Kim, T. Kim, and Y. Park, "Highly efficient green VECSEL with intra-cavity diamond heat spreader," *Electron. Lett.*, vol. 43, no. 2, 2007.

[6] V. G. Savitski, I. Friel, J. E. Hastie, M. D. Dawson, D. Burns, and A. J. Kemp, "Characterization of Single-Crystal Synthetic Diamond for Multi-Watt Continuous-Wave Raman Lasers," *Quantum Electron. IEEE J.*, vol. 48, no. 3, pp. 328–337, 2012.

[7] E. Granados, D. J. Spence, and R. P. Mildren, "Deep ultraviolet diamond Raman laser," *Opt. Express*, vol. 19, no. 11, pp. 10857–10863, 2011.

[8] R. P. Mildren and A. Sabella, "Highly efficient diamond Raman laser," *Opt. Lett.*, vol. 34, no. 18, pp. 2811–2813, 2009.

[9] J.-P. M. Feve, K. E. Shortoff, M. J. Bohn, and J. K. Brasseur, "High average power diamond Raman laser," *Opt. Express*, vol. 19, no. 2, pp. 913–922, 2011.

[10] W. Lubeigt, V. G. Savitski, G. M. Bonner, S. L. Geoghegan, I. Friel, J. E. Hastie, M. D. Dawson, D. Burns, and A. J. Kemp, "1.6 W continuous-wave Raman laser using low-loss synthetic diamond," *Opt. Express*, vol. 19, no. 7, pp. 6938–6944, 2011.

[11] A. A. Kaminskii, R. J. Hemley, J. Lai, C. S. Yan, H. K. Mao, V. G. Ralchenko, H. J. Eichler, and H. Rhee, "High-order stimulated Raman scattering in CVD single crystal diamond," *Laser Phys. Lett.*, vol. 4, no. 5, pp. 350–353, 2007.

[12] D. J. Spence, E. Granados, and R. P. Mildren, "Mode-locked picosecond diamond Raman laser," *Opt. Lett.*, vol. 35, no. 4, pp. 556–558, 2010.

[13] O. Kitzler, A. McKay, and R. P. Mildren, "Continuous-wave wavelength conversion for high-power applications using an external cavity diamond Raman laser," *Opt. Lett.*, vol. 37, no. 14, pp. 2790–2792, 2012.

[14] A. McKay, H. Liu, O. Kitzler, and R. P. Mildren, "An efficient 14.5 W diamond Raman laser at high pulse repetition rate with first (1240 nm) and second (1485 nm) Stokes output," *Laser Phys. Lett.*, vol. 10, no. 10, p. 105801, 2013.

[15] W. Lubeigt, G. M. Bonner, J. E. Hastie, M. D. Dawson, D. Burns, and A. J. Kemp, "Continuous-wave diamond Raman laser," *Opt. Lett.*, vol. 35, no. 17, pp. 2994–2996, 2010.

[16] S. C. Rand and L. G. DeShazer, "Visible color-center laser in diamond," *Opt. Lett.*, vol. 10, no. 10, pp. 481–483, 1985.

[17] A. Penzkofer, A. Laubreau, and W. Kaiser, "High Intensity Raman Interactions," *Prog. Quantum Electron.*, pp. 56–140, 1979.

[18] H. M. Pask and J. A. Piper, "The design and operation of all-solid-state Raman lasers," *Prog. Quantum Electron.*, vol. 27, pp. 3–56, 2003.

[19] S. Reilly, V. G. Savitski, H. Liu, E. Gu, M. D. Dawson, and A. J. Kemp, "Monolithic diamond Raman laser," *Opt. Lett.*, vol. 40, no. 6, pp. 930–933, 2015.

[20] J. Lin and H. M. Pask, "Cascaded self-Raman lasers based on 382 cm^{-1} shift in $Nd:GdVO_4$," *Opt. Express*, vol. 20, no. 14, pp. 15180–15185, 2012.

[21] R. Li, R. Bauer, and W. Lubeigt, "Continuous-Wave $Nd:YVO_4$ self-Raman lasers operating at 1109nm, 1158nm and 1231nm," *Opt. Express*, vol. 21, no. 15, pp. 17745–17750, 2013.

[22] A. Sabella, J. A. Piper, and R. P. Mildren, "Diamond Raman laser with continuously tunable output from 3.38 to 3.80 μm.," *Opt. Lett.*, vol. 39, no. 13, pp. 4037–40, 2014.

[23] A. Sabella, J. A. Piper, and R. P. Mildren, "Efficient conversion of a 1.064μm Nd:YAG laser to the eye-safe region using a diamond Raman laser," *Opt. Express*, vol. 19, no. 23, pp. 23554–23560, 2011.

[24] A. McKay, O. Kitzler, and R. P. Mildren, "Simultaneous brightness enhancement and wavelength conversion to the eye-safe region in a high-power diamond Raman laser," *Laser Photon. Rev.*, vol. 8, no. 3, pp. L37–L41, 2014.

[25] R. W. Boyd, *Nonlinear Optics*, vol. 5, no. 10. Academic Press, 2003.

[26] Y. R. Shen and N. Bloembergen, "Theory of Stimulated Brillouin and Raman Scattering," *Phys. Rev.*, vol. 137, no. 6, p. A1787, 1964.

[27] X. Li, H. M. Pask, A. J. Lee, Y. Huo, J. A. Piper, and D. J. Spence, "Miniature wavelength-selectable Raman laser: new insights for optimizing performance," *Opt. Express*, vol. 19, no. 25, pp. 25623–31, 2011.

[28] H. M. Pask, "Continuous-wave, all-solid-state, intracavity Raman laser," *Opt. Lett.*, vol. 30, no. 18, pp. 2454–2456, 2005.

[29] G. M. Bonner, J. Lin, A. J. Kemp, J. Wang, H. Zhang, D. J. Spence, and H. M. Pask, "Spectral broadening in continuous-wave intracavity Raman lasers," *Opt. Express*, vol. 22, no. 7, pp. 613–620, 2014.

[30] J. Zhao, X. Zhang, X. Guo, X. Bao, L. Li, and J. Cui, "Diode-pumped actively Q-switched Tm, Ho:$GdVO_4$/$BaWO_4$ intracavity Raman laser at 2533 nm," *Opt. Lett.*, vol. 38, no. 8, pp. 1206–8, 2013.

[31] D. C. Parrotta, A. J. Kemp, M. D. Dawson, and J. E. Hastie, "Tunable continuous-wave diamond Raman laser," *Opt. Express*, vol. 19, no. 24, pp. 24165–24170, 2011.

[32] J. Lin, H. M. Pask, D. J. Spence, C. J. Hamilton, and G. P. A. Malcolm, "Continuous-wave VECSEL Raman laser with tunable lime-yellow-orange output," *Opt. Express*, vol. 20, no. 5, pp. 5219–24, 2012.

[33] D. C. Parrotta, W. Lubeigt, A. J. Kemp, D. Burns, M. D. Dawson, and J. E. Hastie, "Continuous-wave Raman laser pumped within a semiconductor disk laser cavity," *Opt. Lett.*, vol. 36, no. 7, pp. 1083–1085, 2011.

[34] G. M. Bonner, "Thermal and Spectral Effects in Intracavity Raman Lasers," Strathclyde University, 2013.

[35] D. C. Parrotta, A. J. Kemp, M. D. Dawson, and J. E. Hastie, "Multiwatt, Continuous Wave, Tunable Diamond Raman Laser With Intracavity Frequency-Doubling to the Visible Region," *IEEE J. Quantum Electron.*, vol. 19, no. 4, 2013.

[36] D. J. Spence, P. Dekker, and H. M. Pask, "Modeling of Continuous Wave Intracavity Raman Lasers," *Sel. Top. Quantum Electron. IEEE J.*, vol. 13, no. 3, pp. 756–763, 2007.

[37] M. Weitz, C. Theobald, R. Wallenstein, and J. A. L'huillier, "Passively mode-locked picosecond Nd:YVO4 self-Raman laser," *Appl. Phys. Lett.*, vol. 92, no. 9, p. 091122, 2008.

[38] A. A. Demidovich, A. S. Grabtchikov, V. A. Lisinetskii, V. N. Burakevich, V. A. Orlovich, and W. Kiefer, "Continuous-wave Raman generation in a diode-pumped Nd^{3+}:$KGd(WO_4)_2$ laser.," *Opt. Lett.*, vol. 30, no. 13, pp. 1701–3, 2005.

[39] Z. H. Li, J. Y. Peng, and Y. Zheng, “CW mode-locked self-Raman 1.17μm Nd: $GdVO_4$ laser with a novel long cavity,” *Opt. Laser Technol.*, vol. 58, no. 3, pp. 39–42, 2014.

[40] Z. G. Wu, Z. H. Cong, X. H. Chen, X. Y. Zhang, Q. P. Wang, W. X. Lan, W. T. Wang, and Y. G. Zhang, “Passively Q-switched 1097nm c-cut Nd:YVO_4 self-Raman laser with Cr:YAG saturable absorber,” *Opt. Laser Technol.*, vol. 54, pp. 137–140, 2013.

[41] Y. F. Chen, “Efficient 1521nm Nd : $GdVO_4$ Raman laser,” *Opt. Lett.*, vol. 29, no. 22, pp. 2632–2634, 2004.

[42] F. Couny, F. Benabid, and P. Light, “Subwatt Threshold cw Raman Fiber-Gas Laser Based on H2-Filled Hollow-Core Photonic Crystal Fiber,” *Phys. Rev. Lett.*, vol. 99, no. 14, p. 143903, 2007.

[43] J. K. Brasseur, K. S. Repasky, and J. L. Carlsten, “Continuous-wave Raman laser in H2,” *Opt. Lett.*, vol. 23, no. 5, pp. 367–369, 1998.

[44] W. K. Bischel and M. J. Dyer, “Wavelength dependence of the absolute Raman gain coefficient for the Q1 transition in H_2,” *J. Opt. Soc. Am. B*, vol. 3, no. 5, pp. 677–682, 1986.

[45] E. J. Woodbury and W. K. Ng, “Ruby Laser Operation in the Near IR,” *Proc. IRE*, vol. 50, p. 2367, 1962.

[46] J. T. Murray, R. C. Powell, N. Peyghambarian, D. Smith, and W. Austin, “Generation of 1.5μm radiation through intracavity solid-state Raman shifting in $Ba(NO_3)_2$ nonlinear crystals,” *Opt. Lett.*, vol. 20, no. 9, pp. 1017–1019, 1995.

[47] Y. F. Chen, “Compact efficient self-frequency Raman conversion in diode-pumped passively Q-switched Nd:$GdVO_4$ laser,” *Appl. Phys. B Lasers Opt.*, vol. 78, no. 6, pp. 685–687, 2004.

[48] A. S. Grabtchikov, V. A. Lisinetskii, V. A. Orlovich, M. Schmitt, R. Maksimenka, and W. Kiefer, “Multimode pumped continuous-wave solid-state Raman laser.,” *Opt. Lett.*, vol. 29, no. 21, pp. 2524–6, 2004.

[49] G. Eckhardt, D. P. Bortfeld, and M. Geller, “Stimulated Emission of Stokes and Anti-Stokes Raman Lines From Diamond, Calcite, and A-Sulfur Single Crystals,” *Appl. Phys. Lett.*, vol. 3, no. 8, p. 137, 1963.

[50] A. K. McQuillan, W. R. L. Clements, and B. P. Stoicheff, “Stimulated Raman Emission in Diamond: Spectrum, Gain, and Angular Distribution of Intensity,” *Phys. Rev. A*, vol. 1, no. 3, pp. 628–635, 1970.

[51] A. A. Kaminskii, V. G. Ralchenko, and V. I. Konov, “Observation of stimulated Raman scattering in CVD-diamond,” *JETP*, vol. 80, no. 4, pp. 298–301, 2004.

[52] A. A. Demidovich, A. S. Grabtchikov, V. A. Orlovich, M. B. Danailov, and W. Kiefer, “Diode Pumped Diamond Raman Microchip Laser,” in *Conference on Lasers and Electro-Optics Europe*, 2005, p. 251.

[53] R. P. Mildren, J. E. Butler, and J. R. Rabeau, “CVD-diamond external cavity Raman laser at 573 nm,” *Opt. Express*, vol. 16, no. 23, pp. 18950–18955, 2008.

[54] A. Sabella, J. A. Piper, and R. P. Mildren, “1240 nm diamond Raman laser operating near the quantum limit,” *Opt. Lett.*, vol. 35, no. 23, pp. 3874–3876, 2010.

[55] Y. Feng, L. R. Taylor, and D. B. Calia, “150 W highly-efficient Raman fiber laser,” *Opt. Express*, vol. 17, no. 26, pp. 23678–23683, 2009.

[56] V. R. Supradeepa, J. W. Nichsolson, C. E. Headley, M. F. Yan, B. Palsdottir, and D. Jakobsen, “A high efficiency architecture for cascaded Raman fiber lasers,” *Opt. Express*, vol. 21, no. 6, pp. 7148–7155, 2013.

[57] V. R. Supradeepa and J. W. Nicholson, “Cascaded Raman Fiber Lasers,” *Opt. Lett.*, vol. 38, no. 14, pp. 2538–2541, 2013.

[58] I. D. Vatnik, D. V Churkin, S. A. Babin, and S. K. Turitsyn, “Cascaded random distributed feedback Raman fiber laser operating at 1.2μm,” *Opt. Express*, vol. 19, no. 19, pp. 130–132, 2011.

[59] X. Dong, P. Shum, N. Q. Ngo, and C. C. Chan, “Multiwavelength Raman fiber laser with a continuously-tunable spacing,” *Opt. Express*, vol. 14, no. 8, pp. 3288–3293, 2006.

[60] C. A. Codemard, P. Dupriez, Y. Jeong, J. K. Sahu, M. Ibsen, and J. Nilsson, “High Power Continuous-Wave Cladding Pumped Raman Fiber Laser,” *Opt. Lett.*, vol. 31, no. 15, pp. 2290–2292, 2006.

[61] J. W. Nicholson, M. F. Yan, P. Wisk, J. Fleming, and F. Dimarcello, “Raman fiber laser with 81 W output power at 1480nm,” *Opt. Lett.*, vol. 35, no. 18, pp. 3069–3071, 2010.

[62] W. Koechner, *Solid-State Laser Engineering*, 6th ed. Springer, 2006.

[63] I. Friel, S. L. Geoghegan, D. J. Twitchen, and G. A. Scarsbrook, “Development of high quality single crystal diamond for novel laser applications,” *Proc. SPIE*, vol. 7838, pp. 783819–1, 2010.

[64] J. Didierjean, E. Herault, F. Balembois, and P. Georges, “Thermal conductivity measurements of laser crystals by infrared thermography . Application to Nd : doped crystals,” vol. 16, no. 12, pp. 8995–9010, 2008.

[65] S. Biswal, S. P. O. Connor, and S. R. Bowman, “Thermo-optical parameters measured in ytterbium-doped potassium gadolinium tungstate,” *Appl. Opt.*, vol. 44, no. 15, pp. 3093–3097, 2005.

[66] D. Ran, H. Xia, S. Sun, Z. Ling, W. Ge, and H. Zhang, “Thermal conductivity of $BaWO_4$ single crystal,” *Mater. Sci. Eng. B*, vol. 130, no. 1–3, pp. 206–209, 2006.

[67] P. Dore, A. Nucara, D. Cannavo, G. De Marzi, P. Calvani, A. Marcelli, R. S. Sussmann, A. J. Whitehead, C. N. Dodge, A. J. Krehan, and H. J. Peters, “Infrared properties of chemical-vapor deposition polycrystalline diamond windows,” *Appl. Opt.*, vol. 37, no. 24, pp. 5731–5736, 1998.

[68] A. T. Collins, “The colour of diamond and how it may be changed,” *J. Gemmol.*, vol. 27, pp. 341–359, 2001.

[69] P. M. Martineau, S. C. Lawson, A. J. Taylor, S. J. Quinn, D. J. F. Evans, and M. J. Crowder, “Identification of Synthetic Diamond Grown Using Chemical Vapor Deposition,” *Gems Gemol.*, vol. 40, no. 1, pp. 2–25, 2004.

[70] A. M. Glazer, J. G. Lewis, and W. Kaminsky, “An Automatic Optical Imaging System for Birefringent Media,” *Proc. R. Soc. London. Ser. A Math. Phys. Eng. Sci.*, vol. 452, pp. 2751–2765, 1955.

[71] M. Wolfer, H. Obloh, O. a. Williams, C.-C. Leancu, L. Kirste, E. Gheeraert, and C. E. Nebel, “Doping of single crystalline diamond with nickel,” *Phys. Status Solidi*, vol. 207, no. 9, pp. 2054–2057, 2010.

[72] M. M. Biener, J. Biener, S. O. Kucheyev, Y. M. Wang, B. El-Dasher, N. E. Teslich, A. V Hamza, H. Obloh, W. Mueller-Sebert, M. Wolfer, T. Fuchs, M. Grimm, A. Kriele, and C. Wild, “Controlled incorporation of mid-to-high Z transition metals in CVD diamond,” *Diam. Relat. Mater.*, vol. 19, no. 5–6, pp. 643–647, 2010.

[73] F. Jelezko and J. Wrachtrup, “Single defect centres in diamond: A review,” *Phys. Status Solidi*, vol. 203, no. 13, pp. 3207–3225, 2006.

[74] R. J. Williams, O. Kitzler, A. Mckay, and R. P. Mildren, “Investigating diamond Raman lasers at the 100 W level using quasi-continuous-wave pumping,” *Opt. Lett.*, vol. 39, no. 14, pp. 4152–4155, 2014.

[75] R. S. Sussmann, G. A. Scarsbrook, C. J. H. Wort, and R. M. Wood, “Laser damage testing of CVD grown diamond windows,” *Diam. Relat. Mater.*, vol. 3, pp. 1173 – 1177, 1994.

Chapter 2 - Measurement of the steady-state Raman gain in diamond as a function of pump wavelength

In this chapter, experiments to measure the Raman gain in diamond will be described. The goal of this work was to provide a systematic study of the dependence of pump wavelength on the steady state Raman gain in diamond. The experiments showed that the Raman gain has a linear dependence on the pump wavenumber.

Absolute and relative measurements of the Raman gain will be presented. A pump probe technique was used to obtain absolute values of the Raman gain in diamond between 355nm and 1280nm. A comparative measurement of the stimulated Raman oscillation threshold between 355nm and 1450nm provided relative values.

To the best of the author's knowledge, this is the first systematic study of the dependence of the Raman gain on pump wavelength in diamond. Using this study, the Raman gain at all wavelengths between 355nm and 1450nm can be estimated, with these values being useful in the design process for diamond Raman lasers.

2.1 – Theoretical considerations

2.1.1- Pump probe

In chapter 1, stimulated Raman scattering (SRS) was discussed. With a Raman medium, in our case diamond, pumped at a wavelength λ_P, there is the potential for amplification of an input beam of wavelength λ_R. This process is illustrated in Figure 2.1. As previously discussed, λ_R is determined by the pump wavelength and the intrinsic Raman shift of the Raman active medium.

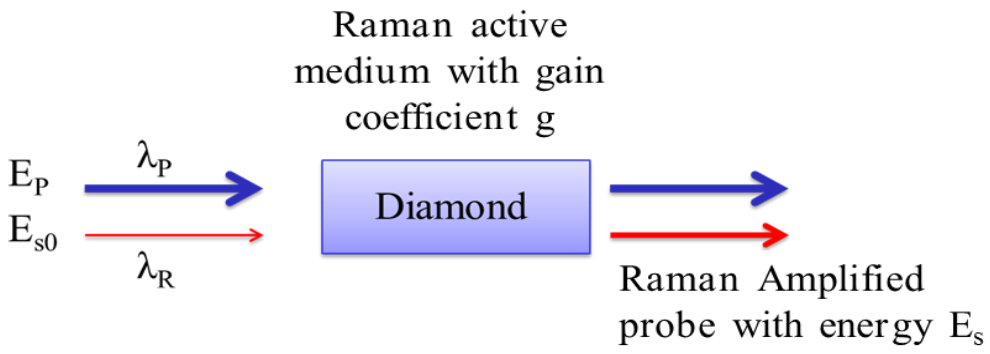

Figure 2.1. Amplification of an incident beam via stimulated Raman scattering

Following the approach set out by Stegeman et al., the Raman amplification process can be described by equation 2.1 [1].

$$\frac{d}{dz}E_R(z) = \frac{1}{2}gE_S(z)I_P(z) \qquad 2.1$$

where g is the Raman gain coefficient, $E_s(z)$ is the incident Raman field, $E_R(z)$ is the generated Raman signal field and $I_p(z)$ is the incident pump irradiance.

Experimentally, the pump and incident Raman field (probe) are pulsed, focused beams. The temporal and spatial profiles of the beams must therefore be taken into consideration when conducting an absolute measurement of the Raman gain. The spatial and temporal profiles of the pump and probe fields, $f_p(x,y,t)$ and $f_s(x,y,t)$, respectively, are assumed to be Gaussian, and can be described by equations 2.2a and 2.2b. The pump and probe beams were spatially and temporally overlapped and collimated throughout the length of the diamond.

$$f_s(x,y,t) = exp\left[-\frac{(x^2+y^2)}{\omega_s^2} - \frac{t^2}{\tau_s^2}\right] \qquad 2.2a$$

$$f_p(x,y,t) = exp\left[-\frac{(x^2+y^2)}{\omega_p^2} - \frac{t^2}{\tau_p^2}\right] \qquad 2.2b$$

So that the generated Raman field $f_R(x,y,t)$ can be defined as [1]:

$$f_R(x,y,t) = f_s(x,y,t)f_p^2(x,y,t) \qquad 2.3$$

Where $\tau_{p(s)}$ are the pulse durations of the respective pulses and $\omega_{p(s)}$ is the pump (probe) beam waist radius.

The Raman and pump fields can then be defined spatially and temporally as follows:

$$E_R(x, y, \mathrm{z}, t) = E_R(\mathrm{z}) f_R(x, y, t) \qquad 2.4a$$

$$E_S(x, y, 0, t) = E_S(\mathrm{z}) f_s(x, y, t) \qquad 2.4b$$

$$E_P(x, y, \mathrm{z}, t) = E_P(\mathrm{z}) f_P(x, y, t) \qquad 2.4c$$

Integrating equation 2.1 over z while assuming negligible pump depletion, we arrive at the term seen in equation 2.5 [1].

$$E_R(z) = \frac{g}{2} L . E_S(0) I_P(0) \qquad 2.5$$

Experimentally, the total Raman energy, E_T, exiting the crystal is measured (i.e. the injected signal plus the generated Raman). This is defined as [1]:

$$E_T(x, y, z) = E_S(0) f_S(x, y, t) + \frac{g}{2} L . E_S I_P(0) f_S(x, y, t) f_P^2(x, y, t) \qquad 2.6$$

Integrating over x, y and t gives the relationship shown in equation 2.7[1].

$$\frac{E_T}{E_s} - 1 = g \left(\frac{\pi}{2}\right)^{-\frac{3}{2}} \left[\frac{E_p L}{\left(\omega_p^2 + \omega_s^2\right)\sqrt{\tau_p^2 + \tau_s^2}}\right] \qquad 2.7$$

In this work, an uncoated diamond sample is studied, therefore, along with bulk absorption losses at both the pump and Raman wavelengths, Fresnel reflections must be taken into consideration. Over the wavelength range of 355nm to 1800nm (the shortest pump wavelength and the longest Raman converted wavelength used experimentally), the refractive index of diamond changes from 2.49 to 2.39. This leads to a variation in the Fresnel reflectivity, R, from 0.18 to 0.167. A value of 0.17 was therefore chosen when calculating the Fresnel reflectivity.

Fresnel reflections at the front diamond surface lead to an energy of E_p (1-R) entering the sample. The back surface of the diamond, however, reflects part of this beam back into the diamond resulting in an overall effective pump energy E_{eff} in the bulk diamond of the form shown in equation 2.8. Due to operation in the small signal regime, it is assumed no depletion occurs.

$$E_{eff} = E_p(1 - R^2) \tag{2.8}$$

Absorption losses, α_L, in the diamond sample of length L also reduce both the pump and Raman pulse energies in the diamond. These losses can be dealt with using the method described in [2]: reducing the samples interaction length to an "effective length", L_{eff}, incorporates the absorption loss in the material, mimicking attenuation of the pump. Equation 2.9 [2] can be used to calculate this effective reduction in the interaction length.

$$L_{eff} = \frac{[1 - \exp(-\alpha_L L)]}{\alpha_L} \tag{2.9}$$

The Raman gain studied in [1] investigates bulk glass samples with a broad Raman linewidth (considerably larger than the pump linewidth). In this study however, the Raman linewidth of diamond Δv_L (2.5cm^{-1} [3],[4]), is comparable to the pump linewidth Δv_P (2cm^{-1} and 5cm^{-1}). It has been previously shown [5],[6] that the threshold of a Raman oscillator increases with the linewidth of the pump laser by reducing the effective Raman gain. In order to calculate the intrinsic Raman gain in diamond, the term $1 + \frac{\Delta v_L}{\Delta v_R}$ [5] has been added to equation 2.7. This effect was investigated experimentally, with the results presented in section 2.3.4.

Considering the above points, equation 2.7 has been modified to take into account the various parameters that affect the measurement of the Raman gain. This results in equation 2.10.

$$\frac{E_T}{E_s F_s \exp(-\alpha_s L)} - 1 = g\left(\frac{\pi}{2}\right)^{-\frac{3}{2}}\left[\frac{E_{eff}L_{eff}}{\left(\omega_p^2 + \omega_s^2\right)\sqrt{\tau_p^2 + \tau_s^2}\left(1 + \frac{\Delta v_L}{\Delta v_R}\right)}\right] \tag{2.10}$$

Where α_s and F_s are the absorption coefficient and Fresnel reflectivity seen by the probe beam in the bulk diamond and at the diamond surfaces respectively. The experimental method for dealing with these losses is discussed in section 2.4.2.

In order to obtain a value for the Raman gain, the ratio of input to output probe pulse energy is monitored. The gain can then be extracted from equation 2.10. This analysis assumes negligible depletion of the pump; hence, the parameters of the pump and probe beam were selected to ensure operation in the small signal regime.

In contrast to ultrafast pump probe experiments, the nanosecond pulse duration used in these experiments deemed it unnecessary to take additional measures to ensure temporal overlap of the pulses. The pulse lengths were chosen to ensure operation in the steady state regime, in which the pump pulse duration is longer than the phonon relaxation time [7]. With the SRS linewidth in diamond Δv_L of 2.5cm^{-1}, the phonon relaxation time T_2 can be calculated from $T_2 = (\pi \Delta v_L)^{-1}$ to give a value of 4.2ps [4]. Using a nanosecond pump source ensures that transient effects will not affect the measurements.

2.1.2 - Stimulated Raman oscillation threshold

Measuring the threshold of stimulated Raman oscillation can provide a complimentary data set to that of the pump probe technique. With Fresnel reflections at the front and back diamond surfaces providing a low Q resonator for the Raman field, the variation in threshold at different wavelengths can be investigated. Although not providing an absolute measurement of the Raman gain, it yields a relative study, showing the trend in the relationship between pump wavelength and Raman gain. Fundamentally, the threshold of a laser system is reached at the point where the gain in the system is equal to the loss. In theory, an absolute measurement of the Raman gain could be obtained using this method; however, a firm grasp of the systems loss is required. Although the losses in the system could be estimated, it is the author's opinion that this could

not be done with enough precision to obtain accurate results. The relationship between the threshold intensity for stimulated Raman oscillations I_{th} and the Raman gain is as follows [8]:

$$g\ \alpha\ \frac{1}{I_{th}L} \tag{2.11}$$

However, as in the pump probe measurement, absorption losses and the pump linewidth must be considered. As can be seen in Figure 2.2, the absorption losses affect each wavelength differently and so must be incorporated into equation 2.11 along with the pump linewidth, which also varied slightly with pump wavelength. The revised relationship set out in equation 2.12 can then be used to obtain a data set detailing the form of the variation in Raman gain with wavelength.

In a similar manner to the pump probe experiment, taking into account the Fresnel reflections from front and back surfaces reduces the incident pump intensity $I_{(inc)}$ to an effective intensity of $I_{(eff)}$ in the bulk diamond sample.

$$I_{th(eff)} = I_{th(inc)}(1 - R^2) \tag{2.12}$$

As this is a comparative study, the Fresnel reflections may be ignored; however, for completeness, they have been included in this analysis.

$$g\ \alpha\ \frac{\left(1 + {\Delta v_L}/{\Delta v_R}\right)}{I_{th(eff)}L_{eff}} \tag{2.13}$$

2.2 – Absorption losses in diamond sample

Absorption loss measurements for the diamond sample used were conducted by Dr Vasili Savitski. As these results are crucial in the measurement of the Raman gain in diamond, a brief overview of the results will be presented. For a more detailed description, see [9], [10].

As discussed in Chapter 1, the absorption in high quality CVD-grown single-crystal diamond is mainly caused by single substitutional nitrogen, with the absorption coefficient increasing towards shorter wavelengths before reaching the band gap of diamond at 226nm [11]. Loss measurements at wavelengths of 1064, 640, 532, 452 and 364nm were taken. The diamond sample was placed on a Peltier element using thermal paste. An increase in temperature caused by absorption of the incident laser resulted in a drop in voltage across the Peltier. It should be noted that a small fraction of light may be scattered onto the Peltier element causing additional heating. The results presented may therefore be slightly higher than the absorption coefficient measured via ISO methods, due to the simplified experimental technique. Figure 2.2 shows a rapid increase in the absorption coefficient with pump photon energy: from 0.03cm^{-1} at 1.17eV (1064nm) to 0.7cm-1 at 3.42eV (364nm).

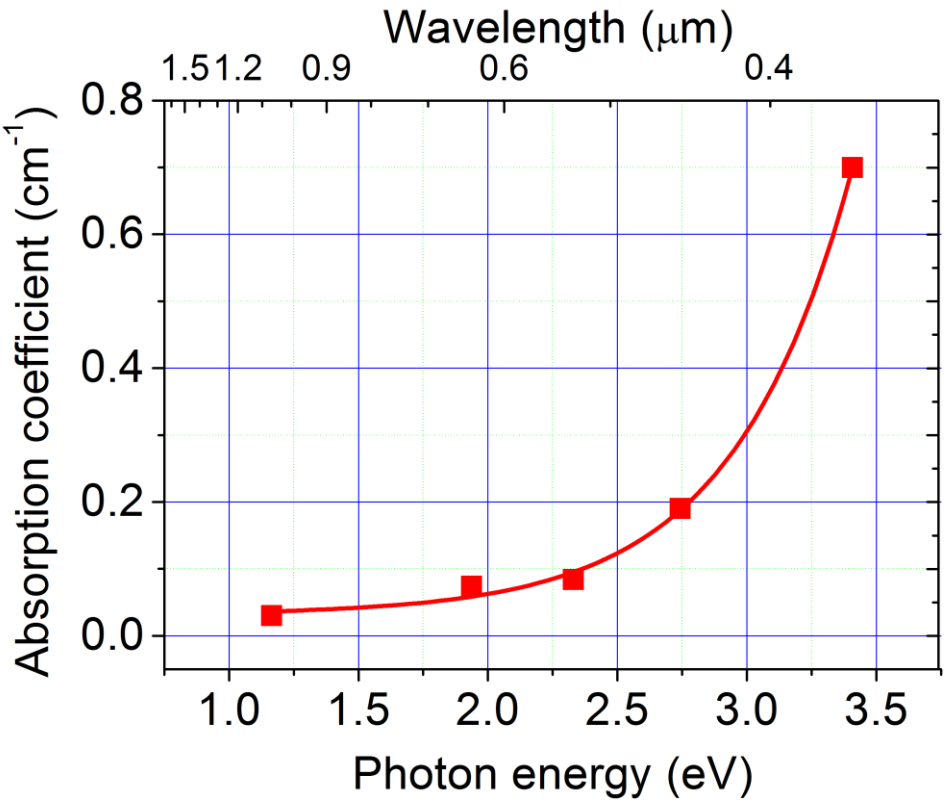

Figure 2.2. Absorption losses in diamond as a function of pump photon energy

An exponential growth function has been fitted to the experimental data. The absorption coefficient is around 10 times larger than in samples used in the

development of the highest power intra-cavity CW Raman laser [10], which had nitrogen content of approximately 20 parts per billion (ppb). From measurements made in [11], the nitrogen content in the sample used can be estimated to be approximately 200 ppb.

2.3 – Measurements of Raman gain in the literature

Although there has been a significant amount of research into the use of diamond as a Raman laser material [4], [10], [12]–[20], values quoted for the Raman gain vary widely. Furthermore, few pump wavelengths have been investigated, with most measurements made at the common Nd:YAG wavelength of 1064nm and its second harmonic at 532nm. Quoted Raman gain coefficients range from 12.5cmGW^{-1} [4] to 21cmGW^{-1} [10] at a pump wavelength of 1064nm and from 50 cmGW^{-1} to 75 cmGW^{-1} at a pump wavelength of 532nm.

Different techniques have been used to deduce the Raman gain. Kaminskii et al [4] compared the intensity required for the onset of significant SRS in diamond at a pump wavelength of 1064nm and Raman wavelength of 1240nm to that of 2-adamanthylamino-5-nitropyridine (AANP) at the same pump wavelength and with a Raman wavelength of 1232nm. The Raman gain of AANP is known at this wavelength and, hence, the gain in diamond can be estimated. The Raman gain can also be estimated from Raman laser performance modelling, which has been done in [4], [7], [8] and [13]. To the best of our knowledge, the steady-state Raman gain in single crystal CVD grown diamond has been measured directly using a pump-probe technique on only one occasion [10] and only at the pump wavelength of 1064 nm.

Although diamond has not been investigated, the Raman gain and its wavelength dependence has been studied in other common Raman materials. Systematic studies of barium tungstate [21] and barium nitrate [22] have been conducted. These measurements were over the relatively small wavelength range between 532nm and 1064nm. The Raman gain was found to decline more

rapidly than the 1/λ dependence predicted and confirmed experimentally in molecular hydrogen[8]. This may be caused by the more complex structure of the crystalline materials studied, compared to the simple H_2 molecules studied in [8].

2.4 – Pump-probe measurement

2.4.1 – Diamond sample

The single crystal chemical vapour deposition (CVD) grown [11], [23] diamonds used in this section were provided by Element 6 Ltd. The sample studied was cut for light propagation along a <110> direction. The dimensions of the sample can be seen in Figure 2.3. The losses of the sample were measured via a simplified calorimetric technique [10] and found to be $0.03cm^{-1}$ at 1064nm, as presented in Figure 2.2. The birefringence (Δn) was approximately 1.3×10^{-6} (relatively uniform across the whole of the sample) along the 6.5mm length of the diamond [10]. The sample had approximately 200 parts per billion (ppb) concentration of single substitutional nitrogen [10]. The diamond was uncoated.

Figure 2.3. Dimensions and crystallographic orientation of diamond sample under investigation

The Raman gain in diamond is dependent on the crystallographic orientation relative to the pump and Raman polarisations and the direction of light propagation. It is shown in [10] and [13] that the maximum Raman gain is realised when the pump and Raman beams are co-polarized along a <111>

crystallographic direction (54.7^0 to a <100> direction) with light propagation along a <110> direction. Theoretically, this is the orientation which allows access to maximum gain: a 33% increase when compared to propagation along a <100> direction [10], [24].

2.4.2 – Experimental method

In order to study the spectral dependence of the Raman gain in diamond over a wide range of pump wavelengths, a Continuum Panther optical parametric oscillator (OPO) was utilised. The OPO was pumped using a frequency tripled, flash lamp pumped Nd:YAG laser, q-switched to produce approximately 6ns pulses with a maximum energy of 400mJ. The laser system was provided by the EPSRC laser loan pool.

The OPO was able to operate in both un-seeded regime and seeded regime, where a narrow linewidth CW diode laser is injected into the Nd:YAG pump cavity. By comparing the results achieved using these two regimes, the effect the linewidth of the pump laser has on the measured Raman gain can be determined. In order to study the dependence of the measured fractional gain on linewidth, the linewidth of the pump laser operating in the seeded and unseeded regime was measured using an optical spectrum analyser.

The pump-probe experimental setup used to measure the Raman gain in diamond is shown schematically in Figure 2.4.

The pulses emitted by the OPO (1) were split at a 50/50 beam splitter (2) with both transmitted and reflected beams being attenuated appropriately using a half wave plate (3) and a Glan Taylor prism (4). The transmitted beam was used to pump the diamond sample under investigation (5) after being focused using a lens of focal length 300mm (6). The reflected beam was focused into a second diamond sample (7) using lens (8). A Raman laser cavity was formed between a dichroic mirror (9) (highly reflective at the Raman wavelength and highly transmissive at the pump wavelength) and the back surface of the diamond,

which reflects approximately 17% (Fresnel reflection). The output from this Raman resonator was used as a weak probe beam.

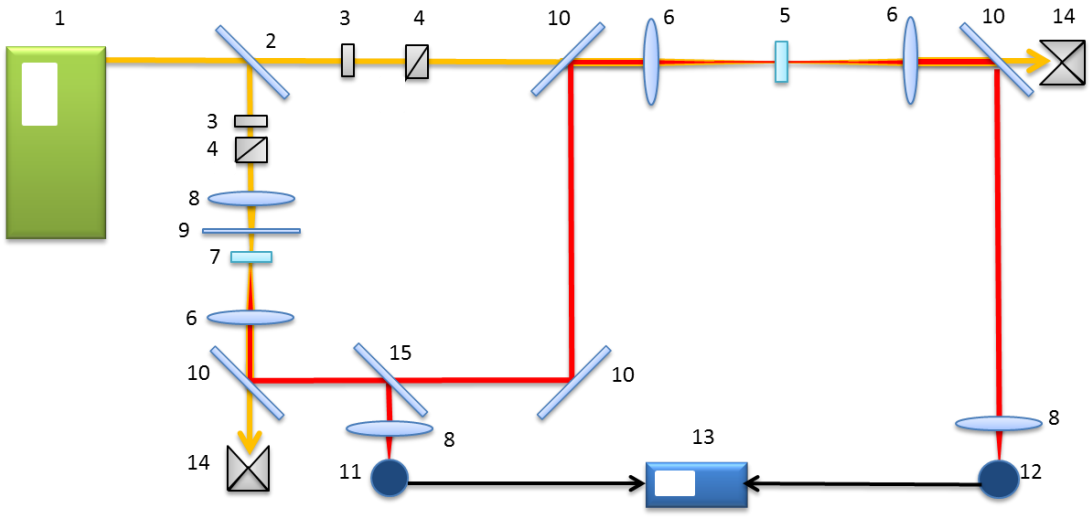

Figure 2.4. Experimental setup used to measure the Raman gain coefficient of diamond as a function of wavelength. (1) Continuum Panther OPO, (2) 50/50 beam splitter, (3) half wavelength plate, (4) Glan Taylor prism, (5) diamond sample under study, (6) focusing/collimating lens, (7) diamond sample used to produce probe beam, (8) focusing lens, (9) dichroic mirror, (10) dichroic mirror, (11) photodetector 1, (12) photodetector 2, (13) oscilloscope, (14) beam dump, (15) glass plate.

A dichroic mirror (10) was used to filter out the residual pump beam from the Raman probe beam. A glass plate (15) was used to pick off a known small fraction of the probe beam, which was then focused into a photodetector (11) to allow the probe pulse energy to be monitored. The remaining probe was then brought collinear with the pump beam using another dichroic mirror (10) with the same properties as before.

After the pump and probe have passed through the diamond, the beams were collimated using a lens of focal length 300mm (10) and separated using a dichroic mirror, with the pump energy being deposited in a beam dump (14) and the amplified probe beam being focused into a second photodetector (12). Silicon based photodetectors were used to take measurements up to

wavelengths of 1100nm, with a germanium based photodetector used for the longer wavelengths. The signals from the photodetectors were averaged over 100 laser pulses, resulting in a signal uncertainty of approximately 1%.

In these experiments, the gain is measured in the linear Raman amplifier regime (i.e negligible pump depletion) [8]. The pump and injected Raman intensities were carefully controlled to ensure this was the case. A wedge of approximately 0.9^0 between the front and back diamond surfaces, as well as slight further tilting (approximately 2 degrees) of the diamond relative to the incident beam prevent stimulated Raman oscillation affecting the measurements.

The amplification factor, i.e. the ratio of amplified Raman signal to that of the input probe beam (LHS of equation 2.10) is now required. The ratio of the signals produced at photodetectors 11 and 12 was taken when the sample under investigation was, firstly being pumped by the OPO (U_p), and secondly not being pumped (U_{np}). The signals produced at the photodetectors are, however, voltages rather than energies. The peak voltages produced by photodetectors 11 and 12 are proportional to energy and can be described in the following way:

$$U_{(11)np} = K_{11}E_s \tag{2.14a}$$

$$U_{(12)np} = K_{12}E_sF_s\exp(-\alpha_s L) \tag{2.14b}$$

$$U_{(11)p} = K_{11}E_s \tag{2.14c}$$

$$U_{(12)p} = K_{12}E_T \tag{2.14d}$$

where K_{11} and K_{12} are the constants of proportionality for photodetectors 11 and 12 respectively.

When the diamond sample under investigation is un-pumped, no Raman amplification occurs. The energy of the Raman beam exiting the diamond sample is therefore equal to the energy of the incident beam, minus the energy

lost via Fresnel reflections (Fs) and absorption. If one divides the ratio of the signals on the two photodiodes under pumped conditions by that under un-pumped conditions, equation 2.15 is obtained.

$$\frac{(U_{12})_p / (U_{11})_p}{(U_{12})_{np} / (U_{11})_{np}} = \frac{\left[K_{12}E_T / K_{11}E_s\right]}{\left[K_{12}E_sF_s\exp(-\alpha_s L) / K_{11}E_s\right]} \qquad 2.15$$

And hence

$$\frac{(U_{12})_p / (U_{11})_p}{(U_{12})_{np} / (U_{11})_{np}} = \frac{E_T}{E_sF_s\exp(-\alpha_s L)} \qquad 2.16$$

The beam waists (at $1/e^2$ of the maximum intensity) were measured using a silicon based CCD camera, where the beam was approximated to be Gaussian. For wavelengths above the band edge of silicon, knife edge measurements were taken using the standard clip levels of 10% and 90% of the pulse energy [25]. The pulse duration was measured using a photodiode and an oscilloscope. The Raman gain coefficient was then calculated using equation 2.10.

2.4.3 – Results

Gain measurements were taken at 355nm, 532nm, 670nm, 800nm, 1064nm and 1280nm. Measurements of the pulse duration, spatial profiles, optical spectra and optical linewidth at a pump wavelength of 670nm will be presented in this section. The results presented at this wavelength are typical of those at each of the wavelengths investigated, and show both the pump and generated probe beam measurements. The probe beam characteristics were measured before Raman amplification occurred in the diamond sample being studied.

The pulse durations of both the pump and the injected Raman probe beam are presented in Figure 2.5 and Figure 2.6 respectively. The Nd:YAG pumping the OPO was operating in unseeded mode.

The pulse duration (FWHM) of the pump beam was measured to be 5.5ns, while the probe beam was measured to be 3.3ns. When the pump was operating in seeded mode, these values changed to 4.9ns for the pump and 2.6ns for the probe beam.

Due to the beam's slightly elliptical shape, the area of the beam was measured and the resulting radii of spherical beams with equivalent area were used in the gain calculation. Typical spatial profiles of the pump and probe can be seen in Figure 2.7 and Figure 2.8, both with the relevant Gaussian fit. As previously, presented graphs are of those measured at a wavelength of 670nm with the pump being operated in the un-seeded mode. A pump radius ($1/e^2$) of 394μm was measured from the Gaussian fit, which was set to have a baseline at zero. As expected, the probe beam was considerably smaller in diameter, with a measured $1/e^2$ radius of 177μm.

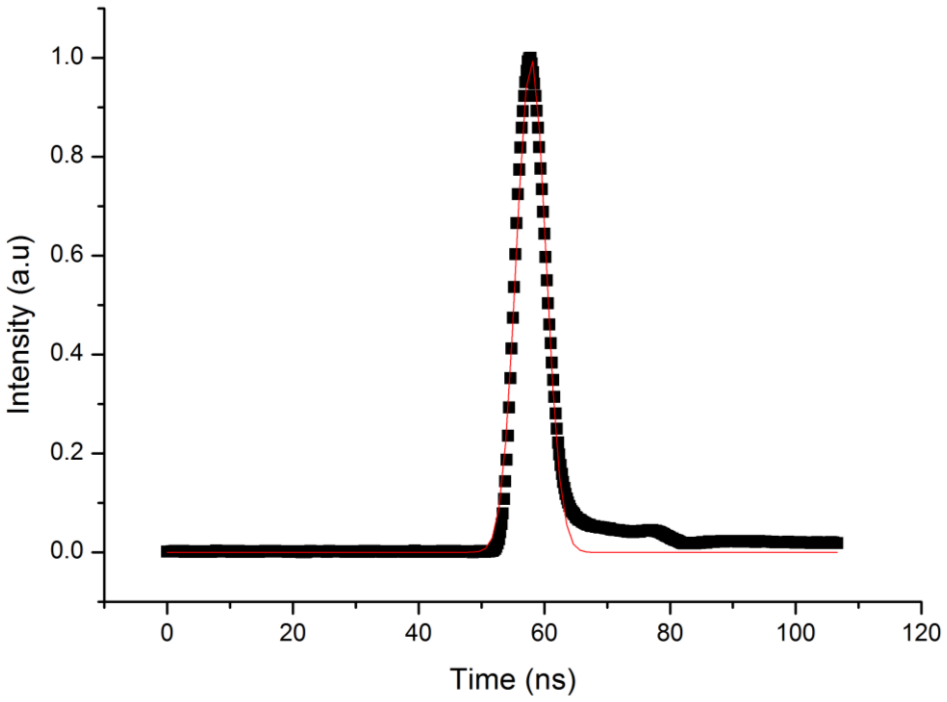

Figure 2.5. Pump pulse temporal profile at 670nm with Gaussian fit. The Nd:YAG pump for the OPO was operating in unseeded mode.

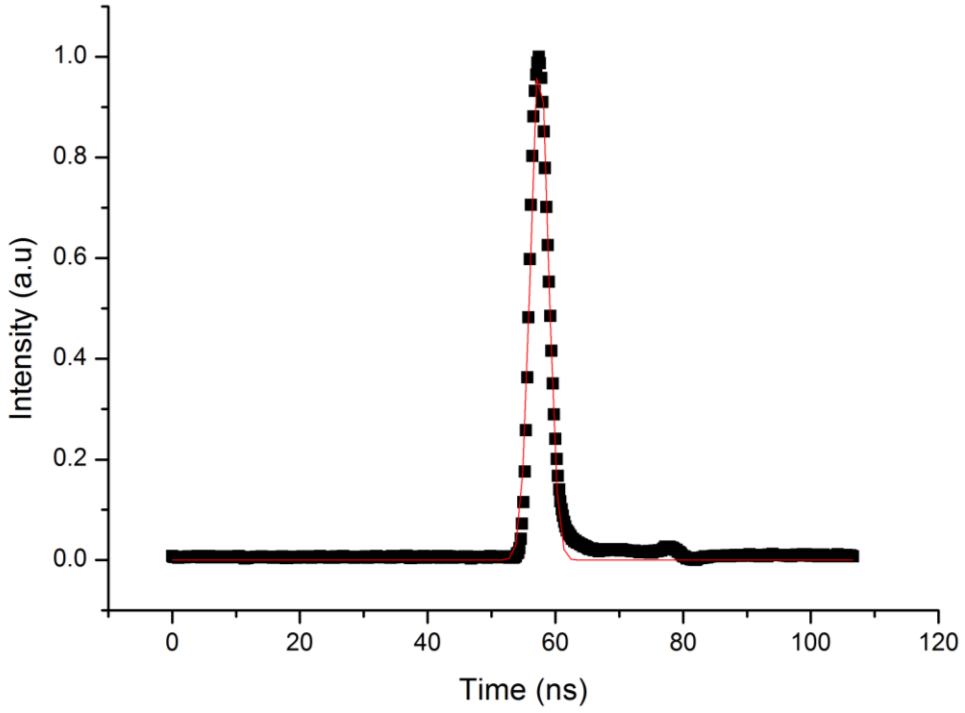

Figure 2.6. Probe pulse temporal profile at 735nm with Gaussian fit The Nd:YAG pump for the OPO was operating in unseeded mode.

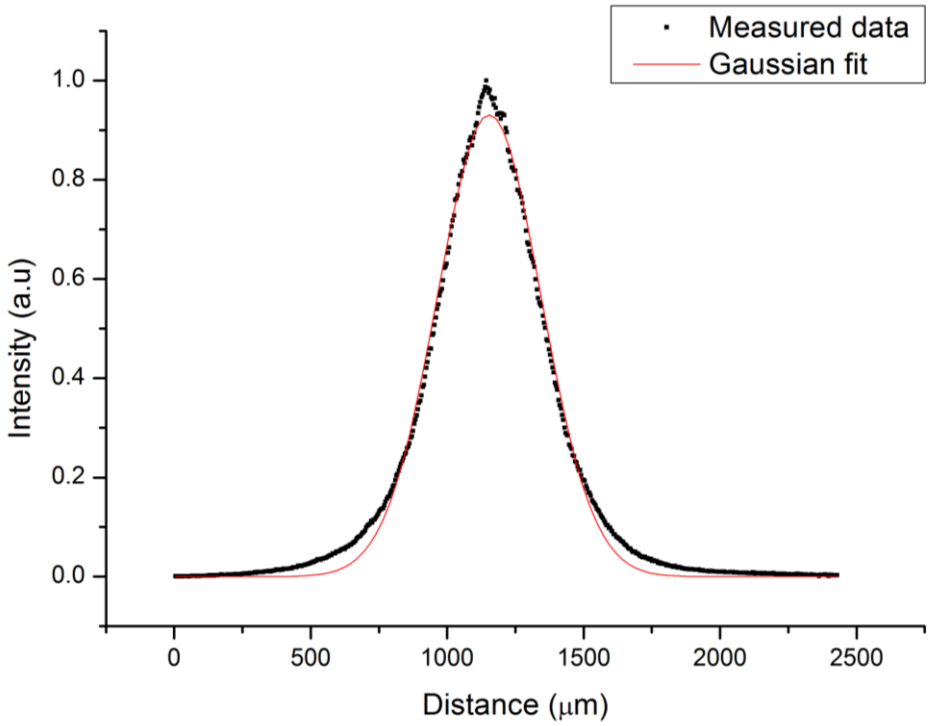

Figure 2.7. Spatial profile of pump beam at 670nm

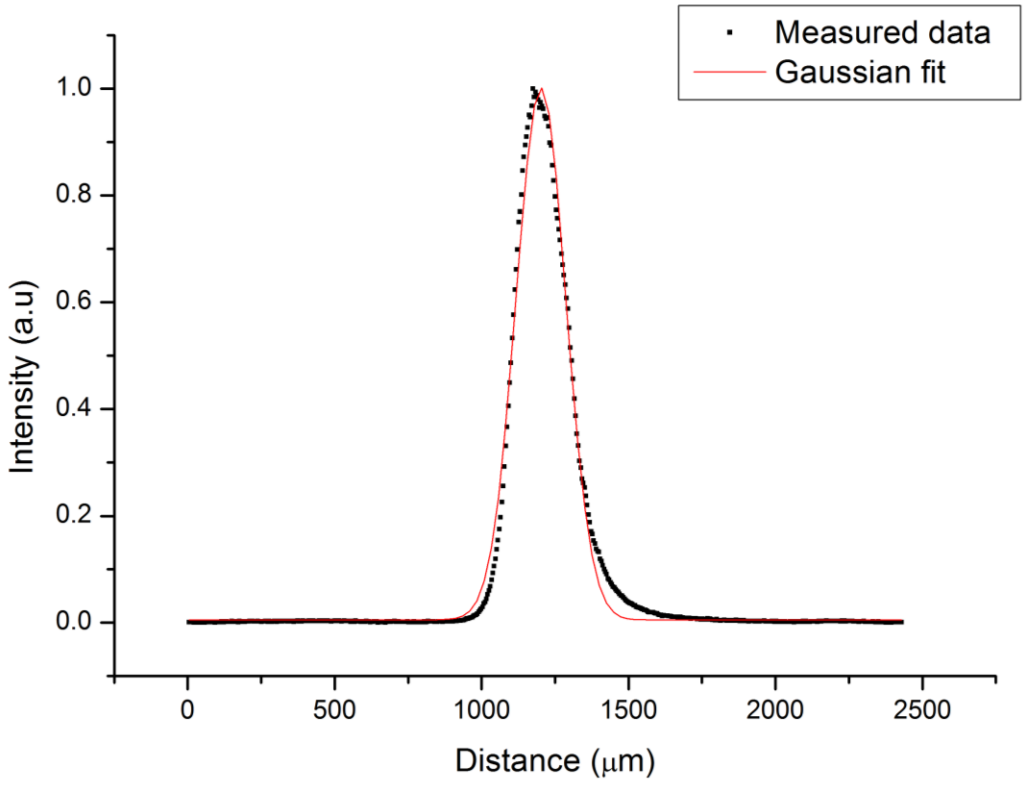

Figure 2.8. Spatial profile of probe beam at 735nm

As previously discussed, the effect the pump linewidth had on the observed Raman gain was investigated. The linewidth of the pump OPO was varied using a CW diode seed laser, injecting this into the OPO's Nd:YAG pump. This narrowed the OPO emission linewidth as well as slightly reducing the pulse duration. The linewidth of the pump at 670nm was measured using an optical spectrum analyser, Figure 2.9 and Figure 2.10 show the measured spectrum with the OPO operating in un-seeded and seeded mode respectively.

As can be seen in Figure 2.11, there is an increase in the fractional gain (represented by the gradient of the least squared linear fit plotted) as the linewidth of the pump laser is reduced. In the unseeded mode the linewidth of the pump was measured to be 5cm^{-1} shown in Figure 2.9. In seeded mode, the linewidth is seen to narrow to 2cm^{-1} shown in Figure 2.10. The size of the increase in gain is consistent with the $1 + \frac{\Delta\nu_L}{\Delta\nu_R}$ dependence, following the expected trend previously presented for Raman fibres [5].

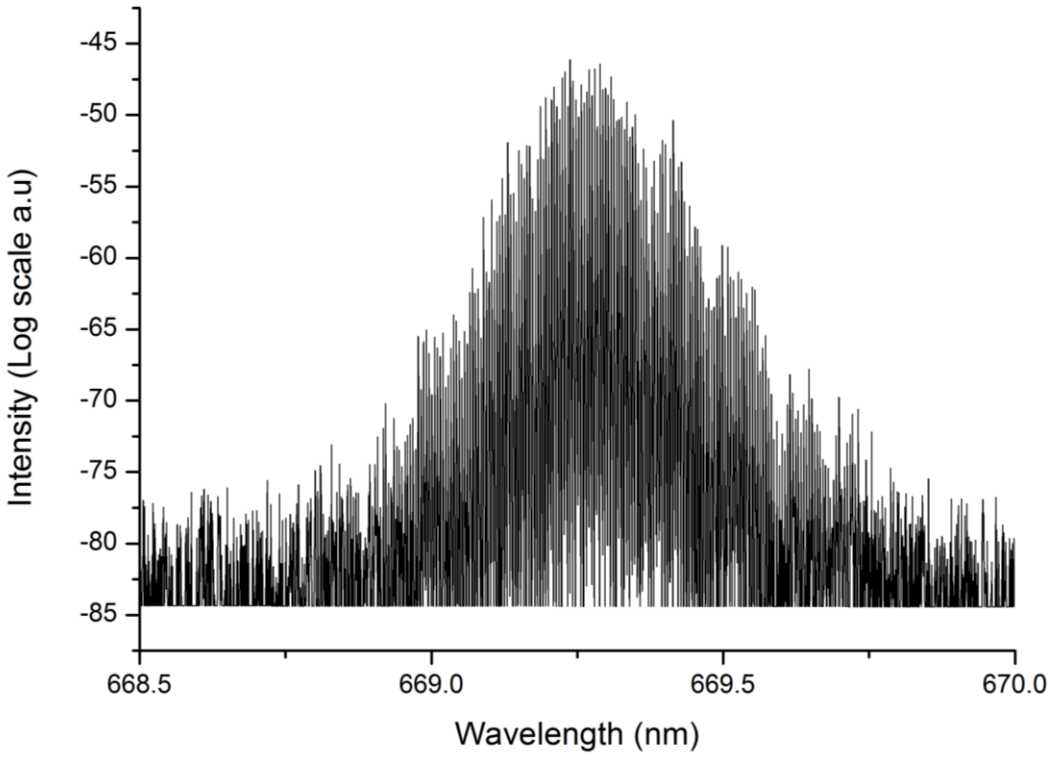

Figure 2.9. Pump spectrum at 670nm with OPO operating in un-seeded mode

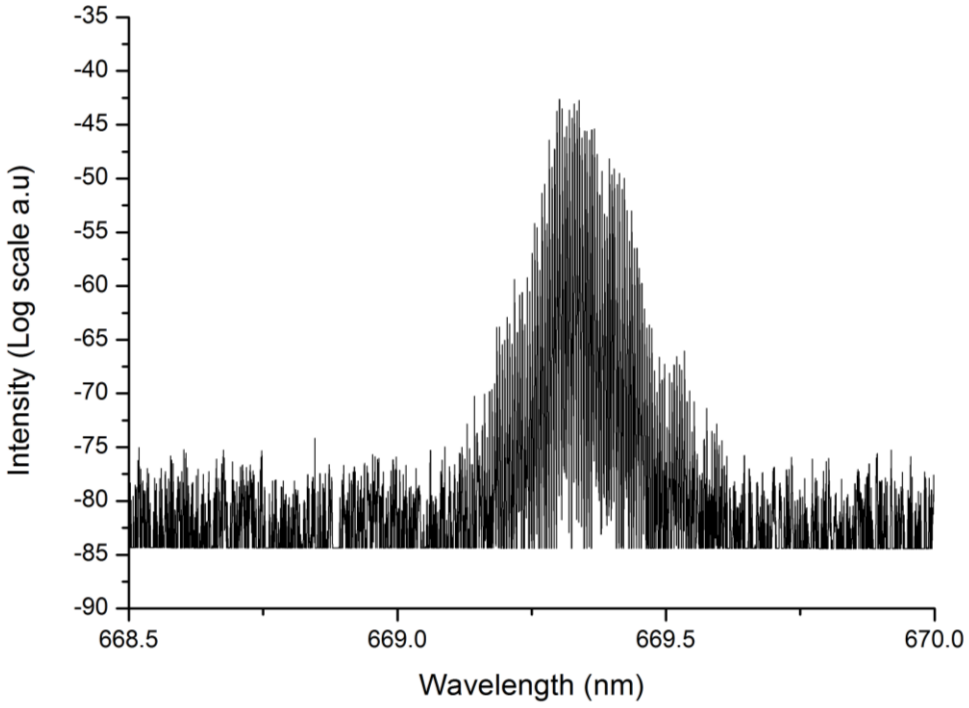

Figure 2.10. Pump spectrum at 670nm with OPO operating in seeded mode

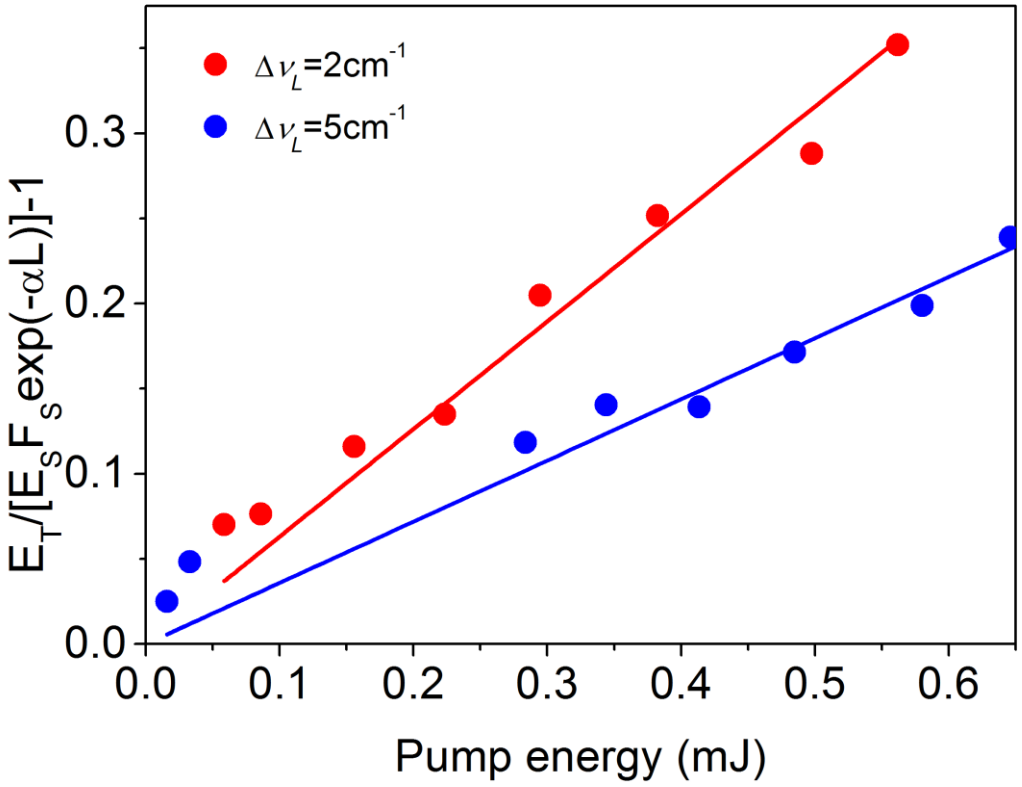

Figure 2.11. Fractional gain as a function of pump energy for pump linewidth of 2cm^{-1} (red) and 5cm^{-1} (blue). The pump wavelength was 670nm.

In order to make physical sense, i.e. zero gain under un-pumped conditions, both linear fits in Figure 2.11 have been constrained to intersect the origin.

Figure 2.12 shows the wavelength dependence of the fractional gain in diamond. The fractional gain is plotted against the pump energy divided by the spatial, temporal and linewidth terms found in equation 2.5. Plotting the data in this way means the gradient of the linear fit is directly proportional to the Raman gain coefficient.

Using the gradient of the slopes produced in Figure 2.12, while taking into account Fresnel reflections and the absorption losses seen in Figure 2.2, absolute values of the Raman gain in diamond can be calculated using equation 2.10, with the results shown in

Figure **2.13**. A linear relationship between the Raman gain and pump wavenumber is shown. The least squared linear fitted to the measured data points was chosen so as to comply with the theoretical prediction of a linear relationship between the Raman gain and the pump frequency[8]. The origin of the uncertainty in each gain value arises from the scatter of points in Figure 2.12.

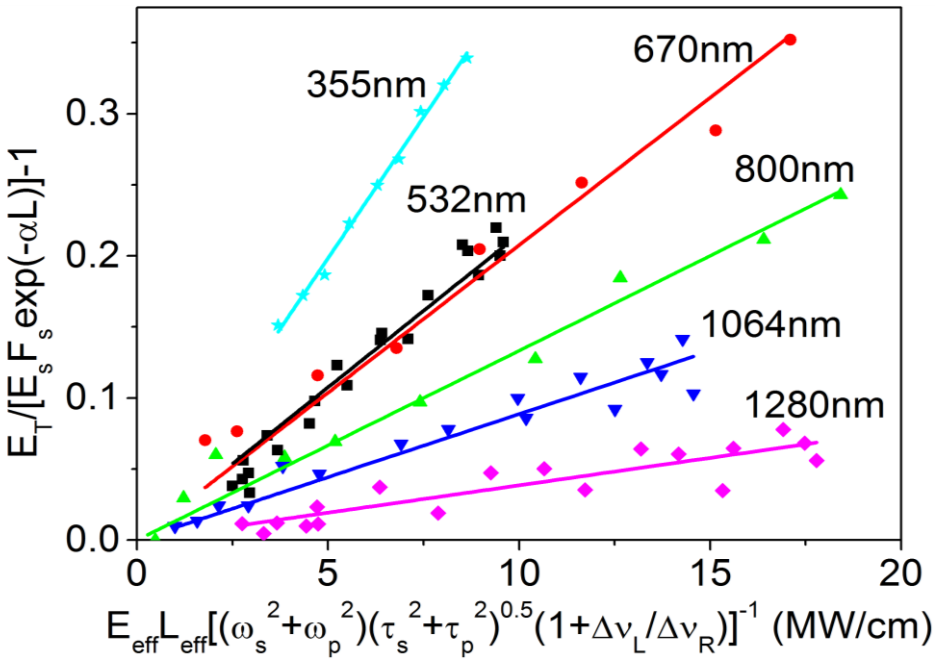

Figure 2.12. Fractional gain measured in diamond using pump-probe technique.

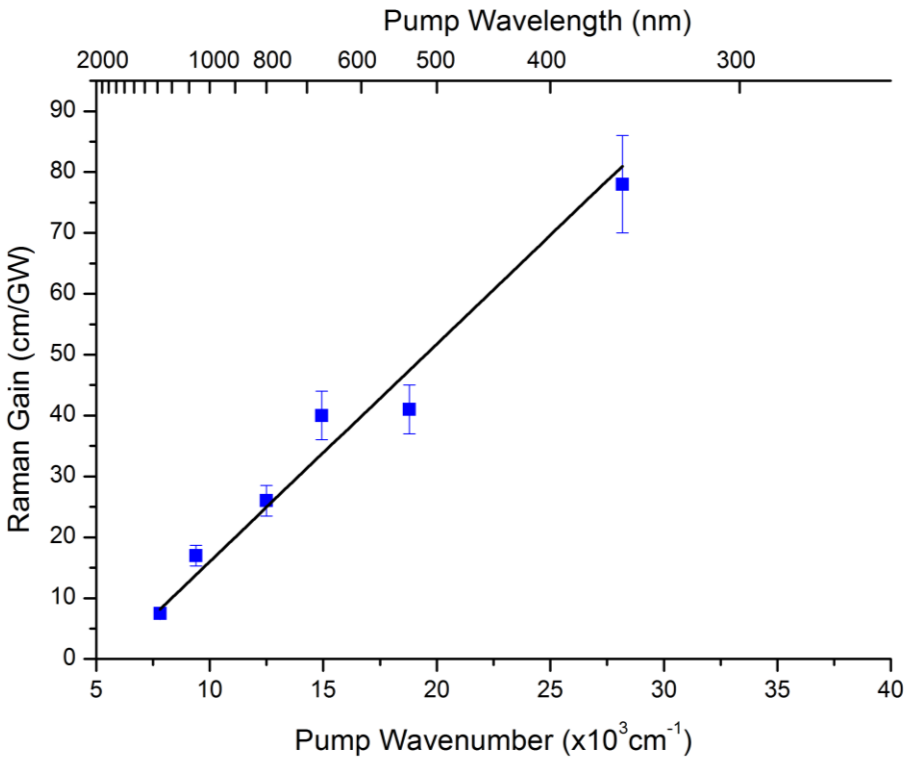

Figure 2.13. Absolute values of Raman gain in diamond as a function of pump wavenumber measured using a pump probe technique. (The pump wavelength is shown on the upper x-axis for reference.)

2.5 Stimulated Raman oscillation threshold

In order to verify the dependence of the Raman gain in diamond on pump wavelength, the stimulated Raman oscillation threshold at various wavelengths was measured. These measurements are a comparative study and do not produce absolute measurements of the Raman gain. Rather, they were conducted to complement the results obtained from the pump probe experiment and confirm the observed linear relationship between the Raman gain and pump wavenumber. As mentioned earlier, although the basic theory suggests a linear relationship between pump wavenumber and Raman gain [8], experimental measurements on other, albeit more complex, Raman crystals

have not shown this dependence [21], [22]. Hence, it was important to obtain corroborating evidence of the linear dependence observed for diamond in the pump probe measurements (shown in Figure 2.13).

2.5.1 Experimental method

The experimental setup used to measure the threshold for stimulated Raman oscillation is shown in Figure 2.14. The threshold of stimulated Raman oscillation was measured for pump wavelengths of 355nm, 450nm, 532nm, 670nm, 800nm, 1064nm, 1240nm and 1450nm. As was the case for the pump-probe measurements, the pump source used was a Continuum Panther OPO, with the same diamond sample under investigation.

The output beam of the OPO (1) was attenuated using a half wavelength plate (2) and Glan Taylor prism (3) before being focused into the diamond sample (4) with a lens of focal length 300mm (5). The uncoated front and back surfaces of the diamond create a low Q Raman laser cavity. The divergent Raman output beam generated in the diamond was then collimated using a lens of focal length 300mm (6) before the residual pump and generated Raman beams were separated using a dichroic mirror (7).

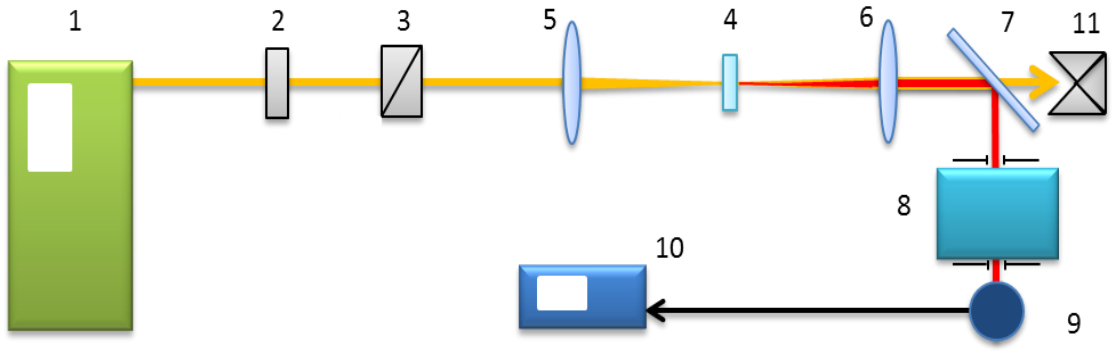

Figure 2.14. Experimental setup to measure threshold of stimulated Raman oscillation. (1) Continuum Panther OPO, (2) half wavelength plate, (3) Glan prism, (4) diamond sample, (5) and (6) lens with 300mm focal length, (7) dichroic mirror, (8) monochromator, (9) photodiode, (10) oscilloscope, (11) beam dump

The Raman beam was then further isolated using a monochromator (8) before terminating in a photodetector (9). The intensity of the stimulated Raman output was monitored with increasing pump powers using an oscilloscope (10). The spatial and temporal characteristics were measured using a silicon based CCD camera and a photodiode respectively. As 1450nm was out with the range of the CCD detector, a knife-edge measurement was taken to determine the beam waist at this wavelength. Clip levels of 10% and 90% of the pulse energy were used [25].

2.5.2 Results

The output of the Raman oscillator at the wavelengths measured as a function of pump intensity multiplied by the effective diamond length can be seen in Figure 2.15. The effective length term is used in the x-axis to compensate for absorption losses to the pump at various wavelengths. As seen in section 2.2, the absorption losses are wavelength dependent and have a larger effect on shorter wavelengths.

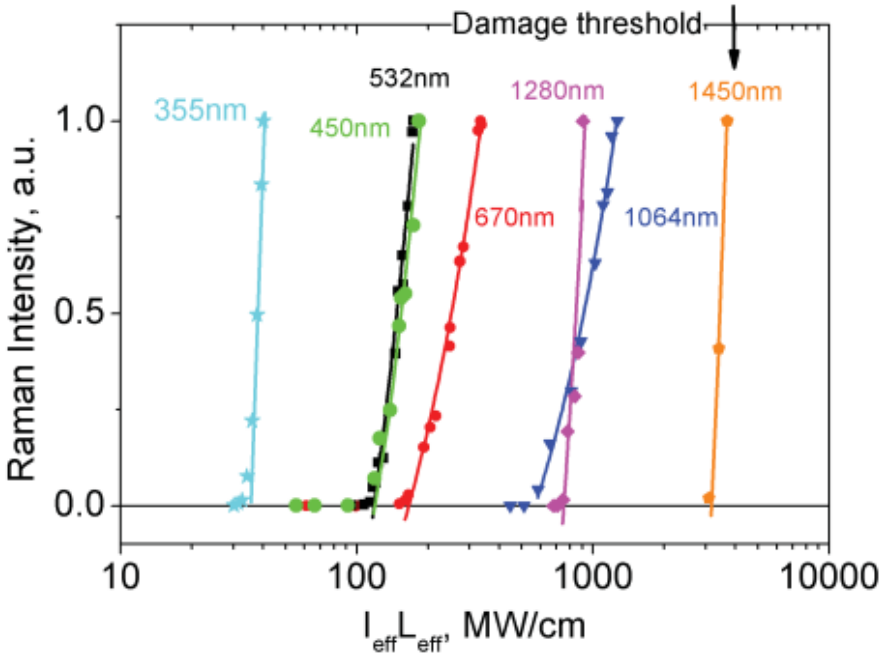

Figure 2.15. Dependence of stimulated Raman intensity on pump intensity at various pump wavelengths. The effective length term has been incorporated

into the x axis to compensate for absorption losses to the pump. Linear fits are added to the above threshold data points to determine the point of intersection on the x-axis.

The incident threshold pump intensity of stimulated Raman oscillation, $I_{th(inc)}$, for each pump wavelength was found from the intersection of the linear fit with the x-axis. Several points were taken at increasing incident pump intensities to obtain an accurate measurement; however, the intensities required to produce stimulated Raman oscillation at a pump wavelength of 1450nm was close to the damage threshold of diamond (with an in depth measurement of the damage threshold of diamond presented in chapter 5). For this reason, only 3 points were obtained at this wavelength.

As mentioned previously, a germanium photodiode was used for 1280nm and 1450nm, which lead to the steeper slope seen in the fore mentioned wavelengths. The unexpected intersection of the 1064nm and 1280nm curves can be attributed to this effect.

Figure 2.16 shows a linear relationship between the Raman gain in diamond and the pump wavenumber. This substantiates the $1/\lambda$ trend observed using the pump probe technique and theoretical expectation [8].

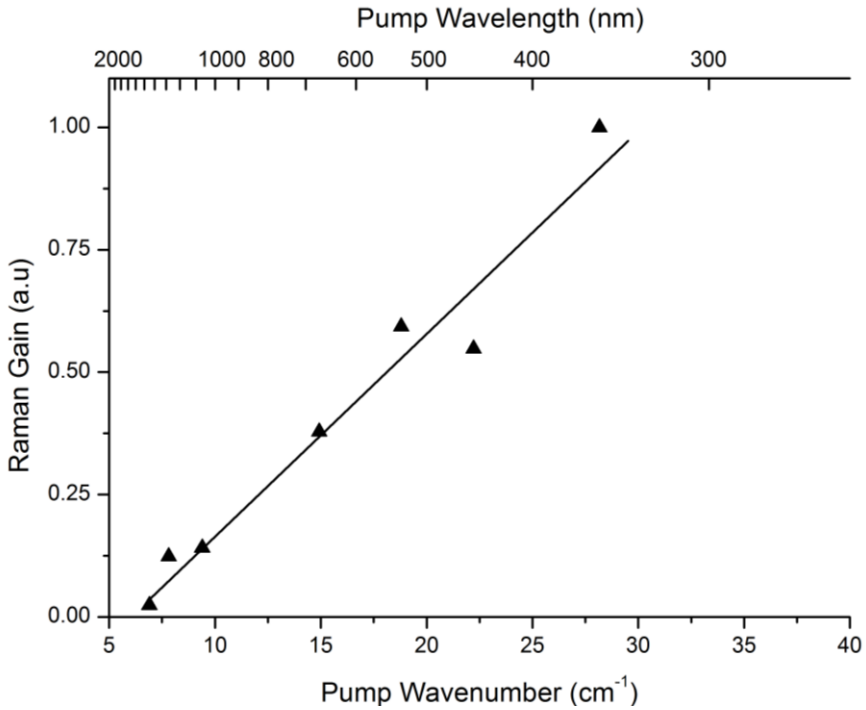

Figure 2.16. Dependence of Raman gain with pump wavelength measured using the threshold of stimulated Raman oscillation.

2.6 Overview

Figure 2.17 shows a comparison between Raman gain values obtained from literature (red circles), the pump probe measurements (blue squares), and the threshold measurements (black triangles). The results obtained are in good agreement with the theory presented by Penzkofer et al. [8]: a linear dependence between Raman gain and wavenumber. It should be noted however that the theory was based on "simple" Raman interactions in an H_2 atom. The single Raman peak in diamond at 1332cm^{-1} is due to the vibration between two face centre cubic sub-lattices [15]. When compared to the more complex nature of the Raman spectra of other common Raman materials such as Barium nitrate and barium tungstate, it is not overly surprising that, in diamond, the Raman gain's wavelength dependence is more closely related to that of simple Raman interactions in H_2 gas.

Figure 2.17 also highlights the large variation in values quoted in literature. This is, to an extent, expected due in part to different sample quality, but more

importantly, due to potential differences in crystal orientation, which in some cases (open red circles) is unknown. This, however, would only explain points lying under our expected trend, as the results presented in this paper are for the orientation at which the maximum Raman gain can be extracted, i.e. with the pump and probe polarised along the <111> direction and propagation is along a <110> direction [10], [13].

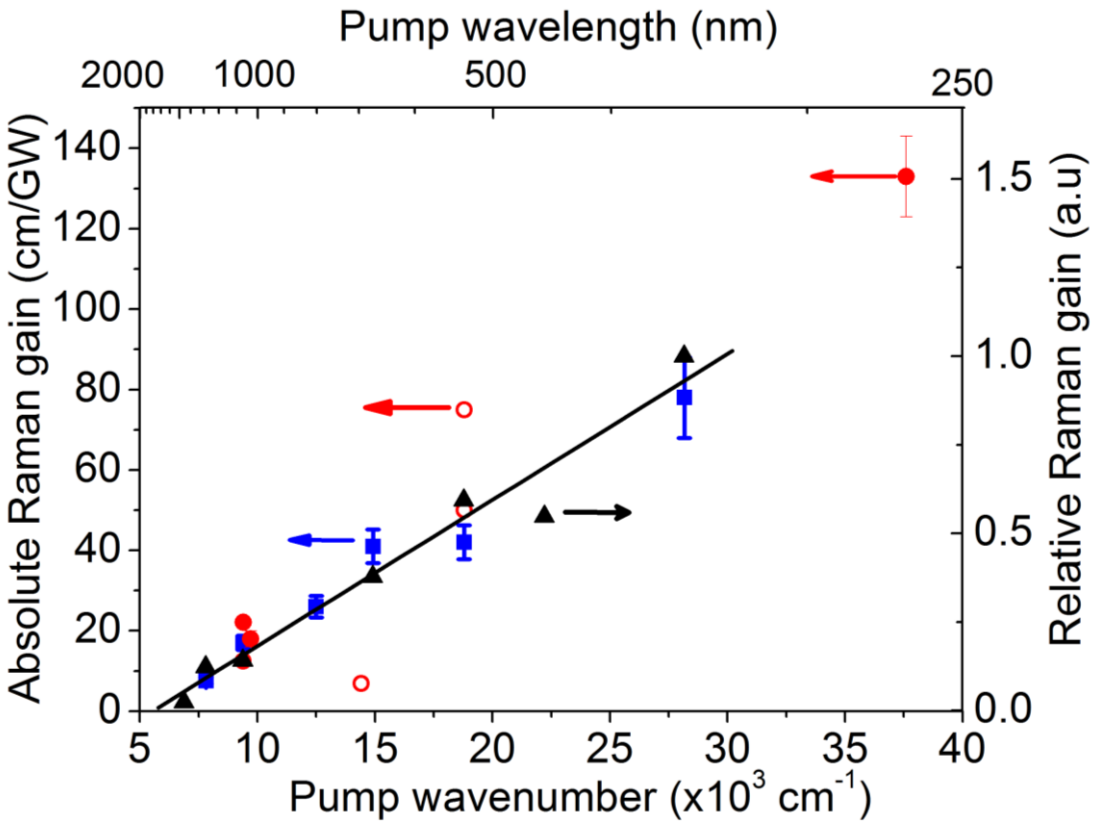

Figure 2.17. Dependence of Raman gain coefficient on wavenumber. Absolute values measured using the pump-probe technique (blue squares) are compared with results obtained from the threshold of stimulated Raman oscillation (black triangles) and results published in literature (open red circles for an unknown crystal orientation, solid red circles for results adjusted for propagation along <111>. Literature values from [4], [10], [12], [14], [15], [26].

The pump probe measurements and the values taken from literature are represented on the left hand axis. The right hand axis representing the relative measurements of Raman gain has been scaled such that the values align to the

least squared fit through the pump probe points. It should be emphasised that the relative measurements obtained from the threshold technique previously discussed do not provide an absolute measurement of the Raman gain and have no association with the left hand y-axis in Figure 2.17.

2.7. Conclusions

In this Chapter, a systematic study of the wavelength dependence of the steady state Raman gain in diamond showed a $1/\lambda$ dependence between pump wavelengths of 355nm and 1450nm. Both a pump probe technique, providing absolute measurements of the Raman gain, and a relative measurement comparing the threshold values for SRS are reported. The measurements were taken with the pump polarisation parallel to a <111> crystallographic direction and propagating along a <110> direction, where, under these conditions, maximum gain is extracted[10], [13]. The values obtained ranged from 7.6cmGW^{-1} at a pump wavelength of 1280nm to 78cmGW^{-1} at a pump wavelength of 355nm. The values obtained allow better design of Raman laser cavities, giving an indication of the correct output coupling and spot sizes required for optimal performance.

Bibliography

[1] R. Stegeman, C. Rivero, G. Stegeman, J. Peter Delfyett, K. Richardson, L. Jankovic, and H. Kim, "Raman gain measurements in bulk glass samples," *J. Opt. Soc. Am. B*, vol. 22, no. 9, pp. 1861–1867, 2005.

[2] G. . Agrawal, *Nonlinear Fiber Optics*, Third. New York: Academic Press, 2001.

[3] A. A. Kaminskii, V. G. Ralchenko, and V. I. Konov, "CVD-diamond – a novelχ^3-nonlinear active crystalline material for SRS generation in very wide spectral range," *Laser Phys. Lett.*, vol. 3, no. 4, pp. 171–177, 2006.

[4] A. A. Kaminskii, R. J. Hemley, J. Lai, C. S. Yan, H. K. Mao, V. G. Ralchenko, H. J. Eichler, and H. Rhee, "High-order stimulated Raman scattering in CVD single crystal diamond," *Laser Phys. Lett.*, vol. 4, no. 5, pp. 350–353, 2007.

[5] A. Grasiuk and I. Zubarev, "High-power tunable IR Raman lasers," *Appl. Phys. A Mater. Sci. Process.*, vol. 17, no. 3, pp. 211–232, 1978.

[6] R. Claps, D. Dimitropoulos, V. Raghunathan, Y. Han, and B. Jalali, "Observation of stimulated Raman amplification in silicon waveguides.," *Opt. Express*, vol. 11, no. 15, pp. 1731–9, 2003.

[7] T. T. Basiev, A. A. Sobol, P. G. Zverev, V. V Osiko, and R. C. Powell, "Comparative Spontaneous Raman Spectroscopy of Crystals for Raman Lasers," *Appl. Opt.*, vol. 38, no. 3, pp. 594–598, 1999.

[8] A. Penzkofer, A. Laubreau, and W. Kaiser, "High Intensity Raman Interactions," *Prog. Quantum Electron.*, pp. 56–140, 1979.

[9] V. G. Savitski, S. Reilly, and A. J. Kemp, "Steady-State Raman Gain in Diamond as a Function of Pump Wavelength," *IEEE J. Quantum Electron.*, vol. 49, no. 2, pp. 218–223, 2013.

[10] V. G. Savitski, I. Friel, J. E. Hastie, M. D. Dawson, D. Burns, and A. J. Kemp, "Characterization of Single-Crystal Synthetic Diamond for Multi-Watt Continuous-Wave Raman Lasers," *Quantum Electron. IEEE J.*, vol. 48, no. 3, pp. 328–337, 2012.

[11] I. Friel, S. L. Geoghegan, D. J. Twitchen, and G. A. Scarsbrook, "Development of high quality single crystal diamond for novel laser applications," *Proc. SPIE*, vol. 7838, pp. 783819–1, 2010.

[12] E. Granados, D. J. Spence, and R. P. Mildren, "Deep ultraviolet diamond Raman laser," *Opt. Express*, vol. 19, no. 11, pp. 10857–10863, 2011.

[13] A. Sabella, J. A. Piper, and R. P. Mildren, "1240nm diamond Raman laser operating near the quantum limit," *Opt. Lett.*, vol. 35, no. 23, pp. 3874–3876, 2010.

[14] D. J. Spence, E. Granados, and R. P. Mildren, "Mode-locked picosecond diamond Raman laser," *Opt. Lett.*, vol. 35, no. 4, pp. 556–558, 2010.

[15] R. P. Mildren, J. E. Butler, and J. R. Rabeau, "CVD-diamond external cavity Raman laser at 573nm," *Opt. Express*, vol. 16, no. 23, pp. 18950–18955, 2008.

[16] W. Lubeigt, G. M. Bonner, J. E. Hastie, M. D. Dawson, D. Burns, and A. J. Kemp, "An intra-cavity Raman laser using synthetic single-crystal diamond," *Opt. Express*, vol. 18, no. 16, pp. 16765–16770, 2010.

[17] W. Lubeigt, V. G. Savitski, G. M. Bonner, S. L. Geoghegan, I. Friel, J. E. Hastie, M. D. Dawson, D. Burns, and A. J. Kemp, "1.6 W continuous-wave Raman laser using low-loss synthetic diamond," *Opt. Express*, vol. 19, no. 7, pp. 6938–6944, 2011.

[18] D. C. Parrotta, A. J. Kemp, M. D. Dawson, and J. E. Hastie, "Tunable continuous-wave diamond Raman laser," *Opt. Express*, vol. 19, no. 24, pp. 24165–24170, 2011.

[19] J.-P. M. Feve, K. E. Shortoff, M. J. Bohn, and J. K. Brasseur, "High average power diamond Raman laser," *Opt. Express*, vol. 19, no. 2, pp. 913–922, 2011.

[20] R. P. Mildren and A. Sabella, "Highly efficient diamond Raman laser," *Opt. Lett.*, vol. 34, no. 18, pp. 2811–2813, 2009.

[21] V. A. Lisinetskii, S. V Rozhok, D. N. Bus'ko, R. V Chulkov, A. S. Grabtchikov, V. A. Orlovich, T. T. Basiev, and P. G. Zverev, "Measurements of Raman gain coefficient for barium tungstate crystal," *Laser Phys. Lett.*, vol. 2, no. 8, pp. 396–400, 2005.

[22] V. A. Lisinetskii, I. I. Mishkil, R. V Chulkov, A. S. Grabtchikov, P. A. Apanasevic, H. J. Eichler, and V. A. Orlovich, "Raman gain coefficient of Barium Nitrate measured for the spectral region of the Ti:Sapphire laser," *J. Nonlinear Opt. Phys. Mater.*, vol. 14, no. 01, pp. 107–114, 2005.

[23] R. S. Balmer, J. R. Brandon, S. L. Clewes, H. K. Dhillon, J. M. Dodson, I. Friel, P. N. Inglis, T. D. Madgwick, M. L. Markham, T. P. Mollart, N. Perkins, G. a Scarsbrook, D. J. Twitchen, a J. Whitehead, J. J. Wilman, and S. M. Woollard, "Chemical vapour deposition synthetic diamond: materials, technology and applications.," *J. Phys. Condens. Matter*, vol. 21, no. 36, p. 364221, 2009.

[24] R. Loudon, “The Raman effects in crystals,” *Adv. Phys.*, vol. 13, no. 52, p. 423, 1964.

[25] A. E. Siegman, M. W. Sasnett, and T. F. Johnston, “Choice of Clip Levels for Beam Width Measurements Using Knife Edge Techniques,” *IEEE J. Quantum Electron.*, vol. 27, no. 4, 1991.

[26] A. K. McQuillan, W. R. L. Clements, and B. P. Stoicheff, “Stimulated Raman Emission in Diamond: Spectrum, Gain, and Angular Distribution of Intensity,” *Phys. Rev. A*, vol. 1, no. 3, pp. 628–635, 1970.

Chapter 3 – CW diamond Raman lasers

In this chapter, CW diamond Raman lasers (DRLs) will be presented. Exploiting the high Raman gain in diamond discussed in Chapter 2, and utilising the favourable thermo-mechanical properties of the material, intra cavity DRLs with multi-watt output are demonstrated. To the best of the author's knowledge, to date, the highest powers from an intra-cavity DRL are demonstrated.

Both an Nd:YAG laser with poor beam quality and polarization which was not strongly constrained, and a polarised thin disk Yb:LuAG with good beam quality are used in order to investigate the power scaling of intra-cavity DRLs. A significant brightness enhancement was achieved in the Nd:YAG pumped system. The work presented also highlights the obstacles inhibiting further power scaling of intra-cavity CW DRLs, including spectral characteristics and optical damage to anti-reflection coatings.

3.1 Current state of the art

The first demonstration of a CW DRL came in 2010 [1], with Lubeigt et al. achieving 200mW of Raman output at 1240nm. This was accomplished using an intra-cavity system, with an Nd:YVO_4 gain material and 3.3mm diamond sharing a 2 mirror, 27mm long cavity. Further power scaling of this system was impeded by thermal issues in the Nd:YVO_4; however quasi CW operation was investigated, with 1.75W on time Raman power achieved, highlighting the potential for multi-Watt Raman output in a DRL.

Shortly after this initial demonstration, and with an improved cavity design as well as a longer 4.1mm diamond with lower loss than that previously used ($0.006cm^{-1}$ compared with $0.03cm^{-1}$ at 1064nm), 1.6W was generated at 1240nm [2].

Expanding on this work, Parrotta et al. [3] designed a tunable CW DRL. As the Raman shift in diamond (and indeed any crystalline Raman active material) is fixed, a tunable VECSEL was employed as the pump source for the intra cavity

Raman laser. A maximum Raman output power of 1.3W was reached at a wavelength of 1227nm, with an overall tuning range from 1217nm to 1244nm demonstrated. Further work on tunable DRLs was undertaken in [4], increasing the Raman output power to over 4W whilst also broadening the spectral output from 1209nm to 1256nm. Using a frequency doubling crystal, emission in the orange spectral region was also demonstrated; with a maximum power of 1.5W achieved at 614nm.

To the best of the authors' knowledge, the highest power CW intra-cavity DRL, to date, was demonstrated by Savitski et al [5]. 5.1W of output at 1217nm was attained converting the emission of a side pumped Nd:YLF rod. An impressive 43-fold brightness enhancement was observed from fundamental to Raman output, with a near diffraction limited beam produced at the 1st Stokes shift.

To date, the highest power CW diamond Raman laser, and indeed that produced by any crystalline Raman material, was achieved by Kitzler et al [6]. 10.1W was achieved in an external cavity when pumped with 30W of 1064nm output from a Nd:YVO_4 laser.

Although this output power is, as of yet, unsurpassed; an investigation into the power scaling of CW DRLs provided promising results. Williams et al [7] achieved 108W on time power from a quasi-CW DRL, with an on time duration of 200μs. This duration was shown to be enough for the DRL to operate in the steady state regime. No damage was observed to the diamond facets under a maximum pump power of 320W, with true CW performance inhibited by thermal effects in the Nd:YVO_4 pump system. Although the authors highlight that the peak temperature on axis increases beyond the time-scales investigated, effects on the Raman gain and line shape are small for temperature changes below a few hundred Kelvin [8].

Literature highlights that, to date, the most favourable approach to achieving high power DRLs is employing an external cavity system. Reported systems have, however, implemented near diffraction limited pump sources, and, if a beam of

poor quality is to be converted, an intra-cavity approach has shown to be a more appropriate route.

3.2 Nd:YAG pumped intra-cavity diamond Raman laser

The 6.5mm long single crystal diamond sample used in this Chapter was grown homoepitaxially by Element Six Ltd using microwave plasma assisted chemical vapour deposition. Growth was along a <100> direction. The diamond was grown specifically for low nitrogen content and hence low absorption loss. The end faces of the sample were antireflection (AR) coated for 1064m and 1240nm by Laseroptik GmbH.

Mirrors used in this section were purchased from Layertec GmbH. HR mirrors were specified to have >99.9% reflectivity at 1064nm and 1240nm, while the dichroic mirror used was AR coated at 1064nm (<0.15% reflectivity) and HR (>99.98% reflectivity) at 1240nm.

The Nd:YAG, 1064nm laser was characterised, using the cavity shown in Figure 3.1, with a 20% output coupling at M1, and no diamond or dichroic in the cavity. The Nd:YAG module used was a side pumped Northrop Grumman laser head capable of a maximum 50W output. The laser rod was 2mm in diameter and 60mm long. A fundamental spot radius of 250μm was estimated inside the Nd:YAG crystal, calculated using laser resonator design software. A maximum output power of 41W was achieved at a diode pump power of 152W, with a slope efficiency of 39% as seen in Figure 3.2. The beam quality was measured to be 20 x 18 using a DataRay Beamscope beam profiler. The Nd:YAG laser was unpolarised. Spectral characteristics of the output were measured using an Agilent 81642 spectrometer. The spectrum can be seen in Figure 3.3, measured with a resolution bandwidth of 0.0002nm.

It should be highlighted that the diode power was calculated assuming no aging of the diodes had occurred; in reality, however, some deterioration would be expected, therefore it is possible the efficiencies quoted are slightly lower than the true values.

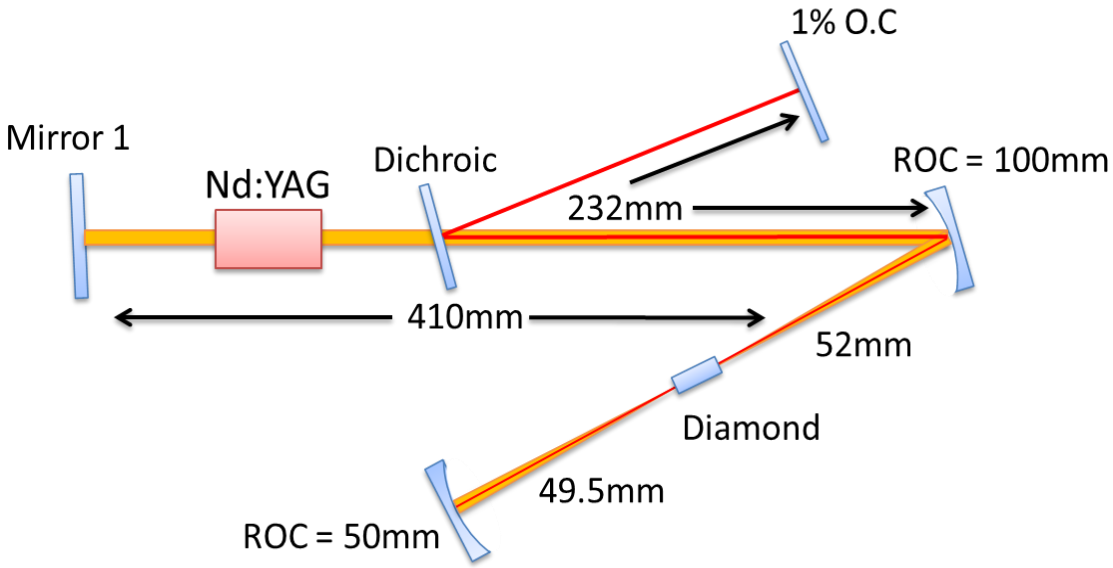

Figure 3.1. Cavity design of Nd:YAG pumped diamond Raman laser.

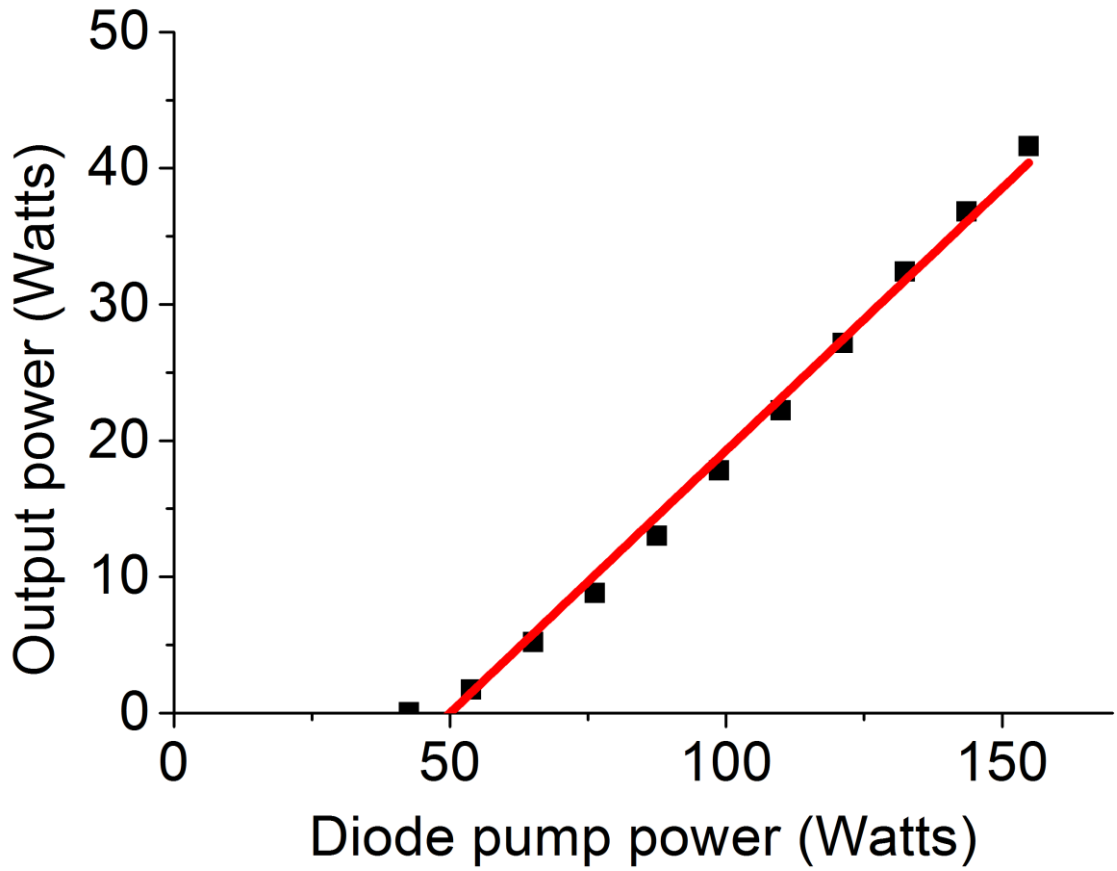

Figure 3.2. Performance of Nd:YAG laser with 20% output coupler and no diamond in the cavity. A slope efficiency of 39% was measured.

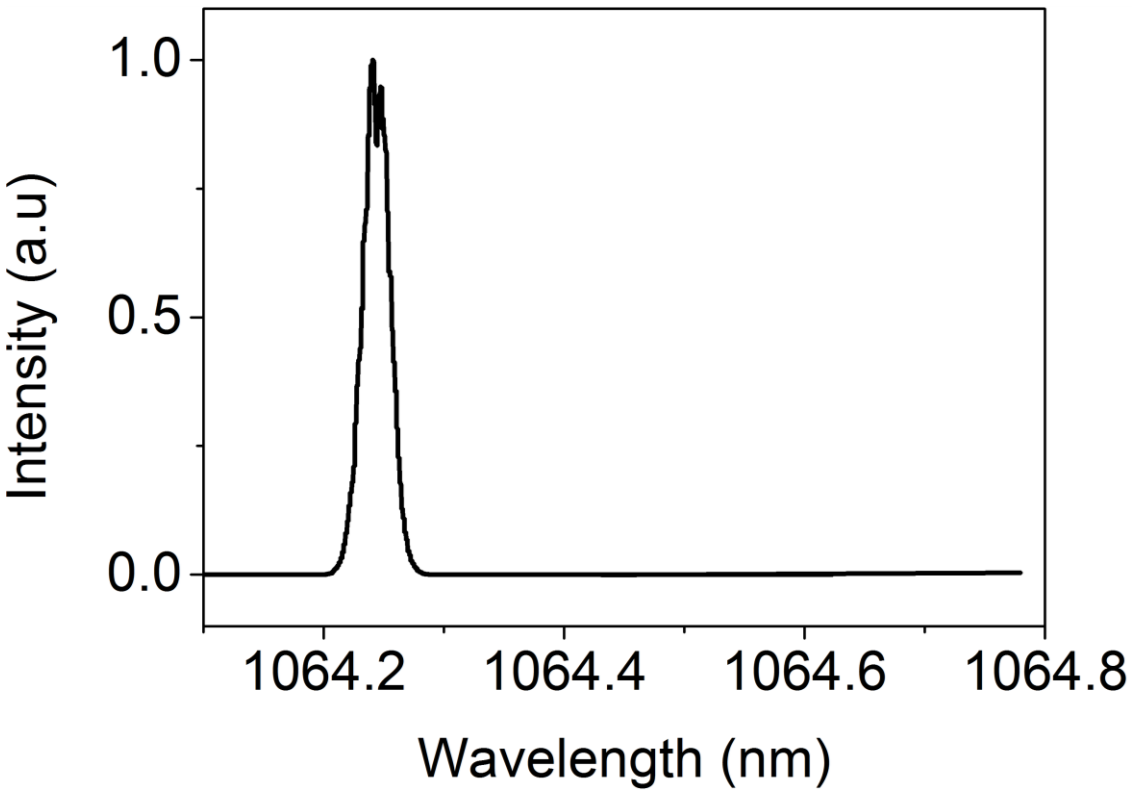

Figure 3.3. Spectral characteristics of the fundamental laser with no diamond in the cavity and a 20% output coupler at Mirror 1.

The 6.5mm diamond and dichroic mirror was then inserted into the cavity as shown in Figure 3.1. A fundamental and Raman spot radius of 37μm was chosen, and provided a maximum Raman output power of 6.1W at the first Stokes wavelength of 1240nm. A diode to Raman slope efficiency of 6.7% was measured, shown in Figure 3.4, resulting in a maximum conversion efficiency of 4%.

This value should not be confused with conversion efficiencies quoted for external cavity systems, which are typically cited as the conversion from the fundamental to Raman output. Any comparison between this value and the conversion from diode to intra-cavity Raman output can be deceptive since it fails to account for the diode-laser to fundamental conversion step in the case of the external cavity system. An approximate comparison of intra-cavity and external cavity conversion efficiencies can, however, be made by measuring the output power of the fundamental laser with optimal output coupling and no Raman oscillation present. A conversion efficiency can then be estimated, comparing the

maximum available output power of the fundamental laser and the Raman output power at the same diode pump power.

With this measure, the DRL presented in this section would have a conversion efficiency of 15%, comparing the 41W maximum output obtained at equal diode pump. Given the poor beam quality of the unpolarised fundamental field, this comparatively low conversion (cf. 30% [6]) is not altogether surprising. Furthermore, the diamond used in [6] was 9.5mm in length, significantly longer than the 6.5mm sample used in this Chapter and had a lower loss (approximately 0.001cm^{-1} at 1064nm).

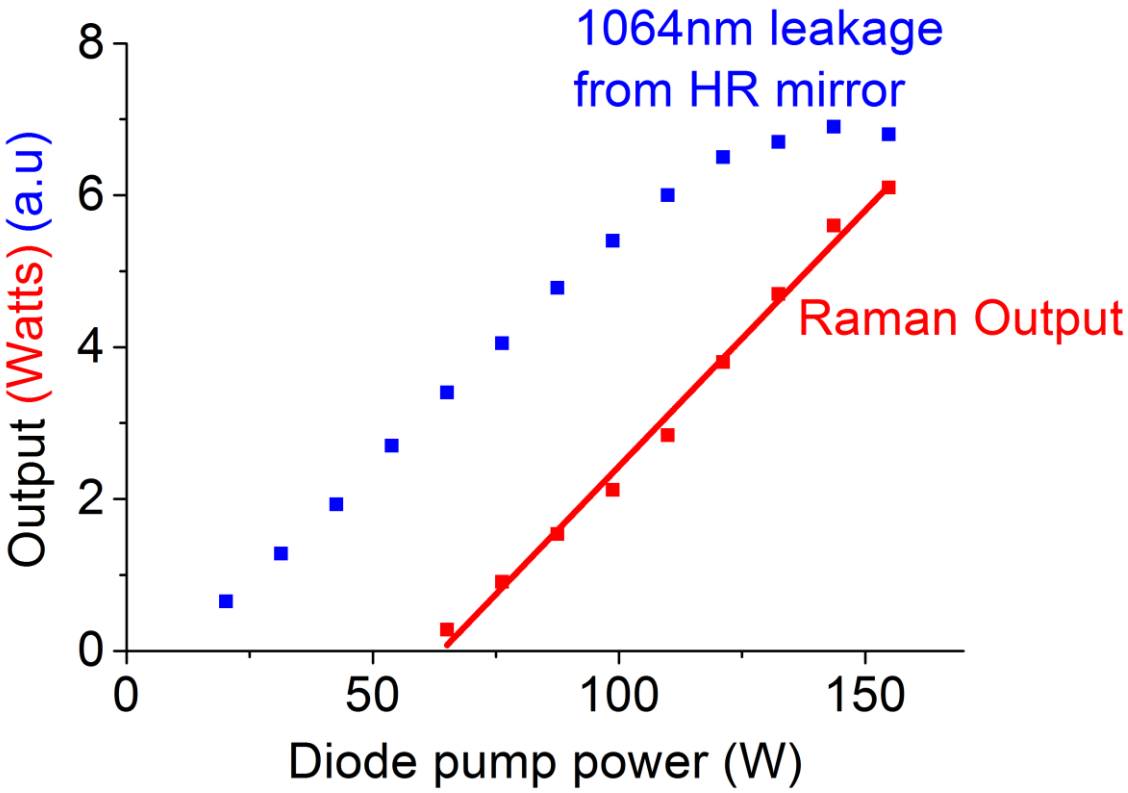

Figure 3.4. Power transfer of Raman laser (red) with comparison of fundamental leakage from HR mirror.

It can be seen from Figure 3.4 that the fundamental field doesn't clamp as the Raman laser threshold is reached. This may be caused by the multi-transverse mode nature of the fundamental field, similar to [5]. Raman lasers pumped with near diffraction limited fundamental beams clamping at threshold has been

observed [3], [4]. To the best of the authors' knowledge, this is the first diamond Raman laser pumped with an unpolarised laser.

Although the fundamental field was unpolarised, the Raman output was polarised along a <110> direction. This is somewhat counterintuitive; due to the nature of the Raman gain in diamond, with the light propagating along a <110> direction, the maximum Raman gain is seen when light is polarised along a <111> direction [5], [9], [10].

The reasoning behind such results can be attributed to birefringence in the diamond sample investigated. It should be highlighted that previously reported DRLs [10] have shown lower threshold when pumping along a <111> crystallographic direction; however, this was implementing a q-switched pump and hence a lower Q Raman cavity, where any retardance caused by birefringence may have reduced effect. This can be emphasised when investigating the average number of round trips taken by a photon in the resonator, N, which greatly decreases with an increasing output coupling, as shown in equations 3.1 and 3.2 [11];

$$N = \frac{\tau_c}{t_r} \tag{3.1}$$

Where

$$\tau_c = \frac{t_r}{T + 2\alpha L + \delta} \tag{3.2}$$

with τ_c representing the average photon lifetime in the cavity, t_r being the round trip time in the cavity, T the transmission of the output coupler, L the diamond length, α the absorption loss in the diamond and δ the term used to encompass other loss in the cavity, such as scatter, absorption, diffraction and birefringence.

As the diamond is birefringent, (and the only birefringent element in the CW Raman cavity discussed in this section), the polarisation eigenmodes of the cavity will be orientated along the fast and slow axis of birefringence in the diamond.

This is due to the requirement for the polarisation of the oscillating Raman field to repeat on every round trip, as is the case with any laser resonator. A single polarisation eigenmode, rather than two perpendicular polarisations, is then selected due to higher Raman gain in one crystallographic direction over the other, which is dependent on both the crystallographic direction and the orientation of the pump. This effect explains the observation of a single polarisation in the laser presented in this section.

The fundamental and Raman spectra are shown in Figure 3.5, Figure 3.6, Figure 3.7 and Figure 3.8. A comparison between the spectral profile of the fundamental output with a 20% output coupling (shown in Figure 3.3) and HR-HR cavity (Figure 3.5) highlights some differences in performance. Firstly, a shift in the emission wavelength is observed, with an output of 1064.2nm in the output coupled cavity compared with a wavelength of 1064.4nm in the HR-HR system. This is not greatly surprising: with a relatively broad gain profile [11], the change of loss in the cavity caused by different mirror coatings has resulted in this observed shift in the output wavelength. The increased structure seen in Figure 3.6 can be attributed to the laser operating extremely far above threshold. Although under initial examination, the spectral characteristics of the fundamental are typical of a cavity with an etalon present, closer inspection of the wavelength seperation between spectral structures doesn't appear to have a consistent value. Furthermore, both the diamond and dichroic (two likely contributors to an etalon effect in the cavity) are AR coated at the fundamental wavelength.

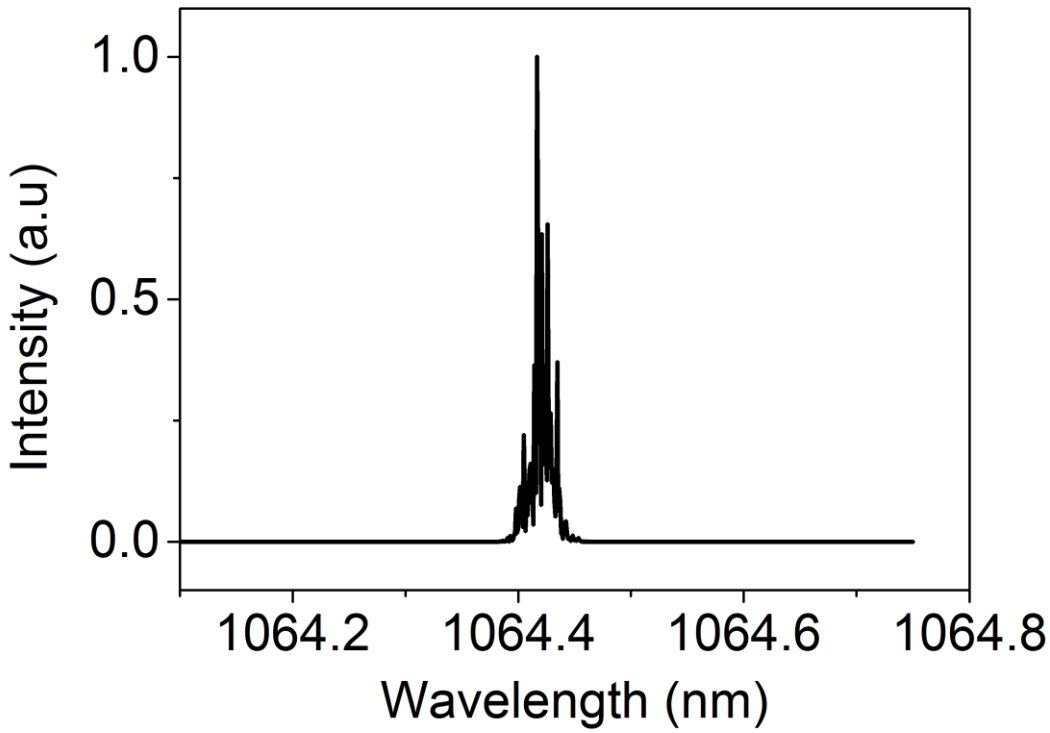

Figure 3.7. Spectrum of Nd:YAG with diamond in an HR-HR cavity below Raman threshold.

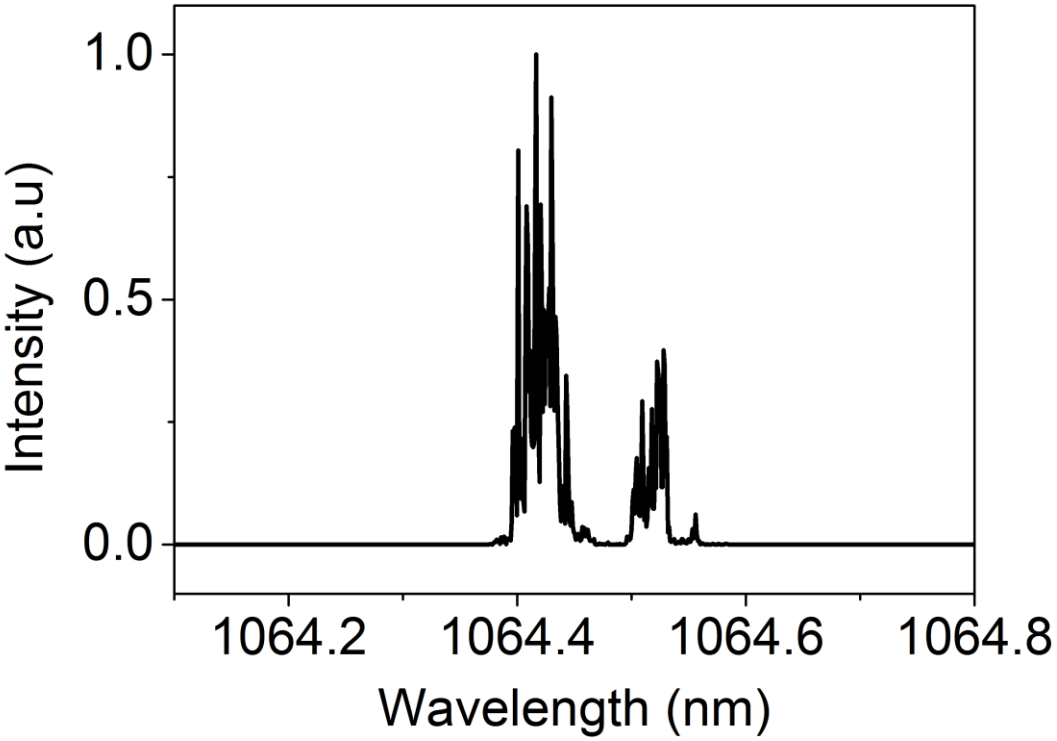

Figure 3.8. Spectrum of Nd:YAG with diamond in an HR-HR cavity at moderate pump powers with a diamond Raman laser output power of 1.5W.

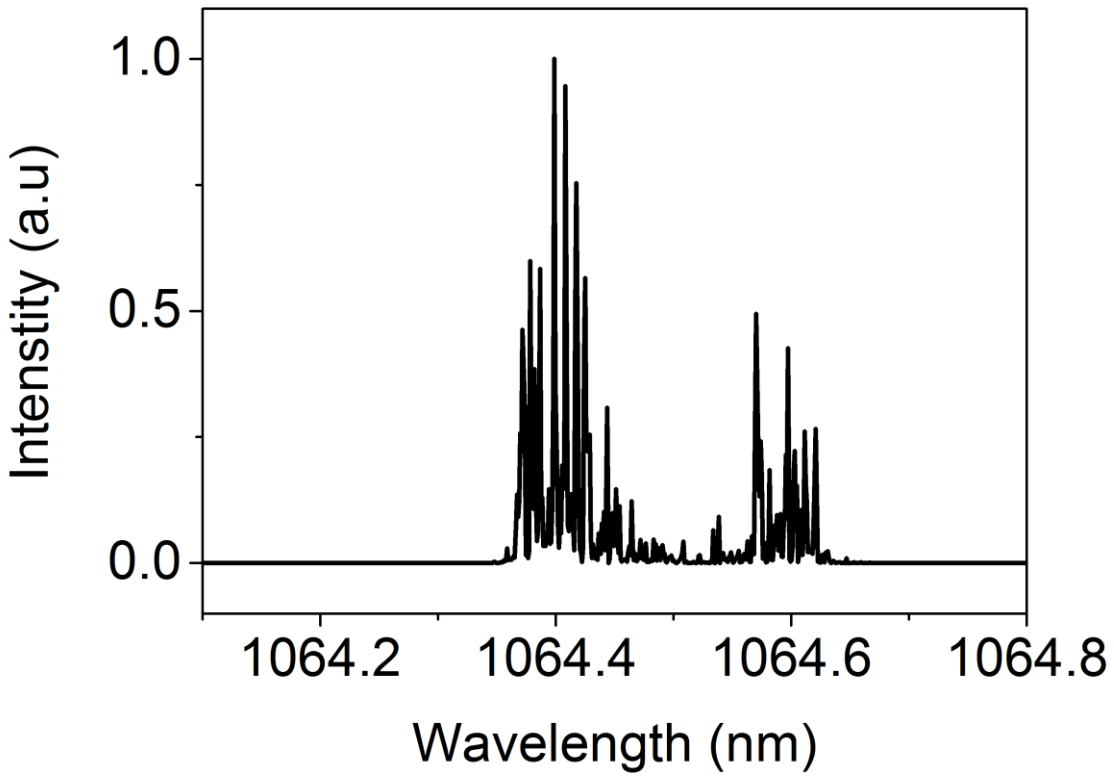

Figure 3.9. Fundamental spectrum at 4.5W of Raman output power.

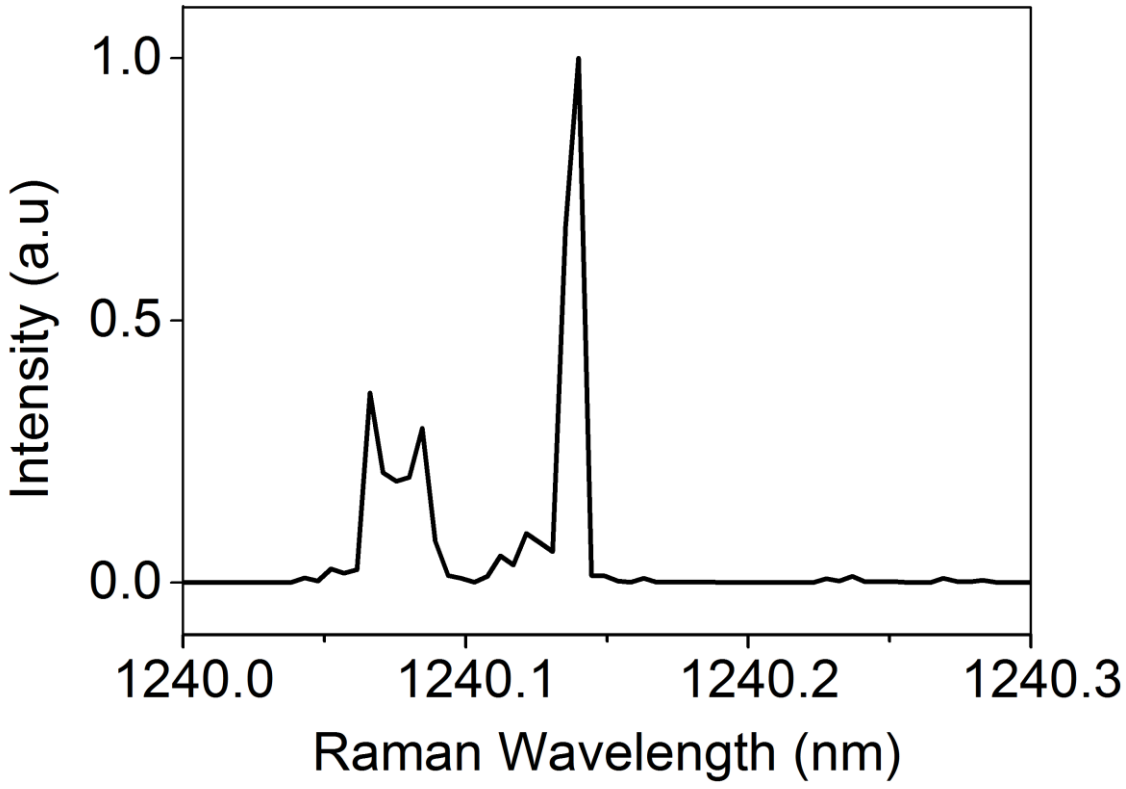

Figure 3.10. Raman spectrum at 4.5W of Raman output power.

A substantial brightness enhancement was attained when comparing the performance of the Nd:YAG laser with an optimal 20% output coupling and the DRL. With the Raman output beam having an M^2 of 2.3 x 1.6, an 11-fold brightness enhancement was achieved, while additionally converting an unpolarised pump into polarised Raman emission.

Attempts were made to improve the Raman output power by using a Brewster plate, inserted between the YAG and dichroic mirror, to force polarised oscillation in the fundamental laser. A quarter waveplate was inserted between "mirror 1" and the Nd:YAG crystal to reduce depolarisation losses, a method reported in [12]. Although the reflected power from the Brewster surface reduced from 8W with no waveplate to 5W with the waveplate, the Raman output power was limited to a maximum of 3.3W. This is not altogether surprising; although the pump was previously unpolarised, several components of the pump beam which are not polarised parallel to the Raman oscillation will still provide gain to the Raman laser. Furthermore, birefringence in the diamond sample is likely to hinder the efficiency of the technique used in [12].

3.3 Yb:LuAG pumped intra-cavity DRL

In this section, further methods of power scaling DRLs will be investigated, this time implementing a thin disk (100μm) ytterbium lutetium oxide (Yb:LuAG) laser. This work was conducted in collaboration with Thomas Südmeyer and Maxim Gaponenko at the Université de Neuchâtel, who provided the Yb:LuAG fundamental laser. The Yb:LuAG was used to convert 1030nm and 1079nm laser emission into the 1200nm spectral range via an intra-cavity DRL. With a pump wavelength of 976nm, the comparatively small quantum defect of the ytterbium laser facilitates high power operation due to the reduced heat load deposited in the gain material per converted pump photon. Due to the large emission bandwidth, tunable operation and ultrafast pulse generation is also possible with this material [13].

The laser cavity used to achieve the results presented in this section can be seen in Figure 3.11. The fundamental cavity mode had a radius of 412μm in the Yb:LuAG crystal, and a mode radius of 25μm in the centre of the diamond. The Raman cavity was designed to match the fundamental cavity mode in the diamond sample. The diamond sample discussed in Section 3.2 was used throughout this section. Mirrors used in this section were purchased from Layertec GmbH. HR mirrors were specified to have >99.9% reflectivity at 1064nm and 1240nm, while the dichroic mirror used was AR coated at 1064nm (<0.15% reflectivity) and HR (>99.98% reflectivity) at 1240nm.

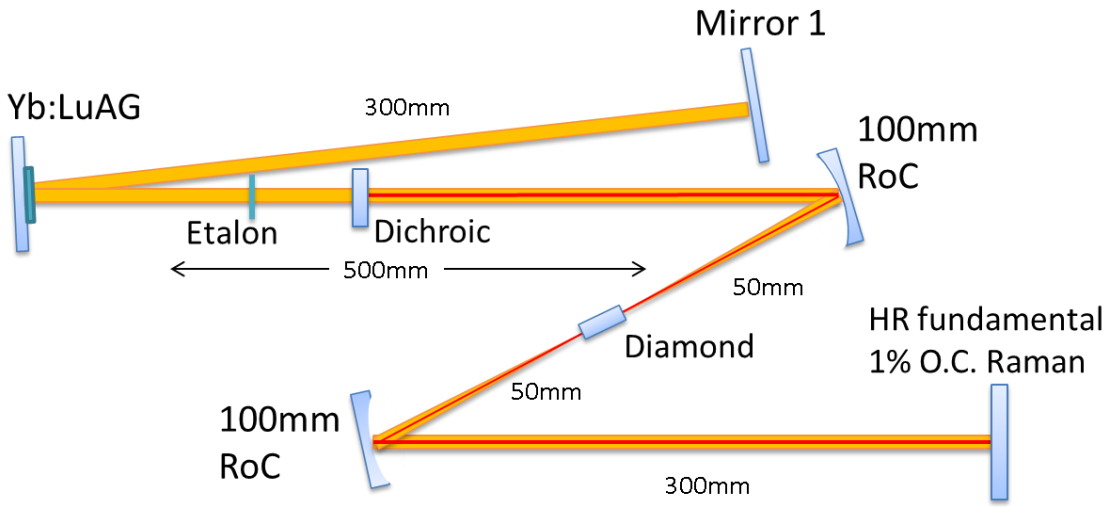

Figure 3.11. Cavity design used in Yb:LuAG intra-cavity Raman laser

Firstly, as before, we will look at the fundamental performance with no diamond in the cavity and a 1% output coupler at Mirror 1. A 24% slope efficiency (incident diode pump to Yb:LuAG output) was measured, comparable to the slope efficiencies observed in [14], with a threshold of 31W, with both shown in Figure 3.12 (black squares).

Next, the fundamental output was investigated, again with a 1% output coupler but this time with the diamond sample inserted into the cavity and Raman laser oscillation present. The fundamental performance under these conditions is represented by red circles in Figure 3.12. In this environment, the slope efficiency dropped to 10.8%, while the threshold dropped slightly to 28W diode pump

power. The similarity in thresholds highlights the low insertion loss of the diamond. The lower slope efficiency is expected, as the Raman output is, in this case, grouped into the residual loss term defining the fundamental slope efficiency.

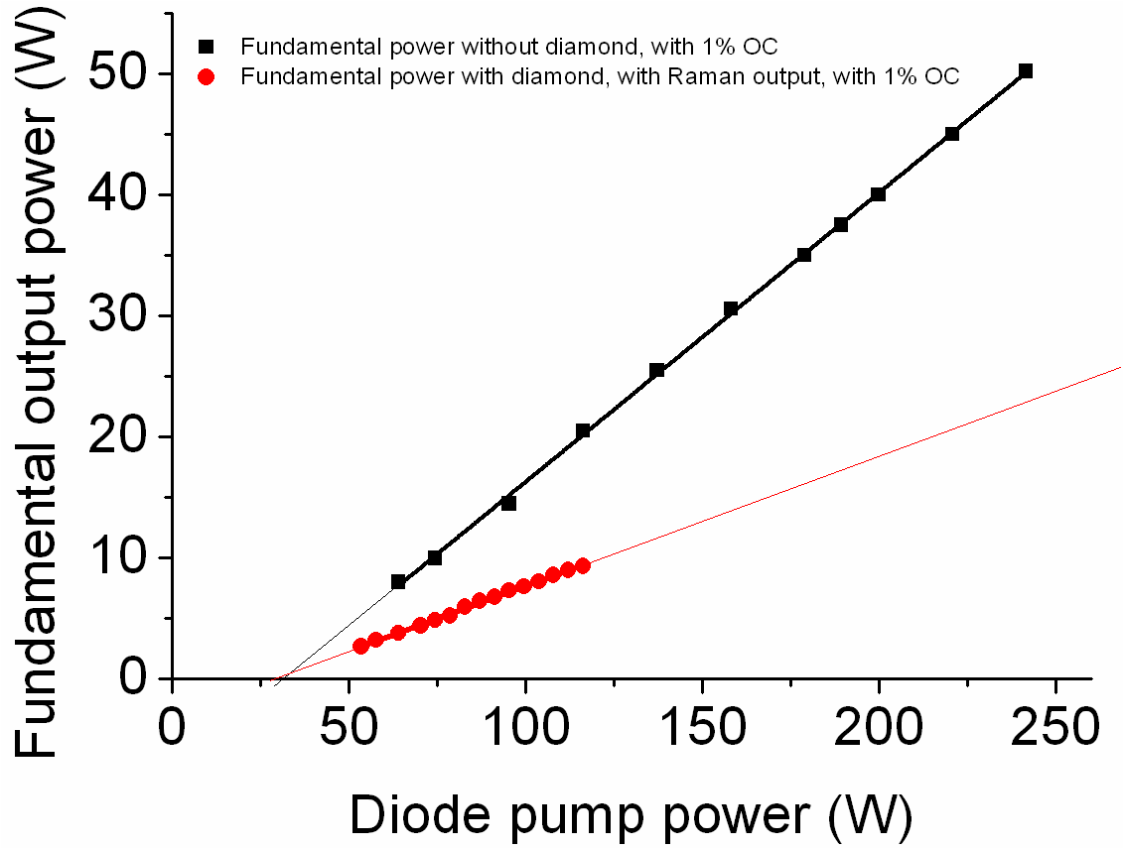

Figure 3.12. Power transfer of the Yb:LuAG with a 1% output coupler without the diamond in the cavity (black squares) and with the diamond in the cavity and Raman laser action present (red circles).

The slope efficiency of the Raman laser under these conditions was 4.3%, with a threshold of 46W diode pump power, shown in (red circles). A 2.6% diode to Stokes conversion efficiency was achieved at a diode pump power of 116W. Although low, this can also be cited as a fundamental to Stokes conversion efficiency of 30%.

With 3.1W of Raman output power achieved with a 1% output coupling on the fundamental laser, the next step was to replace this output coupler with an HR

mirror, reducing the loss in the fundamental cavity. A maximum Raman power of 7.6W was achieved at diode pump power of 190W; the highest reported CW intra-cavity DRL power to date. A slope efficiency of 5.3% was observed, with a threshold of 45W shown in Figure 3.13. This resulted in a maximum diode to Raman conversion efficiency of 4%.

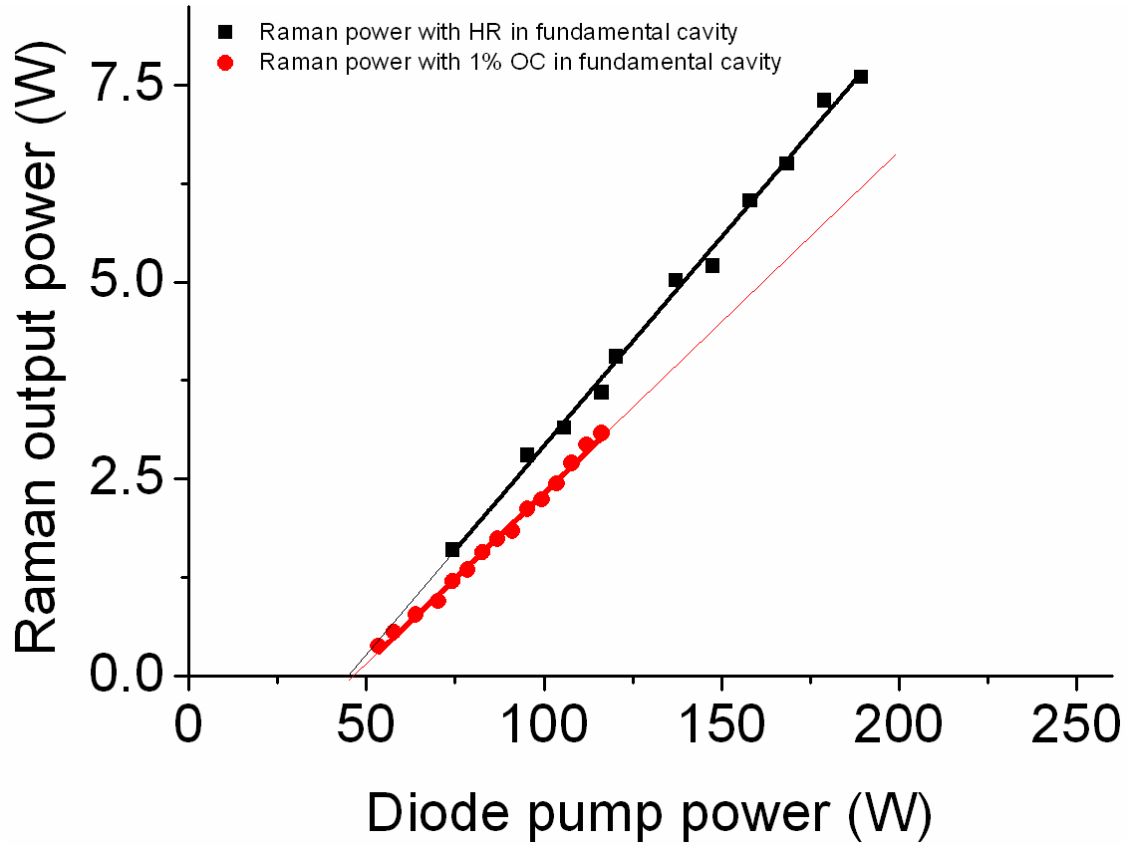

Figure 3.13. Power transfer of the intra cavity DRL with a 1% output coupler on both the fundamental and the Raman cavity (red circles) and that with HR mirror on fundamental cavity (black squares).

It should be noted that the threshold of Raman laser action was almost equal in the cases where the fundamental cavity had a 1% output coupling and an HR mirror at "Mirror 1". This is unexpected; the gain, loss and spot size in the Raman cavity in both cases are identical (assuming optimal alignment). From [15], the ratio of thresholds should be equal to the ratio of the total loss in the fundamental cavity. i.e. (from equation 9 in [15])

$$\frac{P_{Thd(HR)}}{P_{Thd(1\%)}} = \frac{\left(T_{f(HR)} + L_f\right)}{\left(T_{f(1\%)} + L_f\right)} \tag{3.3}$$

Therefore, unless the loss in fundamental cavity is significantly larger than the 1% output coupling, a substantial reduction in Raman threshold should be observed moving from a 1% output coupling to a 0.005% transmission HR mirror.

One potential reason for this apparent abnormality may be down to broadening of the fundamental spectrum. As presented in Section 3.2 (Figure 3.3 and Figure 3.7), the spectrum of the fundamental laser significantly varies moving from an output coupled cavity to an HR-HR cavity. With an etalon in place, this may have resulted in further spectral lines oscillating rather than spectral broadening, which could potentially lead to lower intensities in each spectral line, hence leading to a higher than expected threshold diode pump power in the HR-HR system. Unfortunately, due to time constraints with the work being undertaken off site, and the desire for high power operation, emission with a 1% output coupling was not extensively investigated; therefore this cannot be confirmed. Figure 3.14 does, however, show several spectral lines in the HR-HR case, both at 1030nm and at 1079nm.

The slope efficiency on the other hand, doubles from the 1% case to the HR case. From equation 11 in [15], the slope efficiency should vary with following relationship:

$$\frac{Slope_{(HR)}}{Slope_{(1\%)}} = \frac{A - B\left(T_{f(HR)} + L_f\right)}{A - B\left(T_{f(1\%)} + L_f\right)} \tag{3.4}$$

Where

$$A = \frac{T_S}{(T_S + L_S)}\frac{\lambda_P}{\lambda_S} \tag{3.5}$$

And

$$B = \frac{A_R}{P_P g_R l_R} \frac{\lambda_F}{\lambda_S} \tag{3.6}$$

With A and B equal in the HR and 1% output coupler case.

Equation 3.4 highlights that, if the loss in the cavity is significantly larger than the output coupling, the slope efficiency will remain constant along with the threshold. The observed increase in slope efficiency from the 1% O.C. to the HR system shows that the loss in fundamental cavity is not significantly larger than the 1% output coupling, adding further weight to the theory that interplay with spectral peaks and the corresponding Raman peaks causes the unexpectedly high threshold observed. The importance of the spectral characteristics to the efficiencies of Raman lasers have previously been highlighted in [16]

The spectral characteristics of both the fundamental and Raman lasers were measured using an Agilent 8146 optical spectrum analyser with a resolution of 0.052nm. As can be seen from Figure 3.14, as many as 6 quasi-independent Raman lasers are oscillating at once; independent in the sense that each Raman line is separated by a distance greater than the Raman linewidth in diamond [17], [18], yet coupled by the fundamental laser. It is highly likely that having several laser lines at 1030 and 1079 are inhibiting high conversion efficiencies from the fundamental to the Stokes wavelength. It should be noted that the fundamental output coupler had identical reflectivities at 1030nm and 1079nm, however the Raman output coupler had slightly higher losses at 1079nm (a few tenths of a per cent). Due to extreme coating damage on the diamond facets at high pump powers, laser action became impossible to achieve. For this reason, no M^2 measurements of the Raman output characteristics were taken.

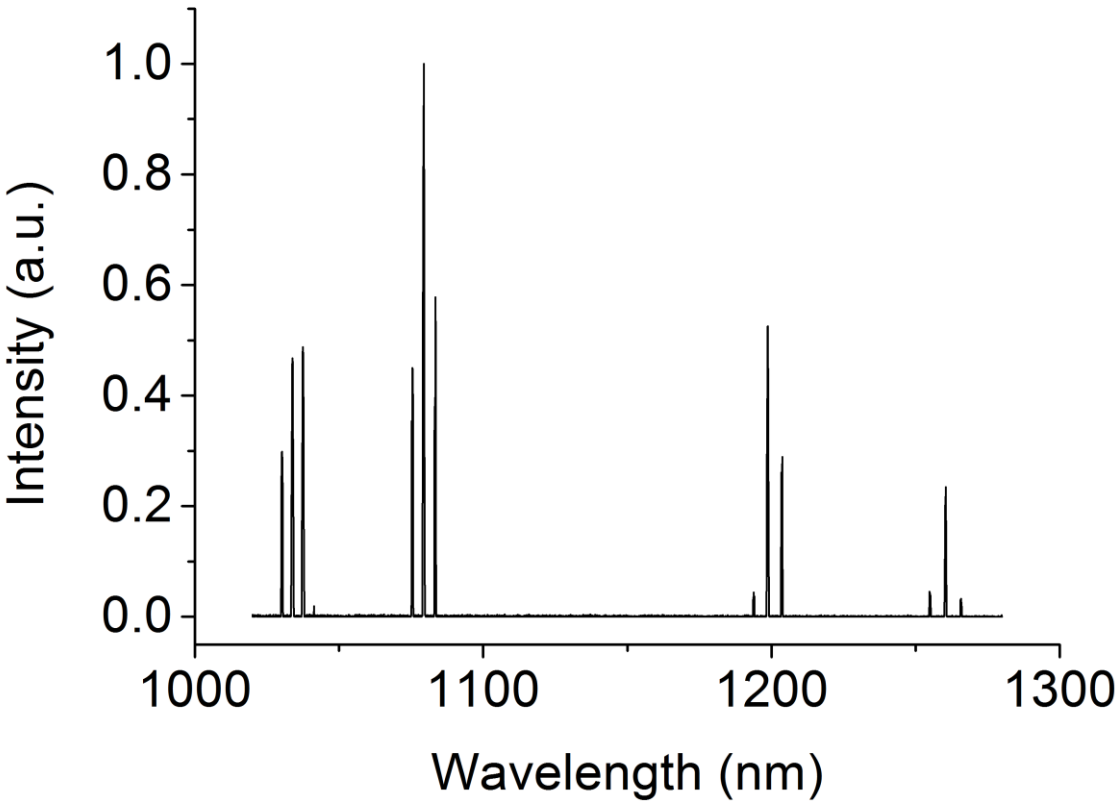

Figure 3.14. Output spectrum of the fundamental and Raman laser emission taken with HR mirror on place of "Mirror 1".

3.4 Summary of Nd:YAG and Yb:LuAG pumped CW DRL's

The performance of both lasers will now be collated in Table 3.1 and compared with the current state of the art CW systems. The brightness is defined as:

$$B = \frac{P}{\left(\lambda^2 M_x^2 M_y^2\right)} \tag{3.7}$$

Where P is the optical power, and M_x^2 and M_y^2 are the M^2 values for the horizontal and vertical directions respectively. Unfortunately, due to coating damage, a beam quality measurement was not taken, meaning a brightness comparison could not be made.

Table 3.1 highlights the potential for intra-cavity diamond Raman lasers to be more than mere frequency converters, as, analogous to a conventional laser and diode pump, they can also significantly improve the optical brightness of a laser

system. This is emphasised with both 11-fold and 43 fold enhancements observed from fundamental to Raman output in DRL's compared with the 2.5 fold enhancement seen in a similar intra-cavity system with KGW acting as the Raman gain material. This table also displays the high power capabilities of external cavity systems, with the previously discussed 10.1W external cavity diamond Raman laser emphasising this fact.

Table 3.1. Comparison of laser systems presented in this chapter with current state of the art systems

Laser Design/ Raman Material	**Fundamental**		**Raman**		
	Output Power (W)	Beam Quality	Output Power (W)	Beam Quality	Brightness Enhancement
Intra-cavity Yb:LuAG DRL	50	1.5	7.6	NA	NA
Intra-cavity Nd:YAG DRL	41	19.9 x 18.3	6.1	2.3 x 1.6	11 fold
Intra-cavity Nd:YLF DRL [5]	18.4	14 x 19	5.1	1.1 x 1.2	43 fold
Intra-cavity Nd:YLF KGW [5]	18.4	14x19	6.1	5 x 6	2.5 fold
External Cavity Nd:YVO_4 DRL [6]	31	1.7	10.1	1.16	0.5 fold (No Enhancement)

Although brightness enhancements (in some cases order of magnitude improvements[5]) have been observed by others as well; the physical mechanism is not well known. Murray et al [19] propose that the Raman gain profile resulting from multi-mode pumping is observed as a quasi-Gaussian gain distribution, which would lead to an improved Raman output beam. This explanation shows that, in theory, brightness enhancements should be achievable in external cavity systems. However, with the decreased Rayleigh length associated with a poorer quality pump beam, along with the requirement to use a focusing lens with a focal length M times shorter to equal the intensities of near diffraction limited beams, reaching threshold for systems similar to that presented in [6] may prove difficult. Hence, with the higher Raman gain in diamond allowing the use of shorter crystals, as well as the excellent thermo-mechanical properties of the material allowing its implementation in intra-cavity systems, it appears intra-cavity DRL's may prove the optimal route in converting poor beam quality laser systems.

3.5 Conclusions and future Work

In conclusion, two of the highest power intra-cavity diamond Raman lasers have been realised; one of which implementing an unpolarised Nd:YAG to obtain 6.1W of polarised Raman output and a 11 fold brightness enhancement from pump to Raman, and the other employing a slightly more exotic Yb:LuAG gain material to produce 7.6W of Raman output. Further power scaling was inhibited mainly by spectral effects in the fundamental laser, with additional complications arising with coating damage to both diamond facets. A comparison between Raman performance with a 1% output coupler on the fundamental Yb:LuAG laser and an HR-HR cavity highlights that, with unexpectedly near identical Raman thresholds, it is possible optimal performance has yet to be achieved. It is likely that, with further spectral control of the fundamental laser, higher power Raman output could be accomplished.

Placing a volume Bragg grating (VBG) in the fundamental cavity to allow further control of the spectrum of the fundamental laser would perhaps increase the

conversion efficiency from fundamental to Raman, similar to work recently presented in [20], with this specific work showing that spectral control of the fundamental cavity can produce improved performance in a KGW Raman lasers.

With regards to the continual problems arising with optical coatings, the use of a Brewster cut diamond would ameliorate the problems introduced by the diamond coatings which has previously been successfully executed in several external cavity DRLs [10], [21]–[24].

Although, in terms of power scaling, external cavity approaches appear, to date, to be the most productive route, intra-cavity systems provide optimal performance in certain circumstances. Similar to results presented in [5], the results presented in this section showed a significant brightness enhancement from fundamental to Raman output when utilizing diamond as a Raman laser gain material. Furthermore, one might argue that, when converting a near diffraction limited pump source, any (potentially expensive) thermal engineering has already been conducted in the fundamental laser. Converting a cheap, robust and "dirty" light source can be done with relative ease using an intra-cavity approach; exploiting Raman beam clean-up and the intrinsic thermal engineering in diamond.

Bibliography

[1] W. Lubeigt, G. M. Bonner, J. E. Hastie, M. D. Dawson, D. Burns, and A. J. Kemp, "Continuous-wave diamond Raman laser," *Opt. Lett.*, vol. 35, no. 17, pp. 2994–2996, 2010.

[2] W. Lubeigt, V. G. Savitski, G. M. Bonner, S. L. Geoghegan, I. Friel, J. E. Hastie, M. D. Dawson, D. Burns, and A. J. Kemp, "1.6 W continuous-wave Raman laser using low-loss synthetic diamond," *Opt. Express*, vol. 19, no. 7, pp. 6938–6944, 2011.

[3] D. C. Parrotta, A. J. Kemp, M. D. Dawson, and J. E. Hastie, "Tunable continuous-wave diamond Raman laser," *Opt. Express*, vol. 19, no. 24, pp. 24165–24170, 2011.

[4] D. C. Parrotta, A. J. Kemp, M. D. Dawson, and J. E. Hastie, "Multiwatt, Continuous Wave, Tunable Diamond Raman Laser With Intracavity Frequency-Doubling to the Visible Region," *IEEE J. Quantum Electron.*, vol. 19, no. 4, 2013.

[5] V. G. Savitski, I. Friel, J. E. Hastie, M. D. Dawson, D. Burns, and A. J. Kemp, "Characterization of Single-Crystal Synthetic Diamond for Multi-Watt Continuous-Wave Raman Lasers," *Quantum Electron. IEEE J.*, vol. 48, no. 3, pp. 328–337, 2012.

[6] O. Kitzler, A. McKay, and R. P. Mildren, "Continuous-wave wavelength conversion for high-power applications using an external cavity diamond Raman laser," *Opt. Lett.*, vol. 37, no. 14, pp. 2790–2792, 2012.

[7] R. J. Williams, O. Kitzler, A. Mckay, and R. P. Mildren, "Investigating diamond Raman lasers at the 100 W level using quasi-continuous-wave pumping," *Opt. Lett.*, vol. 39, no. 14, pp. 4152–4155, 2014.

[8] R. P. Mildren and J. R. Rabeau, Eds., *Optical Engineering of Diamond*. Wiley VCH Verlag GmbH and Co. KGaA, 2013.

[9] V. G. Savitski, S. Reilly, and A. J. Kemp, "Steady-State Raman Gain in Diamond as a Function of Pump Wavelength," *IEEE J. Quantum Electron.*, vol. 49, no. 2, pp. 218–223, 2013.

[10] A. Sabella, J. A. Piper, and R. P. Mildren, "1240nm diamond Raman laser operating near the quantum limit," *Opt. Lett.*, vol. 35, no. 23, pp. 3874–3876, 2010.

[11] W. Koechner, *Solid-State Laser Engineering*, 6th ed. Springer, 2006.

[12] W. A. Clarkson, N. S. Felgate, and D. C. Hanna, "Simple method for reducing the depolarization loss resulting from thermally induced birefringence in solid-state lasers.," *Opt. Lett.*, vol. 24, no. 12, pp. 820–2, 1999.

[13] T. Südmeyer, C. Kränkel, C. R. E. Baer, O. H. Heckl, C. J. Saraceno, M. Golling, R. Peters, K. Petermann, G. Huber, and U. Keller, "High-power ultrafast thin disk laser oscillators and their potential for sub-100-femtosecond pulse generation," *Appl. Phys. B*, vol. 97, no. 2, pp. 281–295, 2009.

[14] S. Veronesi, Y. Z. Zhang, M. Tonelli, A. Agnesi, A. Greborio, F. Pirzio, and G. Reali, "Spectroscopy and efficient laser emission of Yb3+: LuAG single crystal grown by μ-PD," *Opt. Commun.*, vol. 285, pp. 315–321, 2012.

[15] D. J. Spence, P. Dekker, and H. M. Pask, "Modeling of Continuous Wave Intracavity Raman Lasers," *Sel. Top. Quantum Electron. IEEE J.*, vol. 13, no. 3, pp. 756–763, 2007.

[16] G. M. Bonner, "Thermal and Spectral Effects in Intracavity Raman Lasers," Strathclyde University, 2013.

[17] A. A. Kaminskii, R. J. Hemley, J. Lai, C. S. Yan, H. K. Mao, V. G. Ralchenko, H. J. Eichler, and H. Rhee, "High-order stimulated Raman scattering in CVD single crystal diamond," *Laser Phys. Lett.*, vol. 4, no. 5, pp. 350–353, 2007.

[18] A. A. Kaminskii, V. G. Ralchenko, and V. I. Konov, "CVD-diamond – a novel$\chi(3)$-nonlinear active crystalline material for SRS generation in very wide spectral range," *Laser Phys. Lett.*, vol. 3, no. 4, pp. 171–177, 2006.

[19] J. T. Murray, W. L. Austin, and R. C. Powell, "Intracavity Raman conversion and Raman beam cleanup," *Opt. Mater. (Amst).*, vol. 11, pp. 353–371, 1999.

[20] V. G. Savitski, "Experimental analysis of emission linewidth narrowing in a pulsed $KGd(WO_4)_2$ Raman laser," *Opt. Express*, vol. 22, no. 18, pp. 582–585, 2014.

[21] J-P. M. Feve, K. E. Shortoff, M. J. Bohn, and J. K. Brasseur, "High average power diamond Raman laser," *Opt. Express*, vol. 19, no. 2, pp. 913–922, 2011.

[22] R. P. Mildren, J. E. Butler, and J. R. Rabeau, "CVD-diamond external cavity Raman laser at 573nm," *Opt. Express*, vol. 16, no. 23, pp. 18950–18955, 2008.

[23] E. Granados, D. J. Spence, and R. P. Mildren, "Deep ultraviolet diamond Raman laser.," *Opt. Express*, vol. 19, no. 11, pp. 10857–63, 2011.

[24] R. P. Mildren and A. Sabella, “Highly efficient diamond Raman laser,” *Opt. Lett.*, vol. 34, no. 18, pp. 2811–2813, 2009.

Chapter 4 – Pulsed Raman lasers

Diamond Raman lasers producing nanosecond pulses are no longer exceptional [1]–[4], and have been demonstrated at a wide range of hard to reach, but commercially significant wavelengths from the ultraviolet to the mid-infrared [5], [6]. Due to the high peak powers present in q-switched pulses, reaching threshold in external cavities is trivial; however, the additional cavity can, at times, be sizeable and require careful alignment. Additionally, in order to produce pulses in the picosecond regime and below, normally utilizing mode-locked pump sources [7]–[9], the aforementioned drawbacks are coupled with the requirement to synchronously pump the external Raman system.

In this Chapter, two compact methods of generating pulsed Raman laser emission will be discussed, namely: a monolithic diamond Raman laser system pumped externally with a q-switched green laser, and an intra-cavity Raman laser pumped with a mode-locked fundamental laser. A comparison between a monolithic Raman laser using curved microlens structures to form a stable cavity, and that which oscillated in a plane-plane cavity will also be presented.

4.1 Pulsed diamond Raman lasers in the nanosecond regime

Demonstrations of short pulse generation using the Raman effect in diamond have implemented both a q-switched pump [1]–[5], [10]–[12] and a mode-locked pump [7]–[9], [13]. Feve et al [2] , used a cryogenically cooled q-switched Yb:YAG pump laser, emitting at 1030nm, to demonstrate an impressive 24.5W average Raman output power at 1190nm, with a 40kHz repetition rate and a pulse duration of 29ns. It should be highlighted that this was limited only by damage to the optical coatings deposited on the diamond.

With the high peak powers involved in q-switched pump sources, higher Stokes orders have readily been achieved, allowing access to interesting wavelengths such as the “eye safe” region of the spectrum [3]. Pumped with 3.2W of 1064nm

output from a q-switched Nd:YAG laser, an average power of 1.63W was achieved at 1485nm, the 2nd Stokes wavelength of the external cavity diamond Raman laser, with a repetition rate of 5kHz and pulse duration of the order of 10ns.

4.2 Monolithic diamond Raman laser

In this section, two highly efficient compact and robust monolithic diamond Raman lasers will be presented, with their performance discussed. The first laser utilizes microlens structures etched on the front surface of a 4 x 4 x 2 mm^3 diamond to form a stable cavity, and the second, a 3.6 x 2 x 1.6mm^3 diamond implemented in a plane-plane cavity. The simple diamond cavity is near alignment free, and, in comparison to similar external cavity and intra-cavity approaches, reduces the amount of surfaces contributing to round trip loss. There has only been one other demonstration of such a device [14]; however this was merely an observation of SRS in a low Q resonator between 2 uncoated diamond surfaces. The characteristics of the device are not presented in much detail; however, an approximate conversion efficiency of 0.05% from incident pump to Raman output is inferred.

The single crystal synthetic diamond samples used in this section were grown using chemical vapour deposition by Element 6 Ltd, with a birefringence of $<1x10^{-6}$ and a specified absorption coefficient of $<0.005cm^{-1}$ at 1064nm.

4.2.1 Microlens cavity design

Microlens structures (discussed in section 4.2.2) were implemented on the front surface of a diamond sample to form a stable resonator between the front and back surfaces. Dielectric mirror coatings were deposited onto the front and back 4x4mm^2 surfaces by Laseroptik GmbH. The back surface of the diamond was coated for high-reflection (HR) at 532nm, to double pass the pump, and partial reflection (PR) at the first Raman shifted wavelength of 573nm (70% reflectivity). The front surface, with the microlens structures fabricated on it, was coated for high-transmission (HT) at the pump wavelength (~20% reflectivity) and HR coated at 573nm. Due to limitations in the sizes of diamond available from

Element 6, with one length limited to 2mm or less, a diamond cavity length of 2mm was chosen. The longest possible diamond length was selected due to both the increase in available gain, and the slightly larger cavity mode radius associated with the longer resonator length.

Before the demonstration of such a device, several design parameters must be determined. Raman threshold must be reached, which can be controlled via the choice of output coupling and the cavity mode radius (defined by the cavity length and the RoC of the microlens). The choices of these values, however, must be balanced with the threshold powers for optical damage to the dielectric coatings deposited. This section will discuss the parameters selected.

Now, the microlens cavity mode should be defined. Previous microlens structures have been limited to around 10μm[15]–[17], restricting the size of the Raman cavity mode radius to around 20μm in a 2mm long cavity, calculated using equation 4.1 [15] and shown in Figure 4.1.

$$\omega_0 = \sqrt{\frac{L\lambda}{n\pi}\sqrt{nR-1}} \tag{4.1}$$

Where L is the length of the diamond, λ is the wavelength of light, n is the refractive index of diamond and R is the radius of curvature of the microlens.

In order to efficiently convert the pump light into Raman emission, the pump spot radius should be matched to that of the cavity mode radius, which restricts the pump energy which can be used without damaging the diamond surfaces and coatings. Furthermore, the intra-cavity Stokes field presents a threat to the optical coatings. With this in mind, the choice of output coupling becomes pivotal.

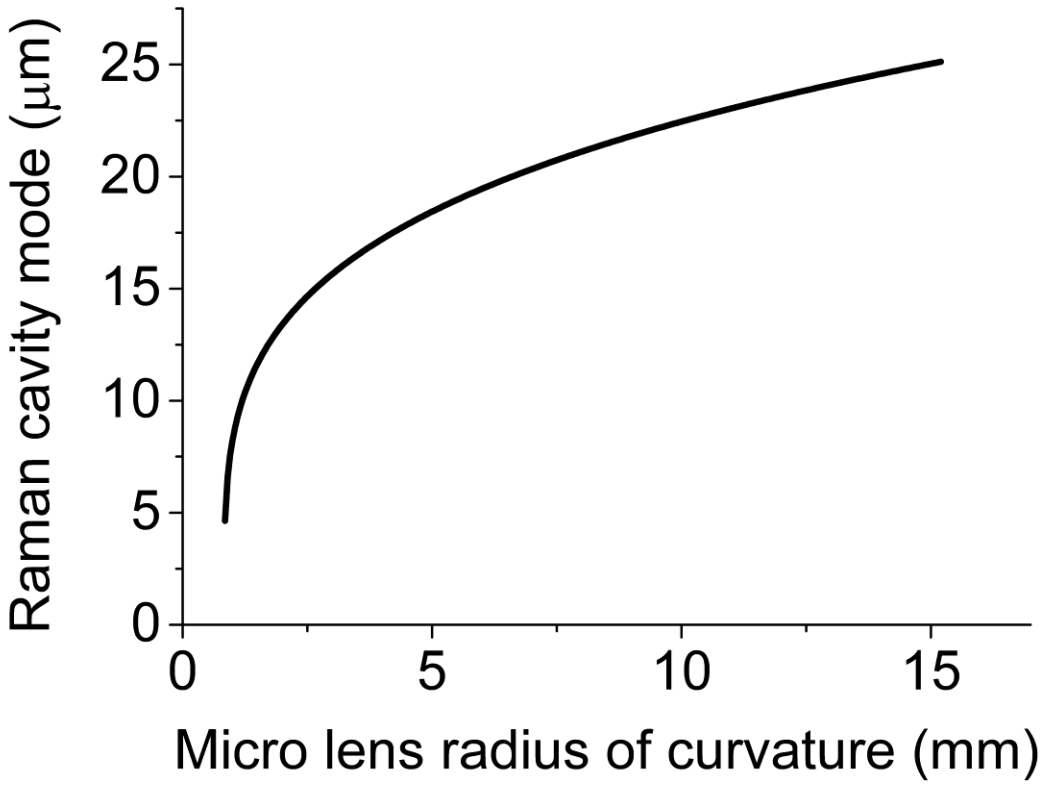

Figure 4.1. Dependence of the Raman cavity mode radius with varying microlens radius of curvature in a 2mm long diamond cavity.

With a 1.5ns, 10kHz q-switched Elforlight SPOT laser as a pump source, an average pump power of 240mW was available. Estimating the damage threshold of the coatings to be 5Jcm^{-2}, a conservative value given past experience with adhesion issues and the comparatively thick HR coatings compared to the previously used AR coatings, a range of output couplers were considered. It became evident that the main threat to coating damage arose from the intra-cavity Raman field (highlighted in Figure 4.2 and Figure 4.3); therefore a large output coupling was originally tested. Initial tests were carried out by optical contact bonding the microlens diamond onto a mirror, HR at both the pump and Raman wavelength, and using Fresnel reflections from the opposite diamond surface, effectively acting as an 83% output coupling for the Stokes wavelength. The modelled performance and damage limits are shown in Figure 4.2. Values of the threshold pump power, Pp, were calculated using equation 4.2 [18], [19].

$$P_p = ln\left[\frac{1}{R_{oc}\, e^{-2\alpha l}\, R_{HR}}\right]\frac{\pi r^2}{4 g_R l} \qquad 4.2$$

Where R_{oc} is the reflectivity of the output coupler at the 1st Stokes wavelength, $e^{-2\alpha L}$ represents the absorption losses in the diamond, R_{HR} is the reflectivity of the HR mirror at the 1st Stokes mirror and l is the length of the diamond sample.

The slope efficiency (η) of the diamond laser was calculated using equation 4.3 [20].

$$\eta = \frac{\lambda}{\lambda_s}\frac{\ln(R_{OC})}{ln[R_{OC}\, e^{-2\alpha l}\, R_{HR}]} \qquad 4.3$$

Where λ is the pump wavelength at 532nm and λ_s is the Raman wavelength at 573nm.

Preliminary tests of the diamond bonded to the mirror, however, proved unsuccessful; with no laser action achieved. Mindful of this, a more cautious 30% (transmission) output coupling was chosen for initial tests, with the modelled performance and damage characteristics for such an output coupling presented in Figure 4.3. Figure 4.2 and Figure 4.3 highlight that, until exceeding an output coupling of around 85%, coating damage caused by the intra-cavity Raman field will be the factor limiting power scaling. Advances in the fabrication of longer radius of curvature microlens structures may allow an increase in the resonator mode, permitting further power scaling.

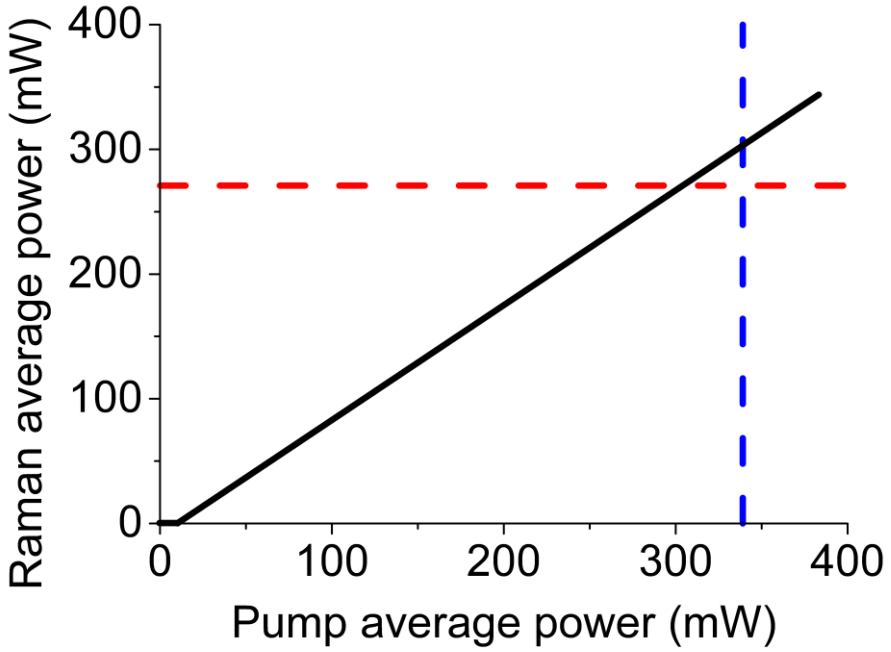

Figure 4.2. – Modelled performance of monolithic diamond Raman laser, with the pump (blue dash) and intra-cavity Raman (red dash) estimated coating damage threshold when using an uncoated diamond surface as an output coupler.

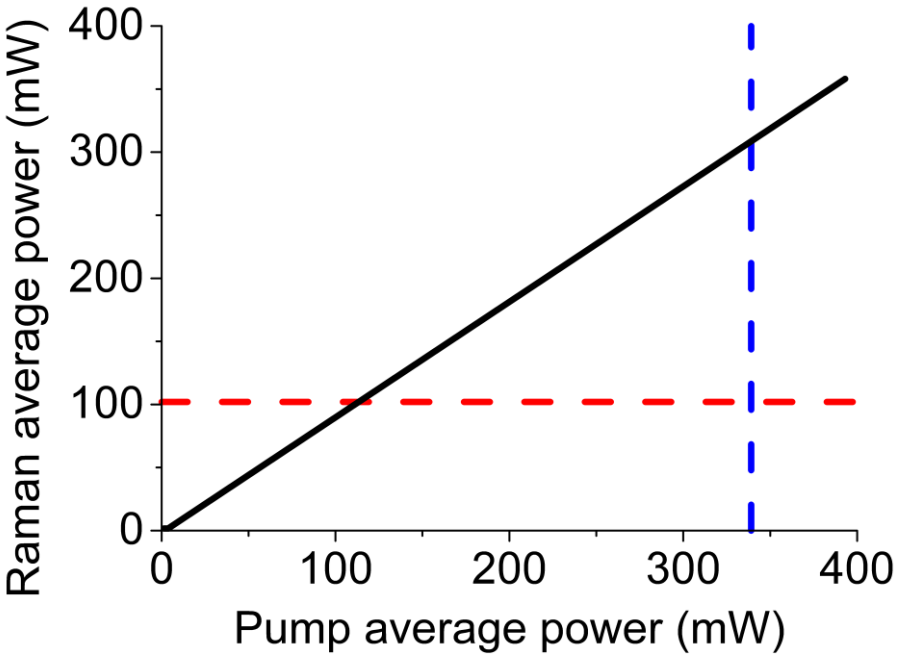

Figure 4.3. Modelled performance of monolithic diamond Raman laser, with the pump (blue dash) and intra-cavity Raman (red dash) estimated coating damage threshold when using a 30% output coupler.

4.2.2 Microlens fabrication and characterisation

The microlens fabrication and characterisation was conducted by fellow PhD student Hangyu Liu. The fabrication was carried out to the laser cavity design discussed in Section 4.2.1. A process developed from the "resist-reflow" process discussed in [21] was used to produce spherical lens-like structures in a Shipley SPR220 photoresist deposited on the diamond surface. Firstly, the photoresist is deposited on the diamond surface, which is then covered in a mask and treated with UV light. The untreated photoresist is then removed using acetone, leaving spherical pillars on the diamond. The "resist-reflow" process heats and melts the photoresist, which due to surface tension, forms spherical lens-like structures. These are then transferred to the diamond surface via inductively coupled plasma etching. In order to achieve lens structures with as long a radius of curvature as possible, (as per the reasons discussed in Section 4.2.1), an Ar/Cl_2 plasma etch was used. This plasma has a lower etch rate and etch selectivity than that of the, perhaps more conventional, Ar/O_2 plasma etch. This allows the fabrication of shallower structures [22]. The radius of curvature is limited by the deposition of the photoresist, with problems arising when the surface tension of the photoresist cannot sustain the lens shape, causing the centre of the photoresist to collapse.

After the lens structures were fabricated on the surface of diamond, shown in Figure 4.4, a Dektak profilometer was used to characterise each structure, with an example of this shown in Figure 4.5. With the measured data, a spherical shape is assumed and a circular fit is plotted on each lens in order to measure its radius of curvature. Although there is a slight difference in the fit and measured data points at the edges of the lenses, the more important central section, where the pump and Raman beam will propagate (a beam radius of 24μm is used while the lens is around 400μm in diameter), the fit is in good agreement with the data. Values of around 13mm ROC were achieved. AFM profiles of the lens structures showed that there was no significant deterioration in surface roughness, with values of R(a) found to be 1.1nm post etch, compared with 0.6nm before the etch.

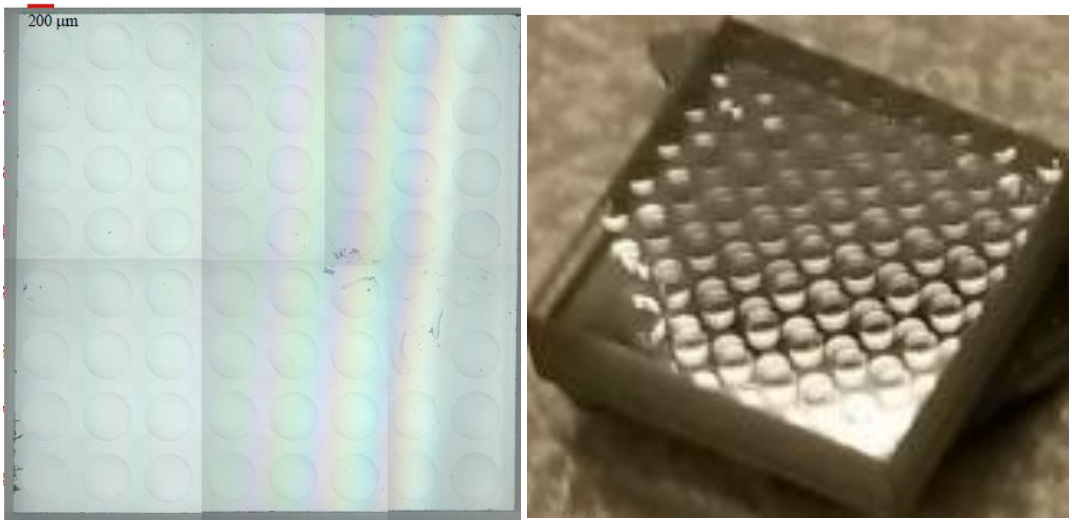

Figure 4.4. Images of the microlens structures etched into the diamond surface.

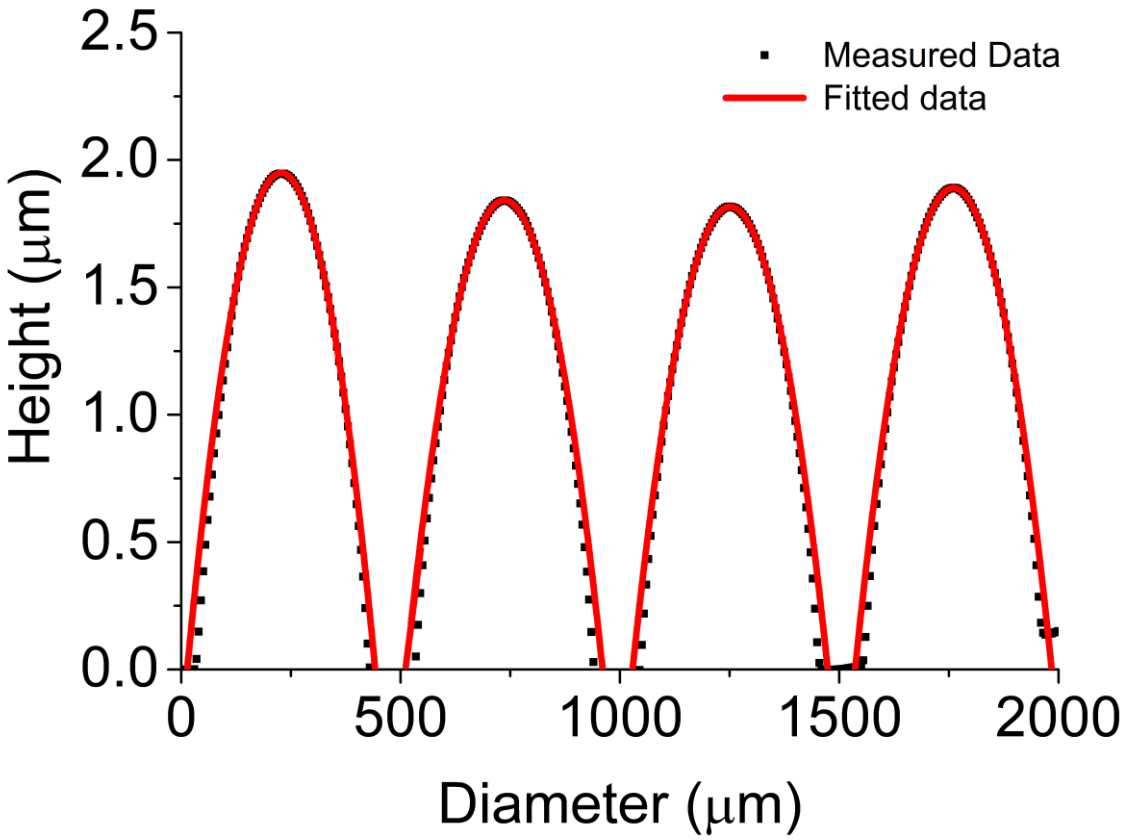

Figure 4.5. Example of lens profiles measured using Dektak profilometer. Radii of curvature of 11.7mm, 13.6mm, 13.6mm and 13.3mm were measured (left to right).

4.2.3 Plane-plane cavity

In order to test a plane-plane cavity, a diamond sample with no microlens structures fabricated on the surface was coated in the same run as the microlens sample. The resonator length in this case was slightly shorter than the 2mm microlens cavity; with the plane-plane diamond measuring 1.6mm. With diamonds thermo-mechanical properties, the thermal loads potentially deposited in the sample are unlikely to cause any significant thermal lensing, therefore any modal confinement in the Raman resonator is likely to come from other means, discussed in Section 4.2.5.

4.2.4 Experimental method

The experimental setup is shown schematically in Figure 4.6. Both the microlensed and plane-plane diamond resonators were pumped with an Elforlight SPOT laser emitting Q-switched pulses at 532nm with pulse durations of 1.5ns (full width half maximum) and pulse repetition rates between 1kHz and 10kHz. The results presented in this thesis were all taken at 10kHz; however, comparable performance was observed at 1kHz.

The pump was attenuated using a combination of a half wave-plate and a polarizing cube. It was then focused using a 50mm focal length lens. In the case of the microlens sample, it was focused through a single microlens structure onto the plane back surface of the diamond, resulting in a pump spot radius of 9μm, which, although significantly smaller than the Raman mode, was found to provide slightly better performance than a pump spot size of 18μm. The microlens cavity had a fundamental mode radius of 24μm. Pump light propagated along a <110> direction in the diamond, and was polarized along a <100> direction in the micro-lens case, whilst in the plane-plane system, pump light propagated along a <100> direction and was polarized along a <110> direction.

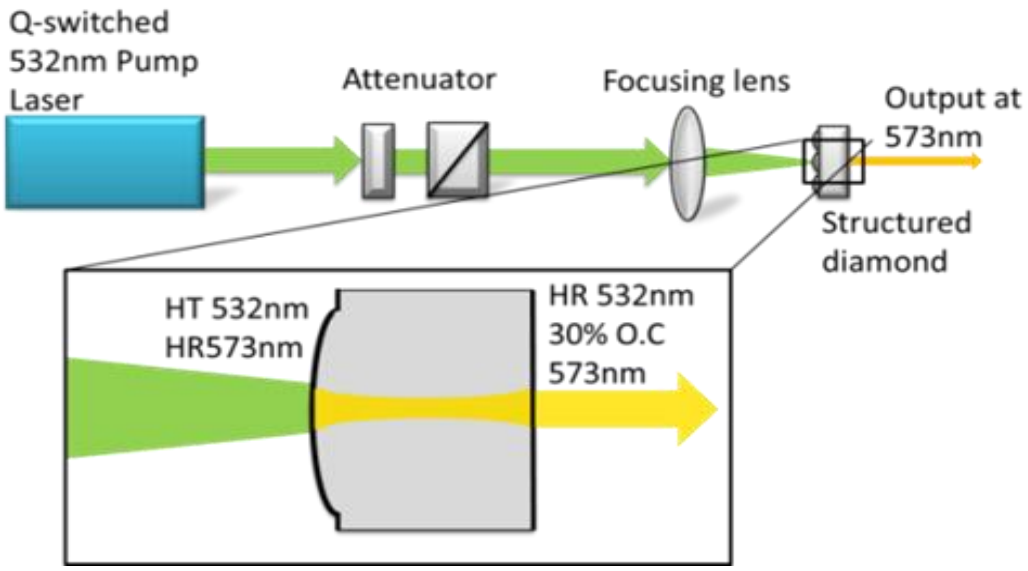

Figure 4.6. Experimental setup used to achieve Raman laser action in microlens and plane-plane diamond. HT: high transmission; HR: high reflectivity; O.C.: output coupling.

Initial alignment of the pump laser was conducted using a set of filters and a Canon EOS digital camera directly behind the diamond sample. Although the back surface was HR at the pump wavelength, a small amount of leakage allowed for rough alignment through specific microlens structures, as shown in Figure 4.7.

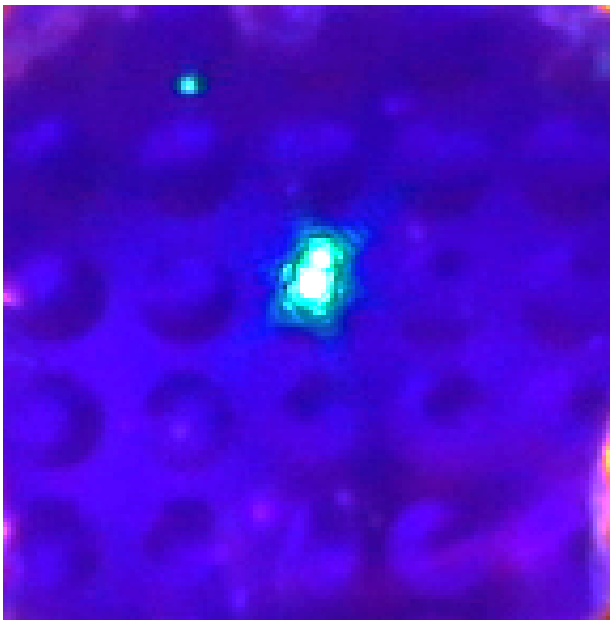

Figure 4.7. Photographic image of initial alignment of the pump beam.

Optimisation of the pump beam position on the microlens was then conducted just above threshold of Raman oscillation, in order to achieve maximum Raman output power. Adjustments at higher incident pump energy (around 10μJ) readily lead to damage of the optical coatings.

4.2.5 Diamond Raman laser performance

Raman conversion of the green pump at 532nm to the yellow at 573nm was observed when the pump pulse energy reached 1.5μJ for the micro-lens case and 3.7 μJ for the plane-plane case (the pump energies quoted are corrected for the 20% reflectivity of the front coating on both diamonds, i.e. are the energies entering the diamond). At large pump energies, Raman emission was also observed at the 2^{nd} and 3^{rd} Stokes wavelengths of 620nm and 674nm respectively. A photograph of the experimental setup is shown in Figure 4.8, with the maximum pump energy available incident on the diamond sample and all three Stokes shifts present in the output.

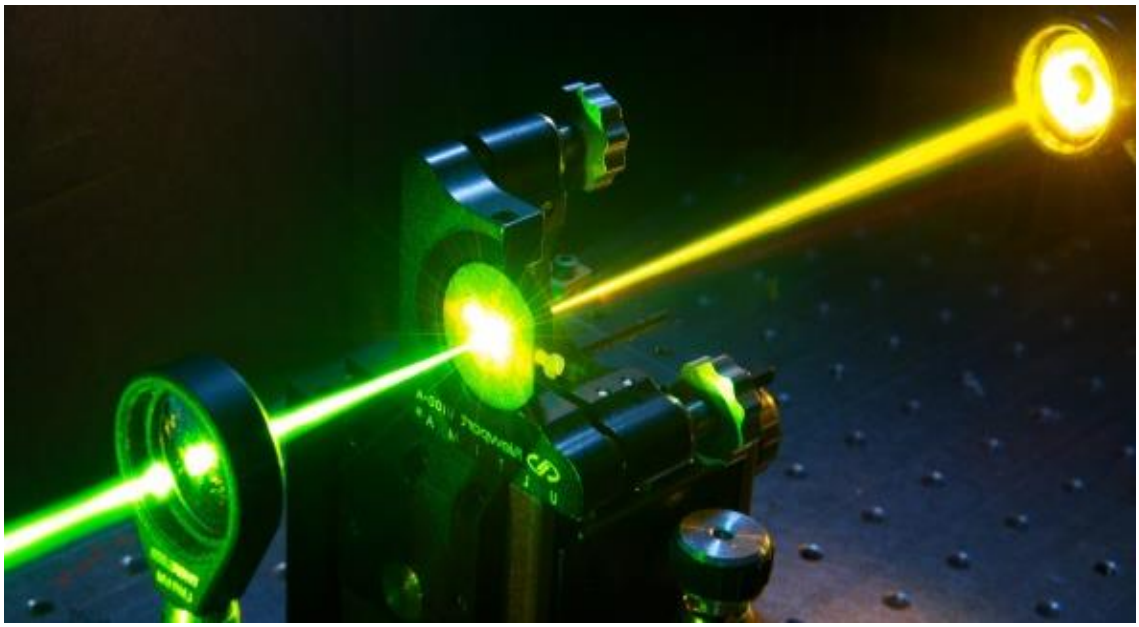

Figure 4.8. Green to yellow/orange conversion using a monolithic diamond Raman resonator. The photograph was taken at maximum pump power with all three Stokes orders present.

The reflectivities at the 2nd Stokes wavelength (620nm) of the coatings deposited on the back and front surfaces of the diamonds were 50% and 40% respectively. Even with this relatively high combined output coupling of 80% per round trip, a significant fraction of the pump power was converted to the 2nd Stokes wavelength: 59% and 25%, respectively, for the microlens and plane-plane cases at maximum pump power (blue triangles in Figure 4.10(a) and Figure 4.11(a), respectively). A small amount of 3rd Stokes emission was also present in both cases, 10% in the microlens system and 1% in the plane-plane, as the pump pulse energy reached maximum (red circles in Figure 4.10(a) and Figure 4.11(a)). Clamping of the 1st Stokes (green squares in Figure 4.10(a)) is observed for the microlens resonator when the 2nd Stokes rises above threshold, but not in the plane-plane case (green squares in Figure 4.11(a)). The power transfer curves were measured using a set of calibrated filters. The output at 620nm was measured in both the forward and backward (towards the pump) directions, as backward emission contributed a significant fraction of the total power in this case. Output at the 3rd Stokes in the backward direction was not measured because the dichroic mirror required to make the measurement reduced the incident pump power to below the threshold for the 3rd Stokes.

A slope efficiency of 88% for the combined Raman output energy was measured for the microlens cavity, with an 84% pump to combined Raman conversion efficiency at the highest pump pulse energy of 16μJ, seen in Figure 4.10(b). A reduced conversion efficiency of 59% was measured in the plane-plane case, shown in Figure 4.11(b), with a slope efficiency of 74%. The maximum average powers of the combined Raman outputs were 134mW and 96mW, respectively for the micro-lens and plane-plane cases.

The Raman output in the microlens case had an M^2 of 6.8 x 4, 1.9 x 1.5 and 1.5 x 1.3 for the 1st, 2nd and 3rd Stokes respectively at maximum pulse energy. The M^2 of the pump was 1.5 x 1.4. Issues with optical damage to the coatings made M^2 measurements difficult for the plane-plane case but values were no better than 3.6 x 3, 3.3 x 2.8 and 2.7 x 2.7 for the 1st, 2nd and 3rd Stokes respectively.

The 1st Stokes emission was polarized along a <110> direction in the diamond for both the microlens and plane-plane cavities, as would be expected given the orientation used and the polarization dependence of the Raman gain [11], [23]. This is seen in Figure 4.9(a), with the plane plane pump and emission characteristics represented as point A, while the microresonator pump and emission characteristics are represented by point B in Figure 4.9(b). With the pump polarization along a <100> direction in the plane-plane cavity, the maximum available gain was likely achieved in this system.

In the microlens cavity, no difference was observed in Raman output power when the microlens diamond was rotated for a pump polarization along a <111> direction, although, in theory, orientating the pump along a <111> direction maximizes the Raman gain for propagation along <110> [11], [23]. With no means to control the Raman polarisation due to the nature of the system, rotation of the pump led to the Raman polarisation rotating, maintaining an approximate 90° angle between that and the pump. Similar observations were made in a more complete study of this phenomenon [24] and have been previously discussed in Chapter 3.

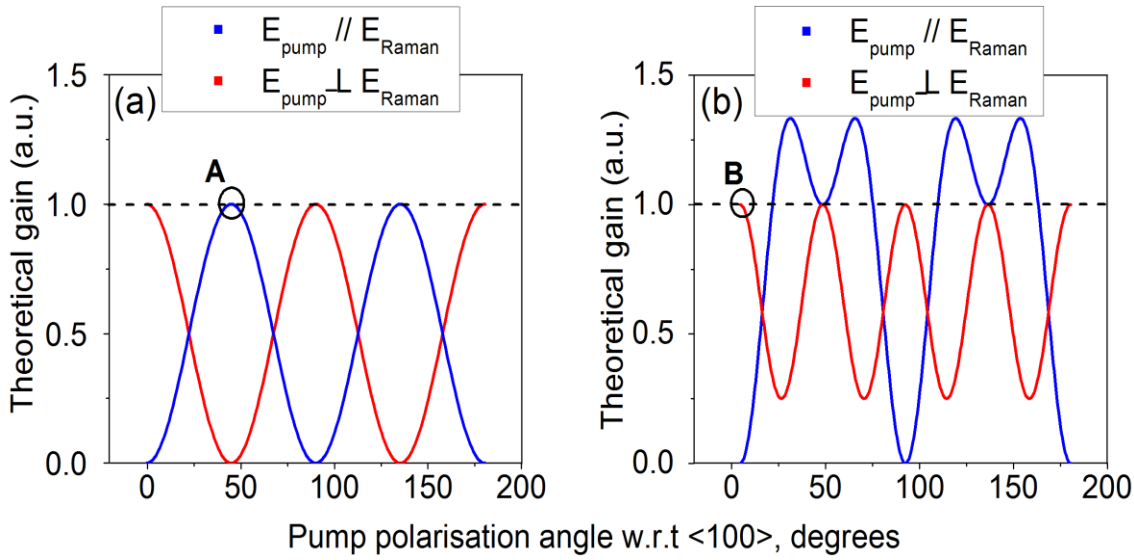

Figure 4.9. Theoretical Raman gain coefficient as a function of pump polarisation angle for the pump propagating along (a) a <100> direction and (b) a <110> direction [23].

Coating damage was observed much more readily on the plane-plane diamond than on the microlens sample. Since the samples were coated in the same run, this might be indicative of poorer diamond surface quality in the plane-plane case.

The 1.5ns incident pump pulse is shown in Figure 4.12(a) (solid) along with the depleted pump (dashed), taken at moderate pump energies. In the microlens and plane-plane cases, the 1st Stokes pulse duration (FWHM) was 1.2ns at low pump energies (below the threshold of the 2nd Stokes), as shown in Figure 4.12(b). At maximum pump energy, however, depletion of the 1st Stokes by the 2nd Stokes, as shown in Figure 4.12(c), meant the FWHM of the 1st Stokes pulse was not well defined. To emphasise this point, a FWHM of 2.1ns was measured for the depleted pump pulse, compared with the 1.5ns incident pump pulse. In the microlens case, the pulse duration of the 2nd Stokes was measured to be 1.6ns and the 3rd to be 0.9ns. Pulse durations of 1.1ns and 0.8ns for the 2nd and 3rd Stokes respectively were measured for the plane-plane device. Due to the significant conversion from 2nd to 3rd Stokes in the microlens cavity, it appears depletion has artificially increased the FWHM of the 2nd Stokes at maximum pump power, as a Raman pulse duration longer than that of the pump pulse is not expected [3], [25]–[27]. This can be seen in Figure 4.13(a), with a slight shoulder seen at the trailing edge of the pulse, while the corresponding 2nd Stokes pulse from the plane-plane resonator, shown in Figure 4.14(a) has no shoulder. The 3rd Stokes pulse from both the microresonator and the plane plane system are shown in Figure 4.13(b) and Figure 4.14(b), respectively.

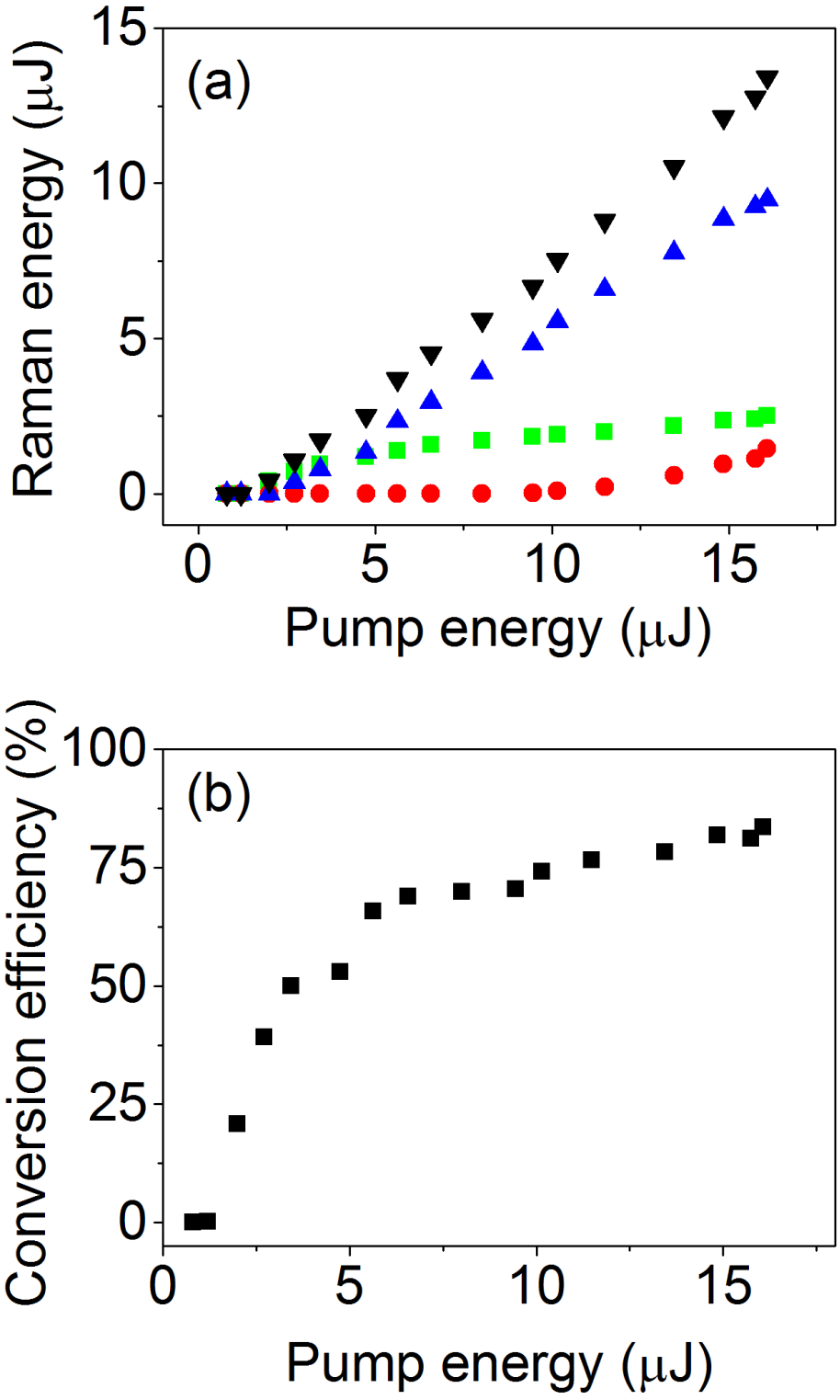

Figure 4.10. (a) Energy transfer characteristics for the 1st (green squares), 2nd (blue triangles), and 3rd Stokes orders (red circles) and the combined Raman output (inverted black triangles) and (b) overall conversion efficiency of monolithic diamond Raman laser using microlens structures.

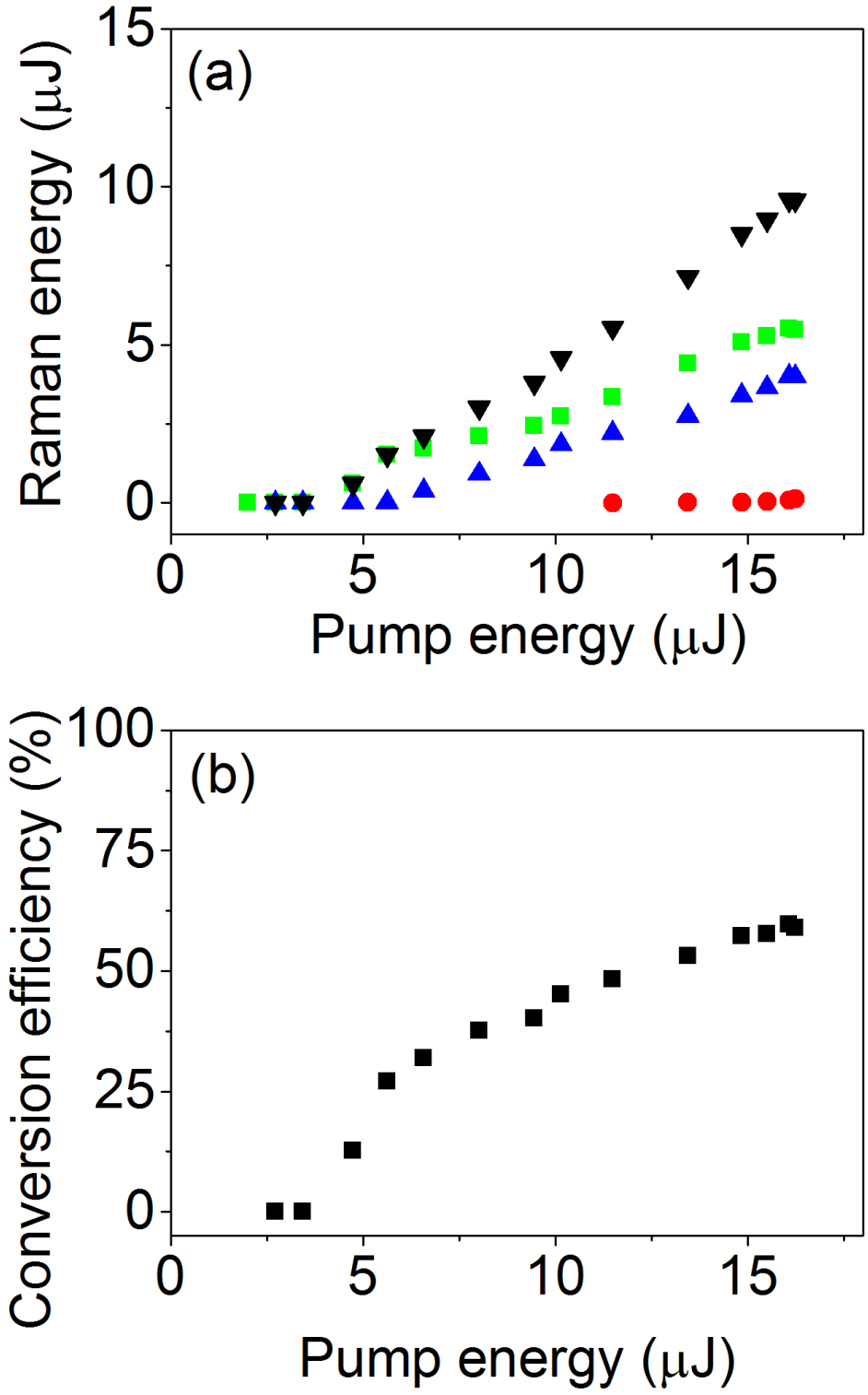

Figure 4.11. (a) Energy transfer characteristics for the 1st (green squares) 2nd (blue triangles) and 3rd Stokes orders (red circles) and the combined Raman output (inverted black triangles) and (b) overall conversion efficiency of monolithic diamond Raman laser in plane-plane cavity

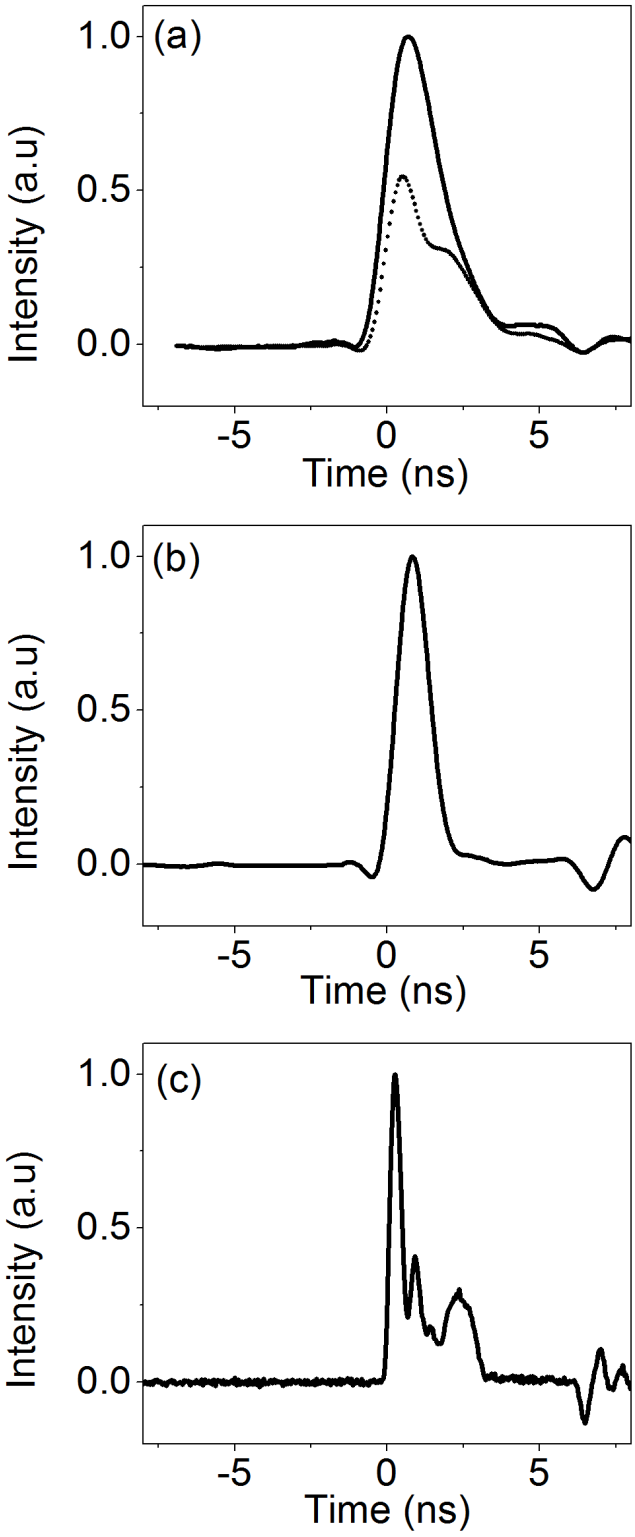

Figure 4.12. (a) Incident pump pulse (solid) compared with depleted pump pulse for the microlens case (dashed black). The 1st Stokes pulse at 573nm in the microlens case: (b) below the second Stokes threshold, and (c) at maximum pump energy with both 2nd and 3rd Stokes oscillating.

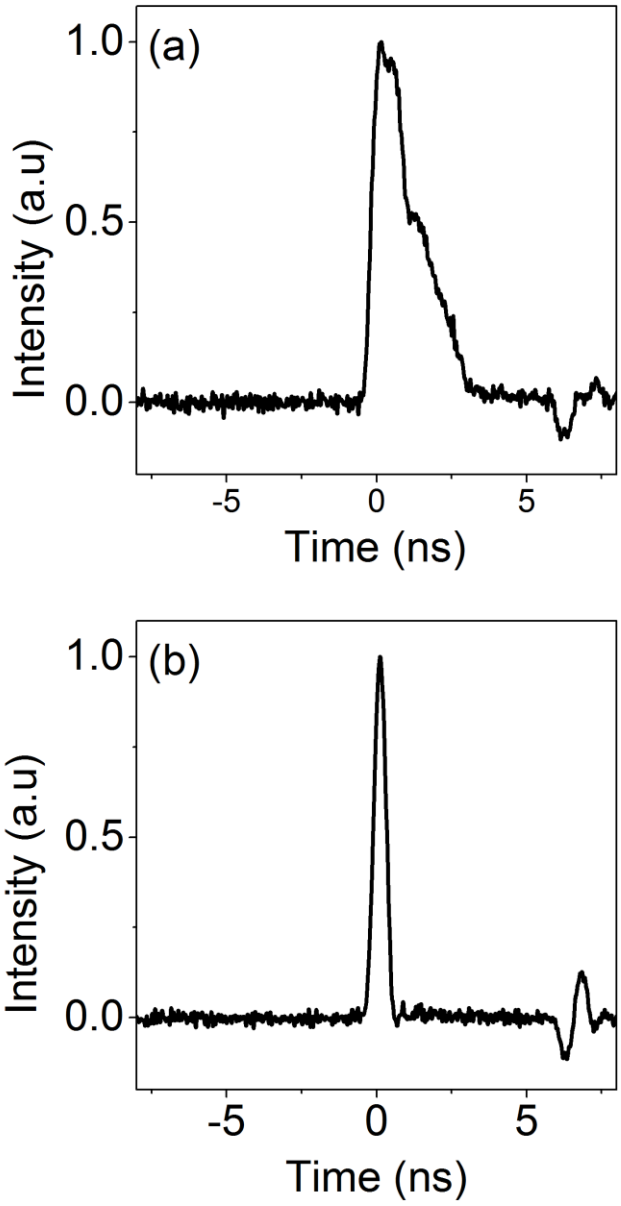

Figure 4.13. Pulse duration of (a) 2nd Stokes and (b) 3rd Stokes emission from the microlens diamond Raman laser.

Although the "cold" plane-plane resonator is on the edge of stability, laser modes suggestive of a stable cavity were observed. In order to estimate the focal length, f, of the thermal lens present in the diamond, equation 4.4 [19] is used, with the thermo optic constant values presented in Chapter 1.

$$\frac{1}{f} = \left(\frac{dn}{dT}\right)\frac{1}{K}\frac{P_s}{\pi\omega_s^2}\left(\frac{\lambda_s}{\lambda_p} - 1\right) \qquad 4.4$$

Where K is the thermal conductivity of diamond, and P_s is the average Raman output power. Given diamonds large thermal conductivity, a thermal lens with a focal length of approximately 5 metres at maximum power is calculated. This suggests the resonator modes (at pump intensities above Raman threshold) are at least in some way determined by a Gaussian duct, also known as the gain-guiding effect [28], caused by a transverse change in the Raman laser gain [29]–[31]. Such cavities have been previously demonstrated in conventional solid state lasers, with marginally stable resonators producing laser operation [28]. Furthermore, emission with Gaussian like intensity profiles has been demonstrated [28]. It is thought that the Gaussian pump profile causes a transverse gradient in the Raman gain profile; which, similarly to [28], causes modal confinement, providing a stable resonator.

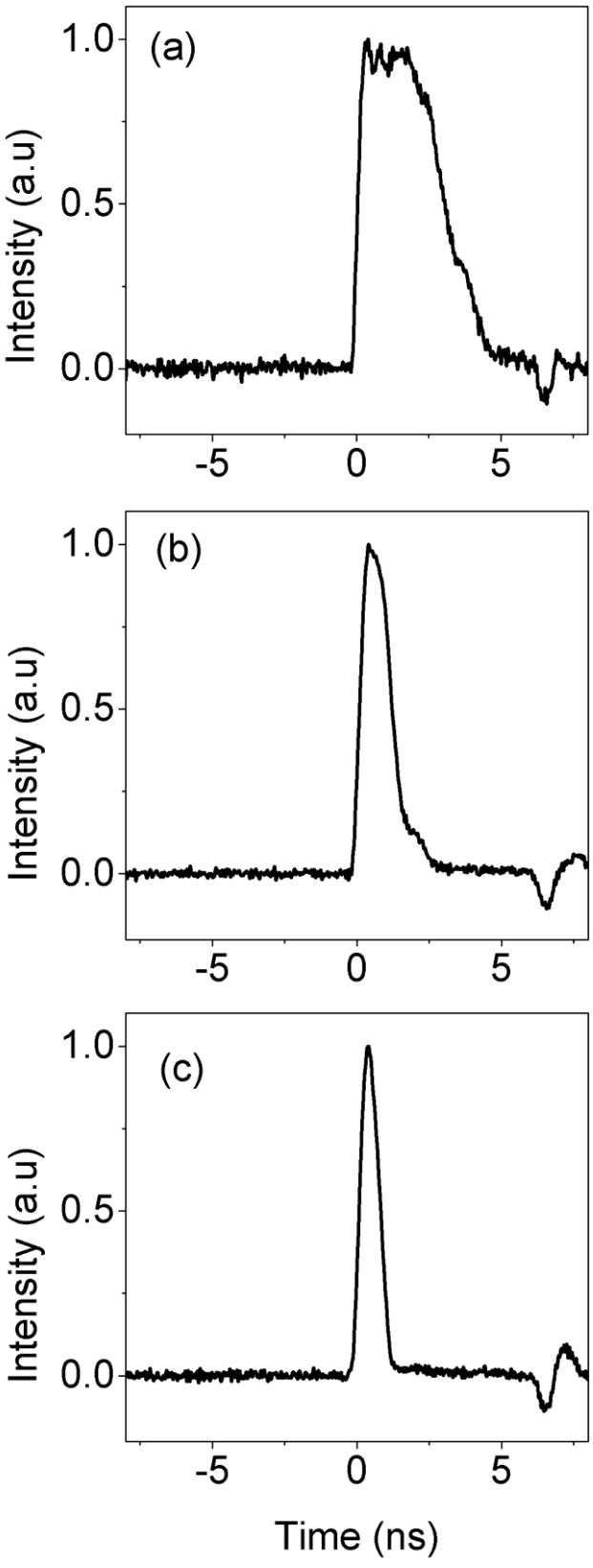

Figure 4.14. Pulse duration of (a) 1st Stokes, (b) 2nd Stokes and (c) 3rd Stokes emission from the plane-plane diamond Raman laser.

A pronounced diffraction pattern is observed in the 1st Stokes output beam from the plane-plane cavity at high pump energies (see Figure 4.15a). This may be the result of interplay between the transverse mode and the spatially varying pump depletion and hence gain. In the case of the microlens cavity, the diffraction pattern is less pronounced (see Figure 4.15b), perhaps due to the microlens structure stabilising the transverse mode. More work is required to confirm these effects.

This demonstration highlights the ease with which emission at the 1st, 2nd and 3rd Stokes wavelengths can be generated in monolithic diamond Raman lasers. However, if only yellow output (573nm) is desired, the use of coatings with greater transmission for the higher Stokes orders is likely to improve the conversion efficiency to the yellow by eliminating cascaded Raman conversion. This may also improve the output beam quality at the 1st Stokes wavelength.

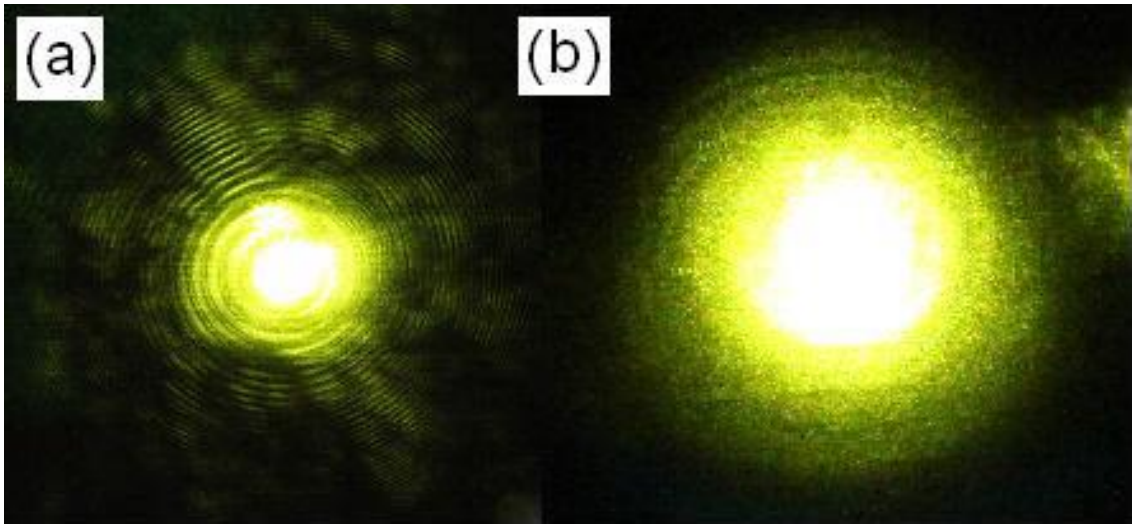

Figure 4.15. The 1st Stokes output beam at maximum pump pulse energy from the plane-plane (a) and micro-lens (b) cavities. (Not to scale.)

4.3 Intra-cavity mode-locked diamond Raman laser

In this section, further shortening of the pulse duration of compact Raman lasers will be investigated. We explore an intra-cavity approach to ultrafast Raman

pulse generation in diamond, implementing a system similar to that shown in Figure 4.18(b). Such a system could lead to the eventual simplification of the generation of picosecond Raman pulses, removing the requirement to match cavity lengths, as well as significantly reduce the size of systems of this nature. Using the high Raman gain of diamond and high intra-cavity fields within a passively modelocked laser, a maximum 1240nm output power of 350mW at a repetition rate of 85MHz was obtained at a diode pump power of 15.5W. There are, however, several hurdles to overcome when taking an intra-cavity approach. On the one hand, this may provide a more compact, cheaper alternative to external cavity approaches by removing the need for a separate mode-locked pump laser, as seen in Figure 4.18(a). Furthermore, introducing a saturable absorber with a dual band rear mirror (1064nm and 1240nm in this case) may, in the future, eliminate the requirement to precisely match cavity lengths, with the principle shown in Figure 4.18(c). On the other hand, an intra-cavity approach couples two competing nonlinearities; the saturable absorber introducing a loss to the fundamental field which reduces with intensity, while the Raman effect introduces a loss which increases with intensity. This has the potential to inhibit stable CW mode-locking [32].

Further problems are introduced by optical damage to the diamond's anti-reflection coatings and to the saturable absorber used in the fundamental cavity. With the damage threshold on both saturable absorber and optical coatings deposited on diamond hindering progress, external cavities have to date produced higher power, more stable results [7]–[9], [13].

Mode locked pump sources have been used in external cavity systems [7]–[9], [13], with Raman pulse durations as short as 95fs achieved when a diamond Raman laser was synchronously pumped with a Ti:Sapphire laser [9]. The external cavity Raman laser had a cavity length tuning range of a mere 2μm, meaning precise alignment was essential. High average powers have also been realised using diamond as the Raman medium, with 2.21W at a Raman shifted wavelength of 573nm was achieved with pulse durations of 21ps at a repetition rate of 78MHz [8].

Self-Raman lasers have also been used to create mode-locked output [32]–[34] which, by nature, utilizes an intra-cavity approach. As discussed in Chapter 1, the Raman active materials used in a self-Raman system must also have the ability to host laser active ions. In these cases KGW, YVO_4 and $GdWO_4$ are used as the laser host/Raman active material, and are doped with neodymium. Stable CW mode-locking has been reported in [32] using an Nd:YVO_4 self-Raman laser. Pumped with a 20W fibre coupled diode, an average output power of 340mW was achieved at a repetition rate of 77MHz, and pulse duration of 3.8ps. It is also noted that a higher power of 420mW was achieved using a longer laser/Raman crystal; however, in depth results are not presented.

Figure 4.18 shows schematic diagrams of three possible ways of achieving ultrafast Raman pulses. Figure 4.16. (a) represents an external cavity synchronously pumped Raman laser, with the requirement of precise cavity length matching. Figure 4.17. (b) shows an intra-cavity Raman laser pumped by a passively mode locked laser, using a dichroic mirror to separate the two cavities, requiring length matching, while (c) represents the use of a dual band saturable mirror (SAM) to remove the arduous task of cavity length matching.

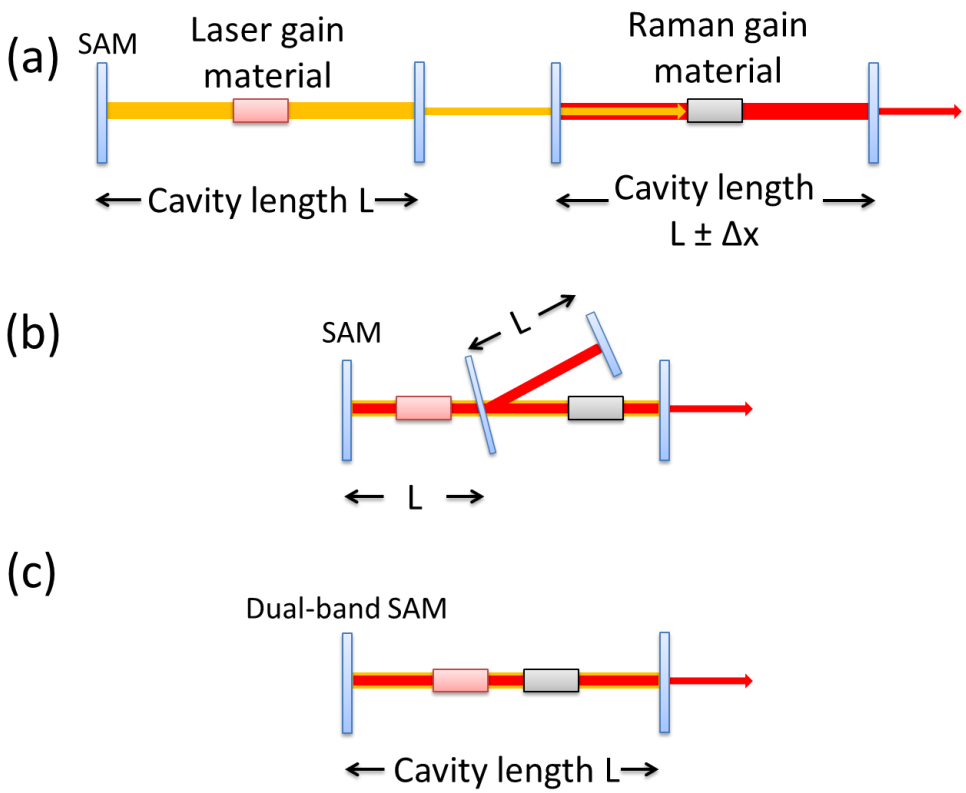

Figure 4.18. Schematic diagram of (a) an external cavity synchronously pumped Raman laser, (b) an intra-cavity Raman laser pumped by a passively mode locked laser, using a dichroic mirror to separate the two cavities and (c) Raman laser pumped in a shared cavity using a dual band SAM used to mode lock the fundamental laser.

4.3.1 Cavity design

The initial cavity design used to produce picosecond pulses at the Raman shifted wavelength of 1240nm can be seen in Figure 4.19. A dichroic mirror, HR at 1240nm and HT at 1064nm was used to couple the fundamental and Raman cavities. This minimized the losses in the Raman cavity, removing loss which would be seen at both Nd:YVO_4 surfaces, as well as high non-saturable losses in the saturable absorber of 1.2%. The fundamental cavity incorporates two mirrors with a radius of curvature of 500mm. The purpose of these mirrors is to control the cavity mode radius both in the gain material and on the saturable absorber with an increasing thermal lens, maintaining mode matching of both the diode

pump and the Raman laser cavity, which does not experience the thermal lens in the laser gain material. The lengths of both cavities were matched in order to ensure the oscillating fundamental and Raman pulses pass through the diamond simultaneously, allowing the Raman pulse to efficiently extract gain. Raman emission was observed over a cavity length range of approximately 1mm. The additional 500mm ROC mirrors do, however, prevent tight focussing in the diamond while maintaining the necessary mode size in the gain medium and saturable absorber; limiting intra-cavity intensities with a relatively large fundamental mode radius of 90μm used. The modelled fundamental cavity mode sizes throughout the cavity can be seen in Figure 4.20. The Raman cavity was designed to have a similar mode radius in the diamond (~80μm) to that of the fundamental mode radius. The cavity mode of the synchronously pumped Raman laser can be seen in Figure 4.21.

A 25W 808nm diode (Coherent FAP81 – 25c – 800b) was collimated and focused to a spot size of 400μm in the Nd:YVO_4 laser crystal. A SAM from BATOP GmbH was used, part number SAM-1064-2-1ps-x, with a modulation depth of 2% and a non-saturable loss of 1.2%. This modulation depth was chosen as it was similar to that used in a Raman system reported in [32].

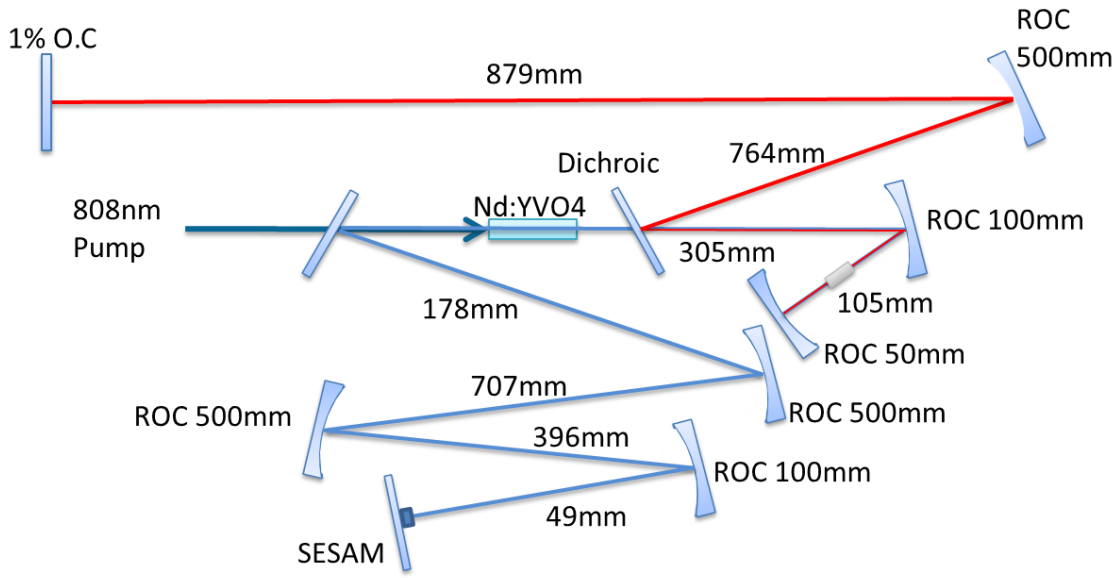

Figure 4.19. Cavity design of mode-locked Diamond Raman laser. An 8mm long Nd:YVO_4 is pumped with an 808nm diode, and mode-locked with a saturable absorber. The fundamental and Raman cavities are coupled with a dichroic mirror, HR at 1240nm and HT at 1064nm.

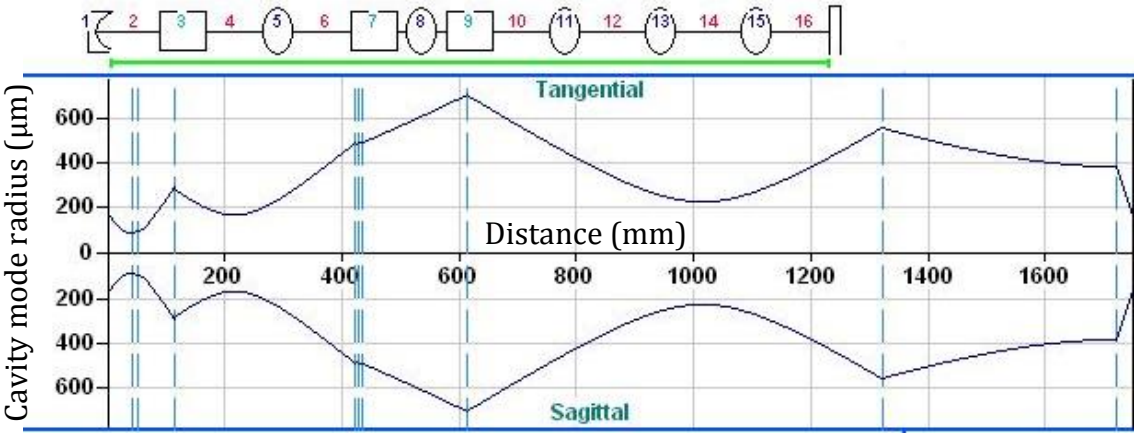

Figure 4.20. Cavity mode of fundamental mode locked Nd:YVO_4 laser.

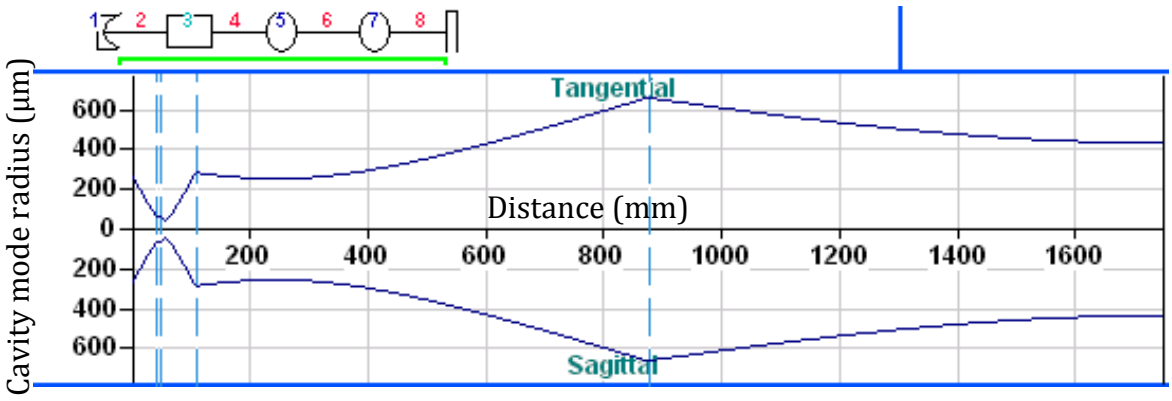

Figure 4.21. Cavity mode of synchronously pumped Raman laser.

A 4:1 ratio of pump spot radius was chosen in the gain medium and SAM. This was found to provide stable CW mode-locking at around 6W of absorbed pump power when the cavity had a 20% output coupling and no diamond in the cavity. In an HR-HR cavity, stable CW mode-locking operation was observed at absorbed pump powers of below 4W.

4.3.2 Results

Stable CW mode-locked Raman output at a power of 350mW and a repetition rate of 85MHz was briefly achieved under a diode pump power of 15.5W. However, due to instabilities in the fundamental oscillation introduced by the Raman conversion process, shown in Figure 4.22, stable CW mode-locking was very difficult to obtain. Figure 4.22 suggests that the Raman process decreases the oscillating fundamental power, which in turn reduces the Raman field until no Raman output is obtained. The fundamental field is then free to increase in intensity which starts the almost cyclical process over again. Weitz et al [32] observed stable CW mode-locking only when the wings of the fundamental pulse were Raman converted; however, this was not observed in this system, possibly due to the Raman laser not running high enough above threshold. This measurement was taking using a photodetector with a 1ns rise time and an Agilent Infiniium oscilloscope with a bandwidth of 2GHz.

Coupled with problems arising from optical damage to both the saturable absorber and the optical coatings deposited on the diamond surfaces, caused

particularly when q-switching instabilities occurred and shown in Figure 4.23, this maximum output power was difficult to reproduce. The results presented in this section were therefore all obtained at an average output power of 40mW.

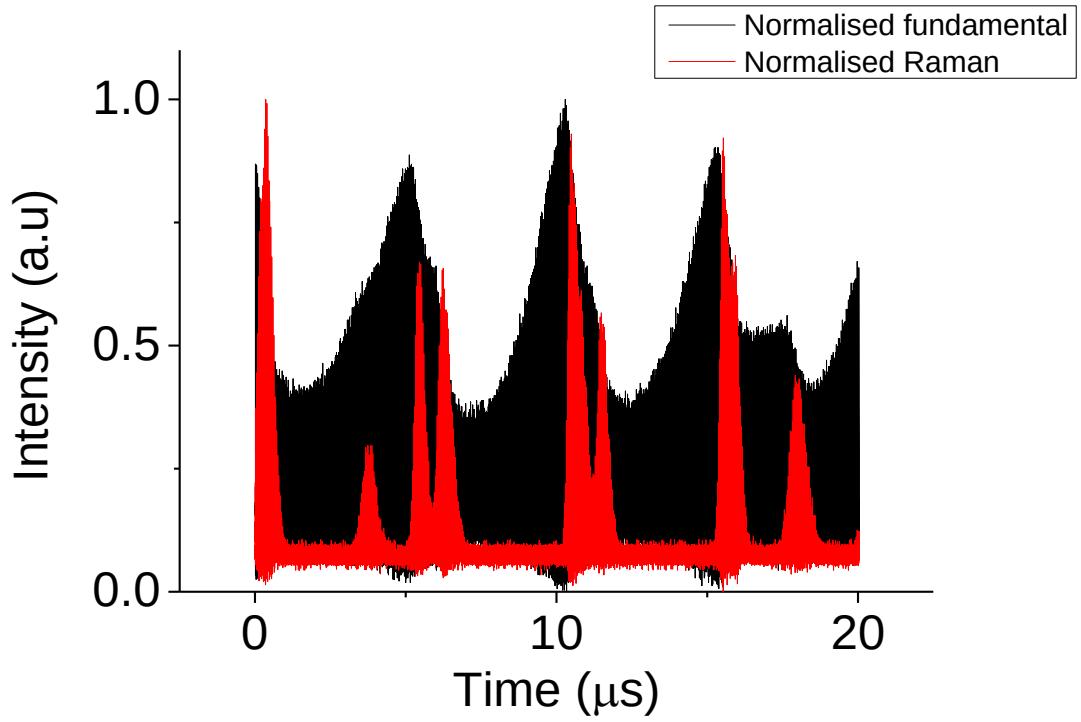

Figure 4.22. Instabilities in fundamental field introduced by Raman field with a Raman output power of 40mW.

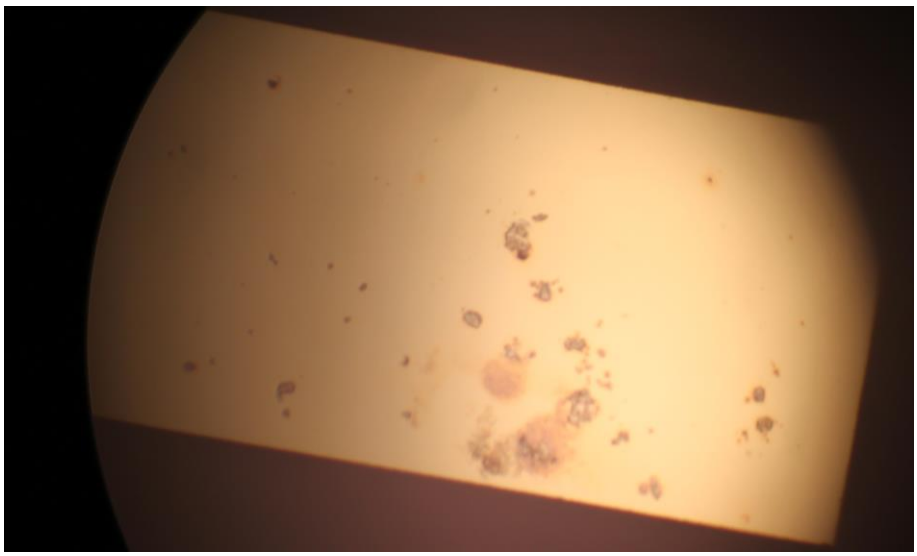

Figure 4.23. Optical damage of diamond coatings caused by high intensity oscillating fundamental and Raman fields.

Mode locking of the fundamental oscillation and Raman output was confirmed via the RF spectra shown in Figure 4.24 and Figure 4.25. Each harmonic is separated by 85MHz, the rep rate of the mode locked laser, which is consistent with the cavity length. The RF spectra were measured using a fibre coupled Agilent E4407B 26.5GHz RF spectrum analyser.

Although the intensities of the peaks in the Raman RF are not all equal (a characteristic of stable mode-locking being equal peaks in the RF spectrum[35], [36]), there is not a steady decline in intensity with increasing harmonic, typical of that seen in the RF spectrum of CW lasers [35]. Similarly varying RF peaks have been reported in mode-locked semiconductor lasers [35]–[37], however the cause of such a phenomena is not clear.

A scanning mirror auto-correlator was used to measure the pulse width, with an 808nm laser diode implemented as a nonlinear detector [38]. A pulse duration of 21ps was measured at the fundamental wavelength, shown in Figure 4.26, produced with a cavity which consisted solely of HR mirrors and a SAM as the active mode locking element, as discussed previously. Pulse shortening was observed in the Raman shifted pulses, where a duration of 15ps was measured from the autocorrelation shown in Figure 4.27.

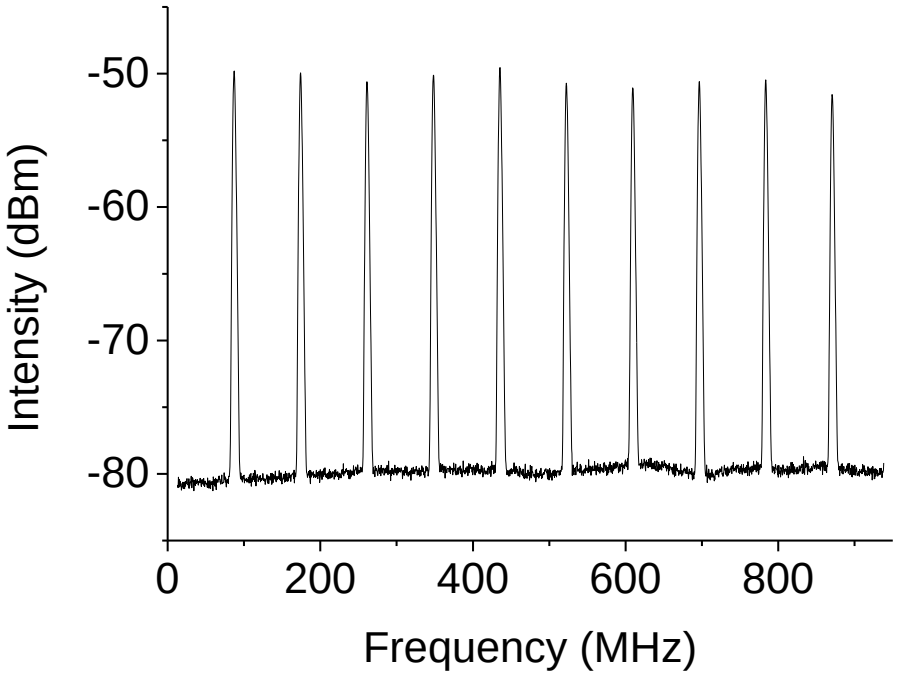

Figure 4.24. RF spectrum of fundamental leakage with Raman oscillation present. Measured at resolution bandwidth of 3MHz.

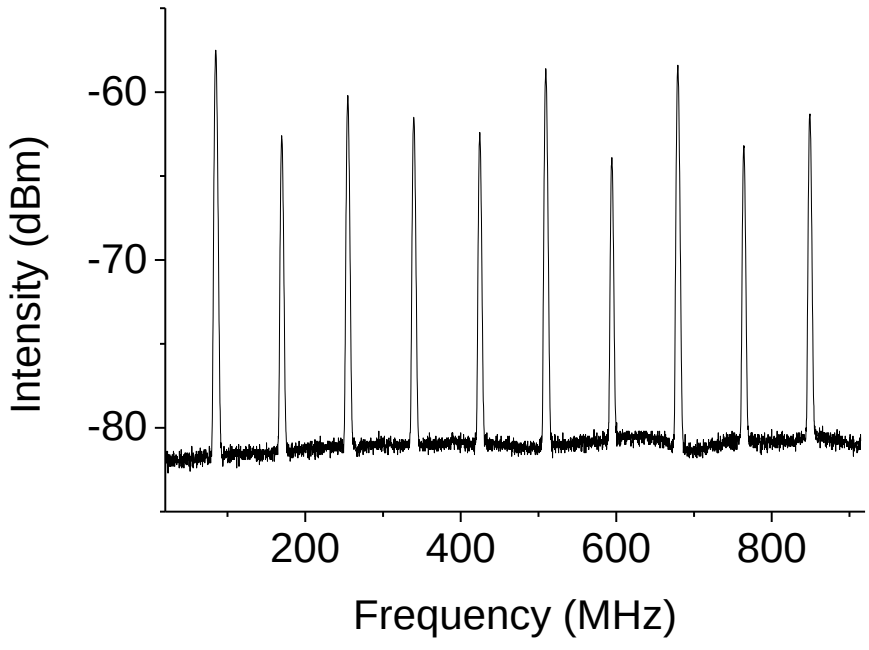

Figure 4.25. RF spectrum of Raman emission at an average output power of 40mW. Measured at resolution bandwidth of 3MHz.

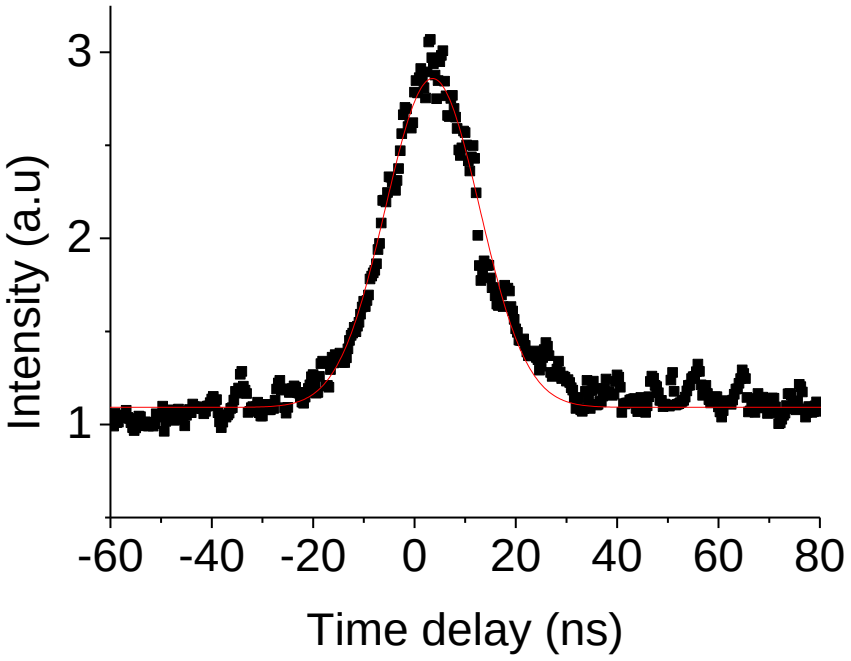

Figure 4.26. Auto-correlator intensity profile of fundamental leakage at 1064nm with no output coupling (HR – SAM cavity) and Raman oscillation present.

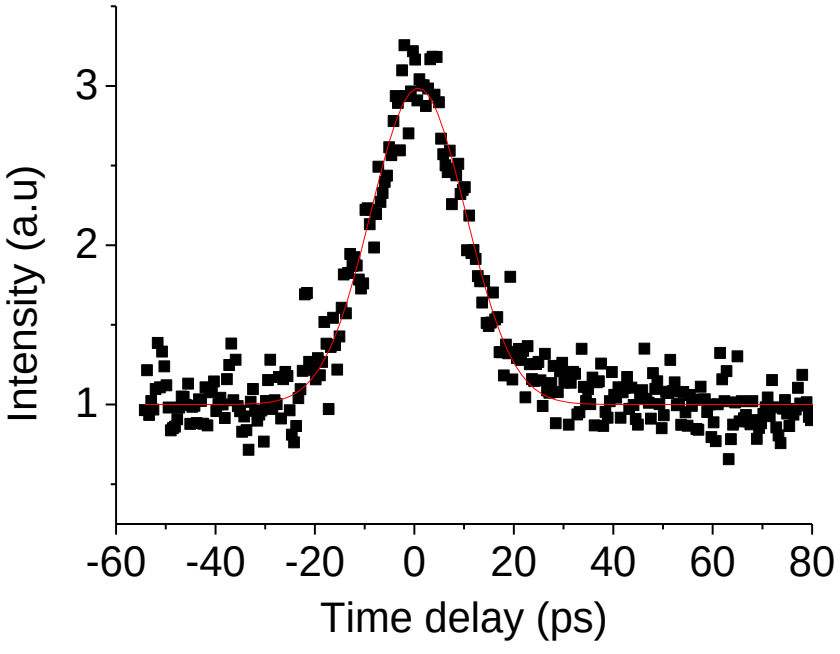

Figure 4.27. Auto-correlator intensity profile of Raman output at 1240nm and an output power of 40mW. A pulse duration of 15ps was measured.

The large scatter range seen in the Raman autocorrelation is thought to be caused by the cavity instability. A value of 15ps is, however, in the range of the expected pulse duration given the 21ps fundamental, with pulse shortening a common occurrence in Raman lasers in both diamond [1], [8], [11], [13] and other conventional Raman materials [26], [39], [40]

4.3.3 Alternate cavity design

In order to reduce the mode radius, and hence increase the intra-cavity intensity in the diamond allowing access to Raman laser action further above threshold, a simplified cavity was used, seen in Figure 4.28.. In this cavity setup, the second mirror with an ROC of 500mm was removed from the cavity, allowing tighter focusing in the diamond. The cavity was designed for optimal operation at an absorbed pump power of 10W, giving an estimated thermal lens of 300mm in the vanadate crystal. With this configuration, the spot size in the diamond was reduced from the 80µm used in the previous cavity design, to approximately 30µm for both the fundamental and Raman beams. The spot sizes are estimated using ABCD matrix software.

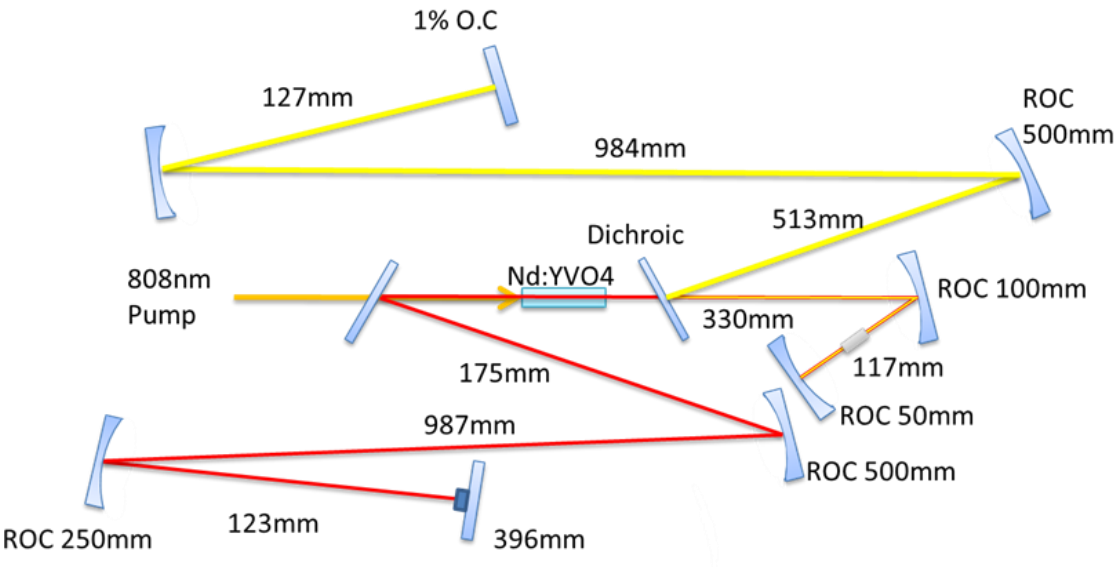

Figure 4.28. Simplified cavity design optimised for 10W absorbed pump power and thermal lens strength of approximately 300mm.

Raman emission was achieved using this cavity, however no improvement in performance was observed, with results very similar to those presented above obtained. This result highlights the difficulty in obtaining stable mode-locked Raman emission using an intra-cavity approach. Even after a reasonably exhaustive search for optimal cavity parameters, stable pulsed output was only briefly observed.

4.4 Conclusions and future work

In conclusion, noteworthy results were obtained with an external cavity monolithic diamond Raman laser, with which attempts to develop a compact, robust device resulted in the achievement of an 84% conversion efficiency. The ease with which the 3rd Stokes was reached, with such a large output coupling on the 2nd Stokes, opens up the opportunity to explore a plethora of new, hard to reach wavelengths, for example in the eye safe region of the optical spectrum, and potentially further into the mid IR region, with potential applications in defence and plastic welding [41]. Further optimisation of optical coatings for the current system, accessing the yellow orange region of the spectrum with applications in ophthalmology [42], [43], will lead to higher conversion efficiencies to the 1st Stokes wavelength of 573nm.

Furthermore, the successful demonstration of a plane-plane monolithic diamond Raman laser may have implications for further work. Unlike the microcavity, which, with a curved end mirror has a pre-determined cavity mode, a plane-plane resonator has no constraints. This permits the use of larger pump spot sizes, allowing increased pump energies whilst maintaining intensities below the damage threshold of the optical coatings, potentially allowing high energy output from a very similar device to that presented in this chapter.

In addition to this work, a compact intra-cavity mode locked diamond Raman laser was designed and built; however, difficulties arising from competition in nonlinearities caused this work to be largely unsuccessful. Furthermore, optical damage to both the optical coatings on the diamond surfaces and the saturable

absorber caused further complications. Although the prospect of developing a simple system which removes the arduous task of cavity length matching is enticing, it appears that this particular method is less fruitful than external cavity approaches [6], [8], [44], which seem to be the more promising route for picosecond Raman generation.

Bibliography

[1] A. McKay, H. Liu, O. Kitzler, and R. P. Mildren, "An efficient 14.5 W diamond Raman laser at high pulse repetition rate with first (1240 nm) and second (1485 nm) Stokes output," *Laser Phys. Lett.*, vol. 10, no. 10, p. 105801, 2013.

[2] J.-P. M. Feve, K. E. Shortoff, M. J. Bohn, and J. K. Brasseur, "High average power diamond Raman laser," *Opt. Express*, vol. 19, no. 2, pp. 913–922, 2011.

[3] A. Sabella, J. A. Piper, and R. P. Mildren, "Efficient conversion of a 1.064μm Nd:YAG laser to the eye-safe region using a diamond Raman laser," *Opt. Express*, vol. 19, no. 23, pp. 23554–23560, 2011.

[4] R. P. Mildren and A. Sabella, "Highly efficient diamond Raman laser," *Opt. Lett.*, vol. 34, no. 18, pp. 2811–2813, 2009.

[5] A. Sabella, J. A Piper, and R. P. Mildren, "Diamond Raman laser with continuously tunable output from 3.38 to 3.80 μm.," *Opt. Lett.*, vol. 39, no. 13, pp. 4037–40, 2014.

[6] D. C. Parrotta, A. J. Kemp, M. D. Dawson, and J. E. Hastie, "Tunable continuous-wave diamond Raman laser," *Opt. Express*, vol. 19, no. 24, pp. 24165–24170, 2011.

[7] E. Granados, D. J. Spence, and R. P. Mildren, "Deep ultraviolet diamond Raman laser.," *Opt. Express*, vol. 19, no. 11, pp. 10857–63, 2011.

[8] D. J. Spence, E. Granados, and R. P. Mildren, "Mode-locked picosecond diamond Raman laser," *Opt. Lett.*, vol. 35, no. 4, pp. 556–558, 2010.

[9] M. Murtagh, J. Lin, R. P. Mildren, and D. J. Spence, "Ti : sapphire-pumped diamond Raman laser with sub-100-fs pulse duration," *Opt. Lett.*, vol. 39, no. 10, pp. 2–5, 2014.

[10] R. P. Mildren, J. E. Butler, and J. R. Rabeau, "CVD-diamond external cavity Raman laser at 573 nm," *Opt. Express*, vol. 16, no. 23, pp. 18950–18955, 2008.

[11] A. Sabella, J. A. Piper, and R. P. Mildren, "1240nm diamond Raman laser operating near the quantum limit," *Opt. Lett.*, vol. 35, no. 23, pp. 3874–3876, 2010.

[12] A. McKay, O. Kitzler, and R. P. Mildren, "Simultaneous brightness enhancement and wavelength conversion to the eye-safe region in a high-power diamond Raman laser," *Laser Photon. Rev.*, vol. 8, no. 3, pp. L37–L41, 2014.

[13] A. M. Warrier, J. Lin, H. M. Pask, R. P. Mildren, D. W. Coutts, and D. J. Spence, "Highly efficient picosecond diamond Raman laser at 1240 and 1485 nm," *Opt. Express*, vol. 22, no. 3, p. 3325, 2014.

[14] A. K. McQuillan, W. R. L. Clements, and B. P. Stoicheff, "Stimulated Raman Emission in Diamond: Spectrum, Gain, and Angular Distribution of Intensity," *Phys. Rev. A*, vol. 1, no. 3, pp. 628–635, 1970.

[15] N. Laurand, C. L. Lee, E. Gu, J. E. Hastie, S. Calvez, and M. D. Dawson, "Microlensed microchip VECSEL.," *Opt. Express*, vol. 15, no. 15, pp. 9341–6. 2007.

[16] N. Laurand, C.-L. Lee, E. Gu, S. Calvez, and M. D. Dawson, "Power-Scaling of Diamond Microlensed Microchip Semiconductor Disk Lasers," *IEEE Photonics Technol. Lett.*, vol. 21, no. 3, pp. 152–154, 2009.

[17] N. Laurand, C. Lee, E. Gu, J. E. Hastie, A. J. Kemp, S. Calvez, and M. D. Dawson, "Array-Format Microchip Semiconductor Disk Lasers," *IEEE J. Quantum Electron.*, vol. 44, no. 11, pp. 1096–1103, 2008.

[18] X. Li, H. M. Pask, A. J. Lee, Y. Huo, J. A Piper, and D. J. Spence, "Miniature wavelength-selectable Raman laser: new insights for optimizing performance.," *Opt. Express*, vol. 19, no. 25, pp. 25623–31, 2011.

[19] H. M. Pask and J. A. Piper, "The design and operation of all-solid-state Raman lasers," *Prog. Quantum Electron.*, vol. 27, pp. 3–56, 2003.

[20] D. J. Spence, P. Dekker, and H. M. Pask, "Modeling of Continuous Wave Intracavity Raman Lasers," *Sel. Top. Quantum Electron. IEEE J.*, vol. 13, no. 3, pp. 756–763, 2007.

[21] H. W. Choi, E. Gu, C. Liu, C. Griffin, J. M. Girkin, I. M. Watson, and M. D. Dawson, "Fabrication of natural diamond microlenses by plasma etching," *J. Vac. Sci. Technol. B Microelectron. Nanom. Struct.*, vol. 23, no. 1, p. 130, 2005.

[22] C.-L. Lee, "Micro-scale Processing of Diamond Structures and Devices," *PhD Thesis*, University of Strathclyde, 2008.

[23] V. G. Savitski, I. Friel, J. E. Hastie, M. D. Dawson, D. Burns, and A. J. Kemp, "Characterization of Single-Crystal Synthetic Diamond for Multi-Watt Continuous-Wave Raman Lasers," *Quantum Electron. IEEE J.*, vol. 48, no. 3, pp. 328–337, 2012.

[24] O. Kitzler, "External Cavity Diamond Raman Lasers for High Power Continuous-Wave Beam Conversion," Macquarie Universty, 2014.

[25] E. Granados and D. J. Spence, "Pulse compression in synchronously pumped mode locked Raman lasers.," *Opt. Express*, vol. 18, no. 19, pp. 20422–7, 2010.

[26] Y. B. Band, J. R. Ackerhalt, J. S. Krasinski, and D. F. Heller, “Intracavity Raman lasers,” *IEEE J. Quantum Electron.*, vol. 25, no. 2, pp. 208–213, 1989.

[27] R. Frey, A. De Martino, and F. Pradbre, “High-efficiency pulse compression with intracavity Raman oscillators,” vol. 8, no. 8, pp. 437–439, 1983.

[28] F. Salin and J. Squier, “Gain guiding in solid-state lasers,” *Optics Letters*, vol. 17, no. 19, pp. 1352–1354, 1992.

[29] A. E. Siegman, *Lasers*. University Science Books, 1986.

[30] H. Kogelnik, “On the Propagation of Gaussian Beams of Light Through Lenslike Media Including those with a Loss or Gain Variation,” *Appl. Opt.*, vol. 4, no. 12, p. 1562, 1965.

[31] L. Casperson, “The Gaussian Mode In Optical Resonators With A Radial Gain Profile,” *Appl. Phys. Lett.*, vol. 12, no. 10, p. 355, 1968.

[32] M. Weitz, C. Theobald, R. Wallenstein, and J. a. L’huillier, “Passively mode-locked picosecond Nd:YVO_4 self-Raman laser,” *Appl. Phys. Lett.*, vol. 92, no. 9, p. 091122, 2008.

[33] Z. H. Li, J. Y. Peng, and Y. Zheng, “CW mode-locked self-Raman 1.17μm Nd: GdVO4 laser with a novel long cavity,” *Opt. Laser Technol.*, vol. 58, no. 3, pp. 39–42, 2014.

[34] D. S. Chunaev, T. T. Basiev, V. a. Konushkin, a. G. Papashvili, and A. Y. Karasik, “Synchronously pumped intracavity YLF–Nd–KGW picosecond Raman lasers and LiF:F_2 amplifiers,” *Laser Phys. Lett.*, vol. 5, no. 8, pp. 589–592, 2008.

[35] K. G. Wilcox and A. C. Tropper, “Comment on SESAM-free mode-locked semiconductor disk laser,” *Laser Photon. Rev.*, vol. 7, no. 3, pp. 422–423, 2013.

[36] L. Kornaszewski, G. Maker, G. Malcolm, M. Butkus, E. U. Rafailov, and C. Hamilton, “Reply to comment on SESAM-free mode-locked semiconductor disk laser,” *Laser Photon. Rev.*, vol. 7, no. 4, pp. 555–556, 2013.

[37] L. Kornaszewski, G. Maker, G. P. A. Malcolm, M. Butkus, E. U. Rafailov, and C. J. Hamilton, “SESAM-free mode-locked semiconductor disk laser,” *Laser Photon. Rev.*, vol. 6, no. 6, pp. L20–L23,○ 2012.

[38] Y. Takagi, T. Kobayashi, K. Yoshihara, and S. Imamura, “Multiple- and single-shot autocorrelator based on two-photon conductivity in semiconductors,” *Optics Letters*, vol. 17, no. 9, pp. 658–660, 1992.

[39] J. T. Murray, W. L. Austin, and R. C. Powell, “Intracavity Raman conversion and Raman beam cleanup,” *Opt. Mater.*, vol. 11, no. March 1999, pp. 353–371, 2010.

[40] A. I. Vodchits, D. N. Busko, V. A. Orlovich, P. A. Apanasevich, V. S. Gorelik, N. V Tcherniega, and A. D. Kudryavtseva, “Kilohertz Raman Lasers Based on BNO and KGW Crystals for a Wide Spectral Range,” *J. Appl. Spectrosc.*, vol. 77, no. 4, pp. 576–582, 2010.

[41] R. Klein, *Laser Welding in Plastics*. Wiley VCH Verlag GmbH, 2012.

[42] J. R. F. De Abreu, “The tunable dye laser in the management of retinal vascular disease,” *Int. Opthalmology*, vol. 196, pp. 193–196, 1988.

[43] F. A. L’Espernace, “Trans-spectral Organic Dye Laser photocoagulation,” *Tr. Am. Opth. Soc*, vol. LXXXIII, no. Fig 1, 1985.

[44] A. M. Warrier, J. Lin, H. M. Pask, R. P. Mildren, D. W. Coutts, and D. J. Spence, “Highly efficient picosecond diamond Raman laser at 1240 and 1485nm,” *Optics Express*, vol. 22, no. 3, pp. 3325–3333, 2014.

Chapter 5 -Laser induced damage threshold of diamond surfaces

In this section, the laser induced damage threshold (LIDT) of state of the art diamond surfaces will be studied and quantified for nanosecond pulse durations. Although not well studied, this value is an important quantity to know, as it gives an upper limit to the intensities used when employing diamond in laser cavities. This chapter also begins the process of analysing the determining factors in the damage threshold of diamond surfaces; whether it is an intrinsic value or whether extrinsic factors such as surface finish have an impact (as has been observed in high optical quality fused silica [1]). If it is the latter, there may be measures available to increase the surface LIDT of the material, potentially close to the far higher bulk damage threshold [2], [3].

Diamond surfaces with different quality finishes, determined by the type of mechanical polish and quantified using atomic force microscopy (AFM), are studied, with the LIDT of each surface compared. Attempts to improve the LIDT of each diamond were also undertaken, using a less aggressive chemically assisted etch to remove 5μm from the surface.

5.1 Laser induced damage threshold

The LIDT of optical surfaces is a crucial value, as going above such intensities/ fluences (pulse energy per unit area) can cause irreversible damage to optical systems. The LIDT of optical quality single crystal CVD diamond has not been extensively investigated. This is probably due to the novelty of material of this grade. The damage characteristics of the more readily available polycrystalline diamond have, however, been examined.

Sussmann et al [4] considered polycrystalline CVD diamond, with the LIDT at several wavelengths and surface finishes investigated. At the widely used Nd:YAG emission wavelength of 1064nm, values between 21 Jcm^{-2} and 31Jcm^{-2} were reported for a pulse duration of 12.5ns. Values at shorter wavelengths were

found to be slightly lower than these values, while at the CO_2 laser wavelength of 10.6μm the LIDT was significantly higher. Natural single crystal type IIa diamond was also investigated in this study; however, only at 10.6μm. Perhaps somewhat expectedly, this material was found to have a higher LIDT than the polycrystalline synthetic material (93 Jcm^{-2} compared to 66 Jcm^{-2}).

Polycrystalline diamond thin films have also been investigated [5]. Using a 50ns, 1064nm q-switched Nd:YAG laser, an LIDT of 7 Jcm^{-2} was observed for a 2.26μm thick diamond film.

Due to interest in the microfabrication of conductive amorphous carbon wires inside diamond, the damage threshold of the bulk material has been the subject of recent studies [2], [3]. Optical breakdown was seen at an incident pulse fluence of very approximately 80Jcm^{-2} in [2], using pulses with durations of 30ps. Significantly lower values are reported using pulses with a duration of 300ps in [3], with polycrystalline CVD diamond damaging at pulse fluences between 2Jcm^{-2} and 4Jcm^{-2}. Interestingly in this study, however, single crystal type IIa natural diamond was found to have a bulk LIDT between 10 Jcm^{-2} and 80 Jcm^{-2}. In the studies discussed in this section, all comparisons show that the LIDT decreases as the pulse lengths shortens, with a systematic study of the LIDT of polycrystalline diamond surfaces confirming this [6]. This relationship with pulse duration has also been confirmed in other, better studied optical materials including fused silica and sapphire[1], [7].

Comparing diamond to the more comprehensively studied fused silica provides some insight. Even with such a widely used optical material, published LIDT results have widely varied; for example Natoli et al [8] observed a value of 70 Jcm^{-2} on the surface of fused silica samples (200 Jcm^{-2} in the bulk material) with a pulse duration of 7ns at 1064nm. Soileau et al [9] presented markedly different values, with a quoted bulk LIDT of 18kJcm^{-2}.

Perhaps the most in depth study of the LIDT of fused silica was conducted by Smith et al [1]. Bulk damage of the material was observed at laser fluences above 3854 ± 85 Jcm^{-2} in the nanosecond regime, whilst picosecond pulses resulted in a

significantly lower damage threshold of 25.4±1.0 Jcm^{-2}. From the point of view of those wishing to utilise diamond in optical systems, promising results were presented when discussing the role the surface finish plays on the surface LIDT. It was found that, implementing the right surface polish, the surface and bulk damage thresholds are "nearly the same", with the large statistical point to point spread of values observed for poorly polished surfaces almost non-existent.

Bloembergen [10] demonstrated that the presence of microstructures and sub-microscopic cracks (potentially prevalent in aggressively polished diamond), can lead to a significant reduction in the LIDT of a transparent dielectrics, which may explain the results observed in [1]. It is demonstrated that these imperfections cause local variations in the electric field, which can lead to an apparent reduction in the damage threshold of the material.

5.2 Experimental method

The diamond samples studied in this section were provided by Element 6 Ltd. The 4 diamond samples were 4mm x 4mm x 2mm long, each with a different mechanically polished surface. The polished samples are defined by the diamond grit size used in the polishing process, namely "grit size 33, 76 and 151" along with a further sample that had a lapped surface finish. Further studies were conducted on 0.5mm thick high optical quality "heatspreader" samples purchased from Element 6; however this investigation was less thorough due to the samples being smaller in dimensions (4mm diameter spherical surface). It should be highlighted that, other than the "heatspreader" sample, the bulk diamond samples studied in this section are of significantly poorer optical quality (high bulk dislocation density) than the Raman material presented in previous chapters.

The experimental setup used to measure the surface LIDT on single crystal diamond can be seen in Figure 5.1. A Continnum Minilite II laser was used to provide single shot laser pulses of up to 20mJ with a duration of 6.5ns, and at a wavelength of 1064nm. The laser was attenuated using a half wavelength plate

and Glan Taylor prism and focused onto the diamond surface with a 200mm focal length lens. Each pulse was fired onto a different spot on the diamond surface, with a total of ten single shots taken at each fluence. The damage threshold is defined as the "highest quantity of laser radiation incident upon the optical surface for which the extrapolated probability of damage is zero" [11]. The experimental method was adapted from ISO 11254-1 [11]. Particular attention should be made when quoting the peak fluence of the incident pulse. The peak fluence is two times the pulse energy divided by the effective beam area [12]. Neglecting the factor of 2 is a common occurrence [12], and it should be noted that it is possible some LIDT values quoted from literature may be a factor of 2 smaller than the true value.

Uncoated glass slides were used to pick off small fractions of the laser pulse to measure its energy, as well as its spatial and temporal characteristics. In order to calculate the incident fluence, the average energy and spot size of the 10 shots was used, with a typical standard deviation of around 2%. The distance between beam splitter 1 and the CCD camera (Ophir spiricon sp620u) was matched to that between beam splitter 1 and the diamond sample to allow for optimal alignment and continual monitoring of the spot size on the diamond. The beam waist was maintained at a radius of around 140μm and 175μm in the horizontal and vertical directions, respectively. In order to calculate the incident laser fluence, the effective beam area is used. Although the laser beam was multimode, the beam shape was near Gaussian; therefore the effective beam area is defined as $\frac{\pi ab}{2}$, where a and b are the beam radii ($1/e^2$) of the approximated Gaussian in the horizontal and vertical directions respectively [11]. The Rayleigh range of the beam used was much longer than the length of the crystal, therefore the spot size on the front and back surface were approximately equal.

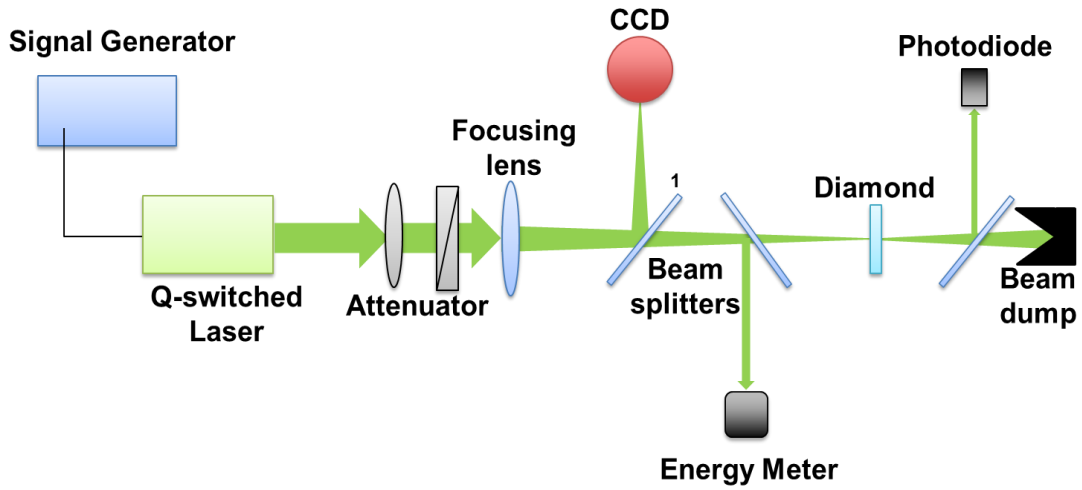

Figure 5.1. Experimental setup used to measure the LIDT of diamond for nanosecond pulses.

The LIDT of four 4mm x 4mm x 2mm diamond samples, each with a different surface finish ("fine lap", grit size 33, grit size 76 and grit size 151), was measured. Starting with a pulse energy well below the LIDT, 10 single shots were fired onto different points of the diamond surface. After the 10 shots were fired onto each diamond, the surfaces were inspected under an optical microscope. The number of damaged spots was recorded and the process was repeated for incrementally higher pulse fluences. Damage was defined as any alteration of the diamond's surface visible under an optical microscope [4], although the Normarski-type differential interference contrast microscope suggested in [11] was not available.

In each case, the value for the LIDT is taken as the x-axis crossing of the least squared linear fit (shown with dashed lines in Figure 5) to the data points between and including the last point with a damage probability of zero and the first point with a damage probability of one. The error bounds include both random errors and a 3% calibration uncertainty in the energy meter used (Ophir PE10-C).

In order to investigate the effects the surface finish has on the surface LIDT of diamond, approximately 5μm of material was removed from the top surface of a

second batch of samples using an Ar/Cl inductively coupled plasma (ICP) etch. The pre-etched samples had the same surface finish as those discussed previously. The etch was conducted by fellow PhD student Hangyu Liu, in an attempt to remove sub-surface damage on the diamond that may potentially be caused by more aggressive mechanical polishing techniques. An Ar/Cl etch was chosen as Friel et al [13] showed that the alternative, an argon oxygen plasma etch, preferentially etches scratches on the diamond surface. In contrast, an Ar/Cl etch has been shown to maintain [13], [14], and in some cases improve [15], the surface roughness of the material.

5.3 Results

Topographic AFM images of the different un-etched surface finishes are shown in Figure 5.2, while the etched surfaces are shown in Figure 5.3. As discussed previously, the diamond optical quality was significantly poorer (high dislocation density) than the Raman materials presented in previous chapters. This is highlighted in the post etch AFM, where craters ranging in depth from 10nm to 120nm appear on the surface. These craters are thought to be caused by dislocations in the bulk material, possibly due to preferential etching around dislocation sites. The pillar effect shown in Figure 5.2(d) is, in our experience, rather unusual. These features were confirmed to be diamond via AFM phase imaging. The grooves seen in Figure 5.2 (c) are typical polishing grooves [16].

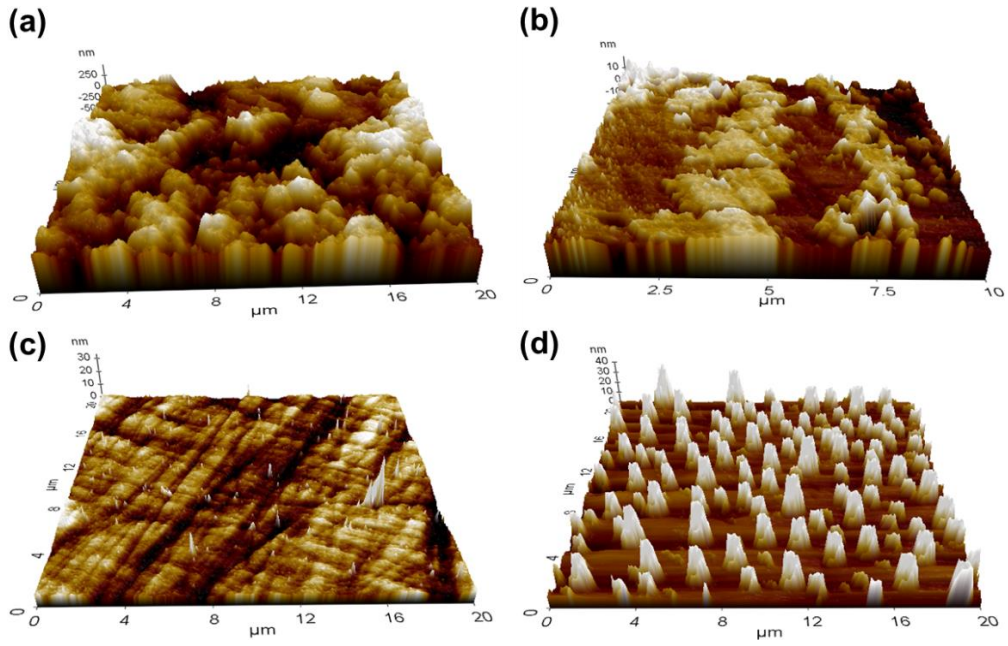

Figure 5.2. AFM images of (a) fine lap with an R(q) of 142nm, (b) grit size 33 with an R(q) of 3.9nm, (c) grit size 76 with an R(q) of 1.2nm, and (d) grit size 151 with an R(q) of 5.6nm. The AFM images have different vertical scales.

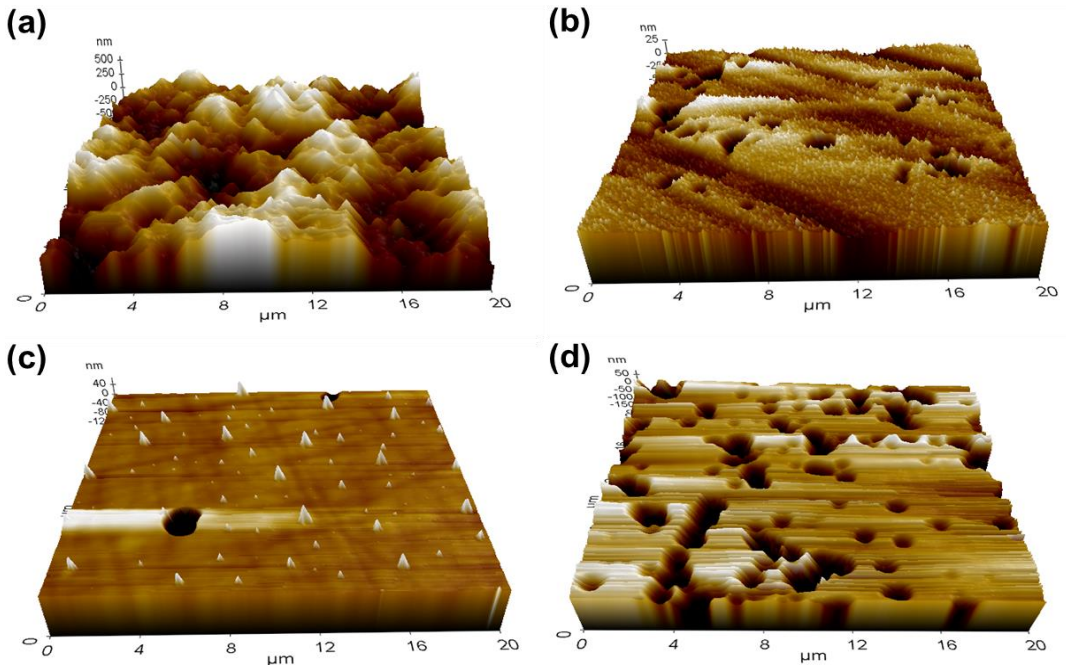

Figure 5.3. AFM images of etched surfaces (a) Fine Lap with an R(q) of 163nm, (b) grit size 33 with an R(q) of 33.8nm, (c) grit size 76 with an R(q) of 7.3nm, and (d) grit size 151 with an R(q) of 7.5nm. The AFM images have different vertical scales.

Problems involving both the etched and unetched “fine lap” samples arose when trying to identify damaged spots, with the undamaged surface being covered in black specs seen in Figure 5.4. The LIDT quoted for these samples is, therefore, only a rough guide; the damaged spots were judged only by eye as they were more discernable here than when inspected under a microscope.

Figure 5.4. Undamaged fine lap diamond surface under 10x magnification.

Figure 5.5 shows LIDT data of the lapped and polished diamond, while Figure 5.6 shows the LIDT of their etched counterparts. The damaged probability was calculated by dividing the number of damaged spots observed on the surface by the number of laser shots (10).

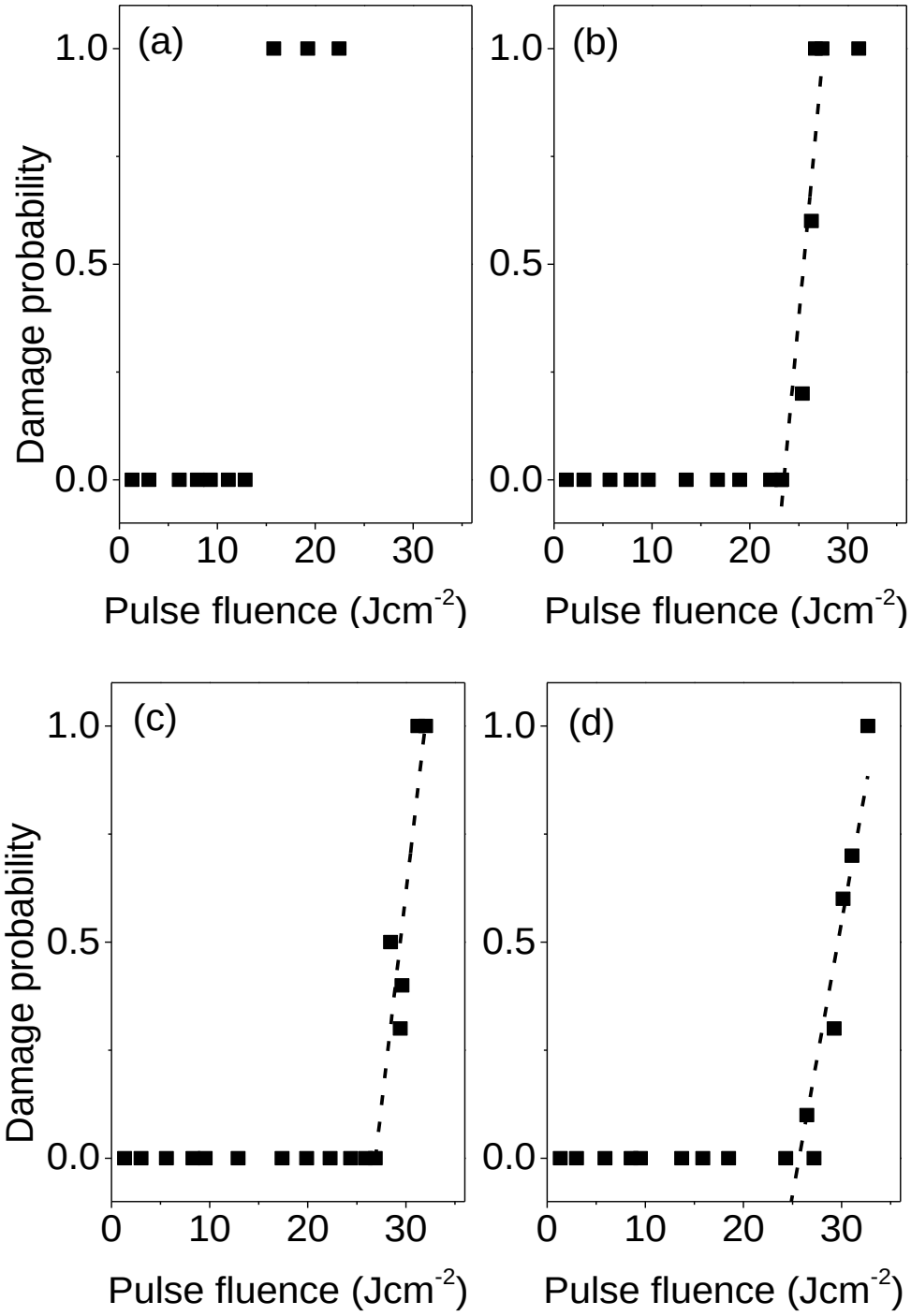

Figure 5.5. Damage threshold measurements for unetched (a) Fine lap, (b) grit size 33, (c) grit size 76, and (d) grit size 151. The damage threshold is defined as the x-axis point of intersection of the least squared fit (dotted line) plotted between the last point of zero damage and the first point with a damage probability of one.

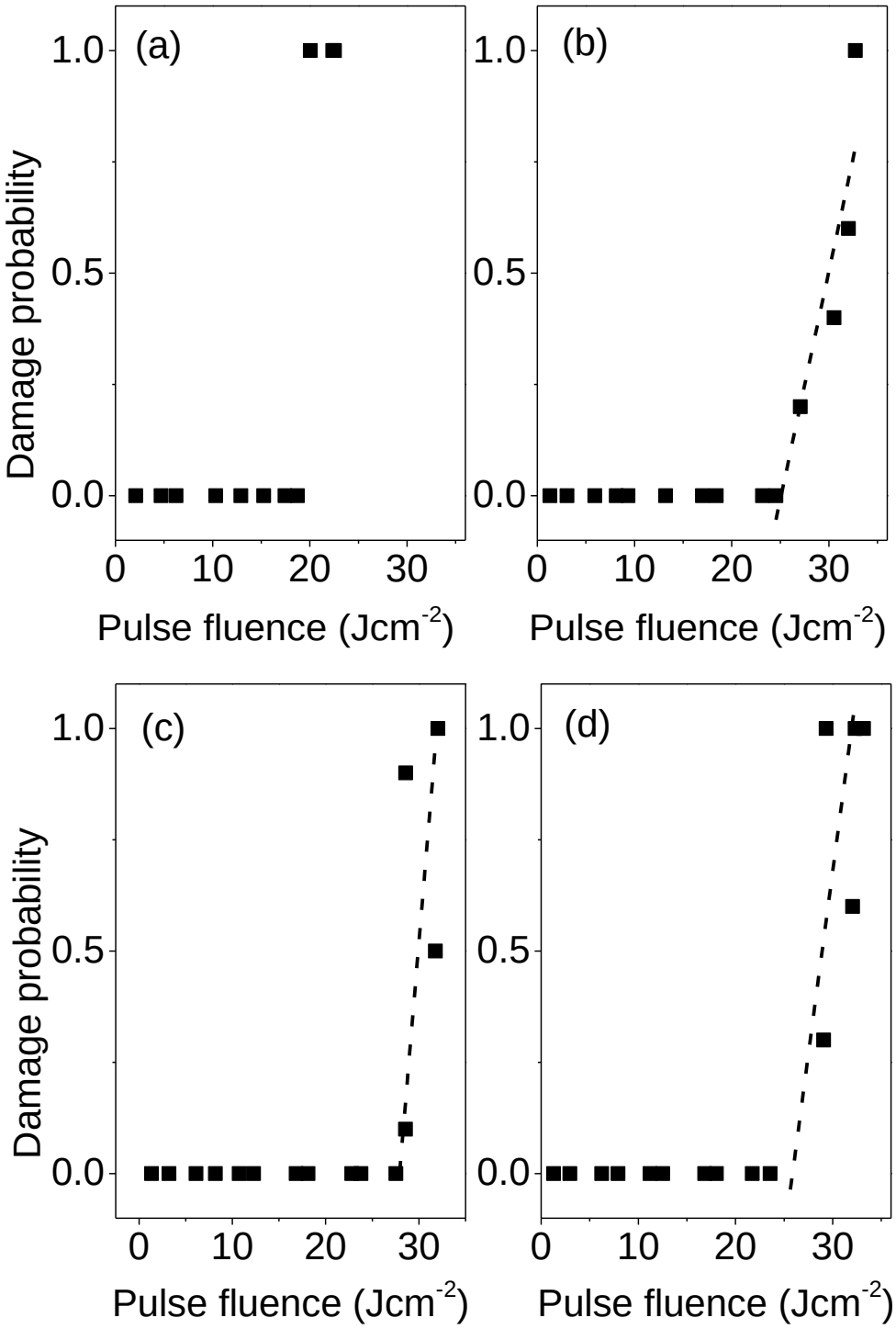

Figure 5.6. Damage threshold measurements for etched (a) Fine lap (b) grit size 33 (c) grit size 76 (d) grit size 151. The damage threshold is defined at the x-axis point of intersection of the least squared fit (dotted line) plotted between the last point of zero damage and the first point with a damage probability of one.

These LIDT values compare to a figure of approximately 23Jcm^{-2}, shown in Figure 5.7, for a 'heatspreader' sample bought from Element Six with an optical quality finish, shown in Figure 5.8 with an (R(q) of 0.63nm); however, the measurements taken on this sample are based on a smaller data set (a maximum of 4 damage spots were obtained) due to the smaller surface area of the diamond available (4mm spherical diameter c.f. 4mm square surface).

It was found that the back surface of the unetched diamond 'heatspreader' consistently damaged at a lower fluence than the front surface, regardless of which way round the sample was orientated. This is consistent with the results presented in [17] and [18]. The reason for this can be attributed to Fresnel reflections: the rear surface is exposed to a laser pulse which experiences constructive interference. The difference in intensity between the entrance surface (with intensity I_{en}) and exit surface (with intensity I_{ex}) can then be calculated using equation 5.1 [19]

$$\frac{I_{ex}}{I_{en}} = \left(\frac{2n}{n+1}\right) \qquad 5.1$$

Where, for diamond with a refractive index of 2.4, this ratio is 1.99.

The observed damage characteristics on the etched sample, however, were markedly different, with optical damage occurring on the front, etched, surface of the diamond. Due to the lower effective intensity incident on the front surface, this indicates that the etch process used, contrary to the desired result, lowers the damage threshold of the surface. The images of the front and back surface damages spots are shown in Figure 5.9(a) and (b). The different morphology of the damage spots can be attributed to the reasons discussed above. With constructive interference occurring a quarter wavelength inside the diamond, the damage at the rear surface should be located approximately 100nm beneath the rear surface. This could not be confirmed due to lack of equipment; however, could be investigated further using optical scanning interferometry.

Prior to any observable damage on the etched surface, i.e. at fluences below the quoted damage threshold, surface "sparking" was observed. This is thought to be

indicative of plasma generation at the entrance surface [2], [20], and, in some cases, is used as an indication of surface damage [4]. This was observed at fluences around 4Jcm^{-2} below that of the quoted LIDT values on the etched surfaces. This sparking was also seen on the unetched samples, at fluences around 2Jcm^{-2} below the quoted LIDT; however, whether the sparking was from the front or back surface of the diamond is unclear.

The mechanism of the laser induced damage in diamond is possibly dielectric breakdown via electron avalanche [2], [3], [6], [21]. This involves the ionization of electrons in the material, with damage occurring when the rate of ionization is larger than the rate of recombination [1]. Due to complexities introduced by possible sub-micron cracks and imperfections, however, the damage mechanism cannot be confirmed as of yet, with further experimental analysis of the material required. It is possible that these cracks and imperfections reduce the local threshold of dielectric breakdown, or cause local field enhancement.

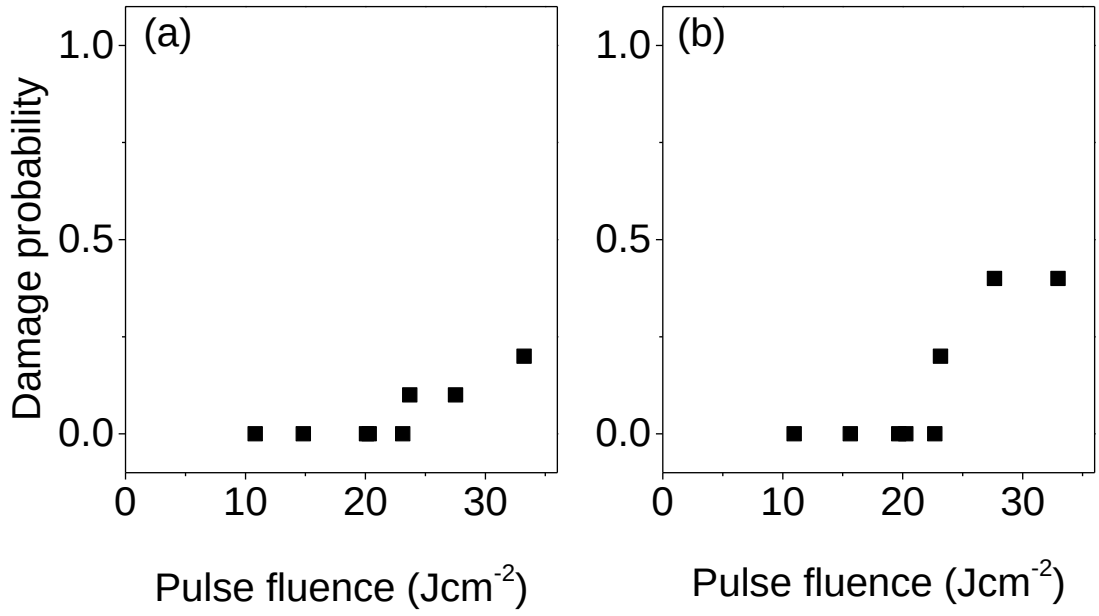

Figure 5.7. – Damage threshold measurements for "heatspreader" samples of (a) unetched and (b) etched surface.

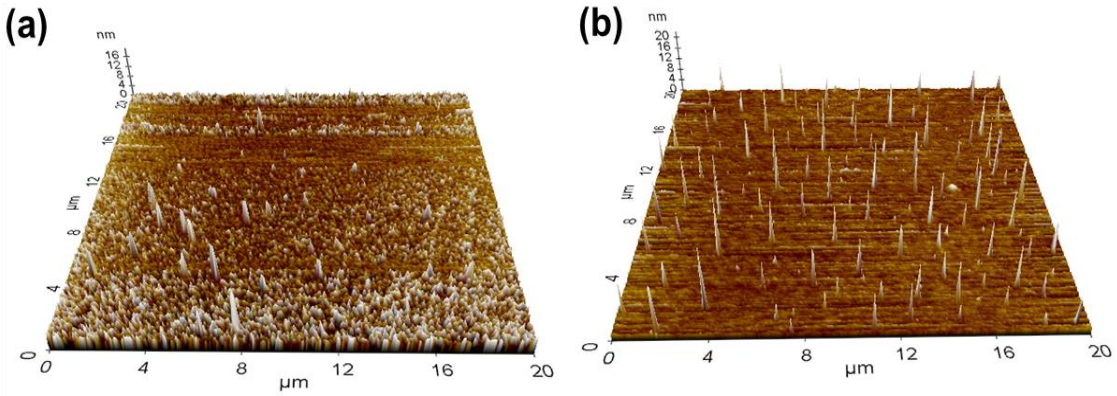

Figure 5.8. - AFM image of (a) unetched "heatspreader" sample (b) etched "heatspreader" sample.

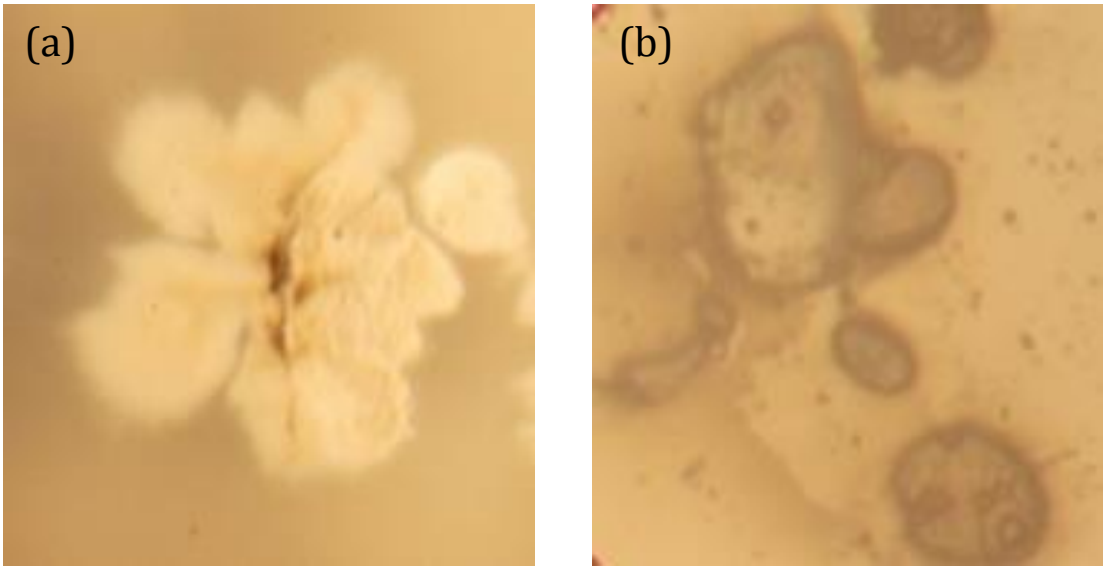

Figure 5.9. Typical characteristic of (a) front surface damage with image taken from etched heatspreader sample and (b) rear surface damage taken from the unetched heatspreader sample.

Sample	Roughness before etch (nm)	LIDT of diamond sample before etch (Jcm^{-2})	Roughness after etch (nm)	LIDT of diamond sample after etch (Jcm^{-2})
Fine Lap	142	~12.5	163	~19
Grit size 33	3.9	23.7±2.0 (rear)	33.6	25.7±2.0 (front)
Grit size 76	1.2	26.8±1.5 (rear)	7.3	28.3±2.1 (front)
Grit size 151	5.6	26.7±1.2 (rear)	7.5	25.7±2.9 (front)
Heatspreader	0.8	~23 (rear)	0.8	~23 (front)

Table 5.1. Summary of the LIDT test results

As Table 5.1 illustrates, the fine lap aside, very little difference is observed between the LIDT measurement for the various surface finishes, before or after etching. In all cases, an LIDT of around $25Jcm^{-2}$ is measured for 6.5ns pulses at 1064nm.

5.4 Conclusion and future work

In conclusions, a laser induced damage threshold of around $25Jcm^{-2}$ is measured for all samples except the 'fine lap' using 6.5ns pulses at 1064nm. No significant improvement is observed if one side of the samples is etched to remove approximately 5μm of material. These results indicate that the laser induced damage threshold of diamond does not vary strongly across the wide range of surface finishes examined here. Comparisons drawn between the nanosecond damage threshold of diamond and fused silica ($25Jcm^{-2}$ compared to 3854±85 Jcm^{-2} for ns pulses) show that diamond surface LIDT is, perhaps, surprisingly low, given the materials impressive thermo-mechanical properties. Reviewing literature, it appears diamond's bulk LIDT is considerably higher than the surface LIDT[2], [3], which offers some promise given the recent results presented by Smith et al [1]; where, under the right surface preparation, fused silica surface LIDT was seen to approach the bulk damage threshold. The low dependence of the diamond surface LIDT on the surface quality observed in this chapter suggests that this may not apply to diamond. If it is the case, however, a more detailed study into the nature of the surface imperfections involved in initiating

below bulk value surface damage needs to be conducted. This information will be crucial in the search for improved surface preparation techniques.

Future work will focus on attempts to improve the surface LIDT of diamond, with a variety of surface finish techniques to be attempted, along with increasing the etch depth to 10μm and beyond. Deposition of AR coatings on the rear surface of the diamond will also reduce the effect of Fresnel reflections, improving the diamond samples damage threshold significantly. With field enhancement thought to be causing a lowering of the measured rear surface LIDT, it is possible that with AR coatings deposited, a value closer to 50Jcm^{-2}

The experimental technique should be modified slightly, as a single mode laser would be preferential when performing damage measurements. Investigations into the morphology of the damage spots should also be conducted to further investigate the cause of the laser induced damage. Alongside this work, an LIDT study of laser materials including YAG and YVO_4 should be conducted to provide a head to head comparison with diamond. Moreover, a study into the temporal and wavelength dependence of the LIDT may provide interesting results. Mildren et al [22] showed that 11ns pulses with fluences of a mere 37μJcm^{-2} at 266nm was sufficient to ablate diamond surfaces, suggesting that the damage threshold may decrease with decreasing wavelength. This would be in line with approaching the band gap of the material, along with the increase in nitrogen absorption discussed in chapter 2.

The value of LIDT in state of the art diamond is an important value to pin down. The values presented in this chapter show that, when implementing diamond in optical systems, the low LIDT could potentially be inhibitive, with optical coatings with damage thresholds as high as 43Jcm^{-2} reported [23]. The high intensities used in intra-cavity Raman lasers could also lead to difficulties involving damage. Determining the upper limit of the material can allow the optimal design of systems involving diamond.

Bibliography

[1] A. Smith, B. Do, R. Schuster, and D. Collier, "Rate equation model of bulk optical damage of silica, and the influence of polishing on surface damage of silica," *Proc. SPIE*, vol. 6873, p. 68730U–68730U–12, 2008.

[2] P. Liu, R. Yen, and N. Bloembergen, "Dielectric breakdown threshold, two photon absorption, and other optical damage mechanisms in diamond," *IEEE J. Quantum Electron.*, no. 8, pp. 574–576, 1978.

[3] T. V. Kononenko, M. Meier, M. S. Komlenok, S. M. Pimenov, V. Romano, V. P. Pashinin, and V. I. Konov, "Microstructuring of diamond bulk by IR femtosecond laser pulses," *Appl. Phys. A*, vol. 90, no. 4, pp. 645–651, 2008.

[4] R. S. Sussmann, G. A. Scarsbrook, C. J. H. Wort, and R. M. Wood, "Laser damage testing of CVD grown diamond windows," *Diam. Relat. Mater.*, vol. 3, pp. 1173 – 1177, 1994.

[5] S. Albin, A. D. Cropper, L. C. Watkins, E. C. Byvik, and A. M. Buoncristiani, "Laser damage threshold threshold of diamond films," *Opt. Eng.*, vol. 28, no. 3, pp. 281–285, 1989.

[6] V. V Kononenko, T. V Kononenko, S. M. Pimenov, M. N. Sinyavskii, V. I. Konov, and F. Dausinger, "Effect of the pulse duration on graphitisation of diamond during laser ablation," *Quantum Electron.*, vol. 35, no. 3, pp. 252–256, 2005.

[7] O. Uteza, B. Bussière, F. Canova, J.-P. Chambaret, P. Delaporte, T. Itina, and M. Sentis, "Laser-induced damage threshold of sapphire in nanosecond, picosecond and femtosecond regimes," *Appl. Surf. Sci.*, vol. 254, no. 4, pp. 799–803, 2007.

[8] J. Natoli, L. Gallais, H. Akhouayri, and C. Amra, "Laser-induced damage of materials in bulk , thin-film , and liquid forms," *Appl. Opt.*, vol. 41, no. 16, p. 3156, 2002.

[9] M. J. Soileau and M. Bass, "Laser-Induced Breakdown in Crystalline and Amorphous Si02," *IEEE J. Quantum Electron.*, vol. 16, no. 8, p. 8114, 1980.

[10] N. Bloembergen, "Role of Cracks , Pores , and Absorbing Inclusions on Laser Induced Damage Threshold at Surfaces of Transparent Dielectrics," *Appl. Opt.*, vol. 12, no. 4, pp. 661–664, 1973.

[11] "Laser and laser-related equipment - Determination of laser-induced damage threshold of optical surfaces," *Int. Stand.*, vol. 11254–1.

[12] R. Paschotta, “http://www.rp-photonics.com/spotlight_2009_10_03.html.” .

[13] I. Friel, S. L. Clewes, H. K. Dhillon, N. Perkins, D. J. Twitchen, and G. A. Scarsbrook, “Control of surface and bulk crystalline quality in single crystal diamond grown by chemical vapour deposition,” *Diam. Relat. Mater.*, vol. 18, no. 5–8, pp. 808–815, 2009.

[14] H. W. Choi, E. Gu, C. Liu, C. Griffin, J. M. Girkin, I. M. Watson, and M. D. Dawson, “Fabrication of natural diamond microlenses by plasma etching,” *J. Vac. Sci. Technol. B Microelectron. Nanom. Struct.*, vol. 23, no. 1, p. 130, 2005.

[15] C. L. Lee, E. Gu, M. D. Dawson, I. Friel, and G. a. Scarsbrook, “Etching and micro-optics fabrication in diamond using chlorine-based inductively-coupled plasma,” *Diam. Relat. Mater.*, vol. 17, no. 7–10, pp. 1292–1296, 2008.

[16] T. Schuelke and T. A. Grotjohn, “Diamond polishing,” *Diam. Relat. Mater.*, vol. 32, pp. 17–26, 2013.

[17] M. D. Crisp, N. . Boling, and G. Dube, “Importance of Fresnel reflections in laser surface damage of transparent dielectrics,” *Appl. Phys. Lett.*, vol. 21, no. 8, p. 364, 1972.

[18] N. L. Boling, M. D. Crisp, and G. Dube, “Laser Induced Surface Damage,” *Appl. Opt.*, vol. 12, no. 4, p. 650, 1973.

[19] W. Koechner, *Solid-State Laser Engineering*, 6th ed. Springer, 2006.

[20] R. M. Wood, R. T. Taylor, and R. L. Rouse, “Laser damage in optical materials at 1064nm,” *Opt. Laser Technol.*, June, pp. 105–111, 1975.

[21] D. W. Fradin, N. Bloembergen, and J. . Letellier, “Dependence of laser-induced breakdown field strength on pulse duration,” *Appl. Phys. Lett.*, vol. 22, no. 12, p. 635, 1973.

[22] R. P. Mildren, J. E. Downes, J. D. Brown, B. F. Johnston, E. Granados, D. J. Spence, A. Lehmann, L. Weston, and A. Bramble, “Characteristics of 2-photon ultraviolet laser etching of diamond,” *Opt. Mater. express*, vol. 1, no. 4, pp. 576–585, 2011.

[23] J. Taniguchi, N. . LeBarron, J. Howe, D. . Smith, C. Stolz, C. Weizapfel, and J. Kimmons, “Functional Damage Thresholds of Hafnia / Silica Coating Designs for the NIF Laser,” *LLE Rev.*, vol. 88, pp. 177–182, 2001.

Chapter 6 – Conclusions and outlook

Diamond's thermo-optic and mechanical properties are unrivalled. With a transparency range spreading across the whole visible spectral region and into the mid IR, the implementation of this impressive material in laser systems has been investigated. The work presented in this thesis, including material characterisation and the exploitation of the material in both CW and pulsed diamond Raman lasers will be summarised in this chapter, with the main achievements discussed.

6.1 Summary

6.1.1 Measurement of the Raman gain in diamond

In chapter 2, a systematic study of the steady state Raman gain in single crystal CVD grown diamond at wavelengths ranging from 355nm to 1450nm is presented. Both a pump probe technique, providing absolute measurements of the Raman gain, and a relative measurement comparing the threshold values for SRS are reported. The measurements were taken with the pump polarisation parallel to a <111> crystallographic direction and propagating along a <110> direction, where, under these conditions, maximum gain is extracted[1], [2]. The results from both experimental methods showed that the Raman gain varies with a $\frac{1}{\lambda}$ dependence, in agreement with theory [3]. The values obtained ranged from 7.6cmGW^{-1} at a pump wavelength of 1280nm to 78cmGW^{-1} at a pump wavelength of 355nm. The results obtained allow better design of Raman laser cavities, giving an indication of the correct output coupling and spot sizes required for optimal performance.

6.1.2 Diamond Raman lasers

In chapters 3 and 4, implementing the high Raman gain in diamond presented in chapter 2, CW and pulsed diamond Raman lasers are presented. Two of the highest power CW intra-cavity diamond Raman lasers have been demonstrated,

one implementing a side-pumped Nd:YAG laser rod to obtain 6.1W of Raman output, and the second achieving 7.6W employing a thin disk Yb:LuAG. Both an 11 fold brightness enhancement and polarisation conversion from a unpolarised pump to polarised Raman output was achieved in the Nd:YAG pumped system, while, to the best of the author's knowledge, the 7.6W achieved from the Yb:LuAG pumped system is the highest power achieved from an intra-cavity Raman laser to date.

Pulsed Raman lasers were also investigated, with an external cavity monolithic diamond Raman laser achieving up to 84% conversion efficiencies presented. Two compact and robust devices are reported, one of which utilises lens-like structures etched into a diamond surface to create a stable resonator between opposing mirror coated faces, and the other demonstrating Raman output from a resonator formed between two mirror coated parallel plane faces. Pumped at 532nm, 1st, 2nd and 3rd Stokes shifts were observed in the Raman output from both the plane-plane and microlens sample. In addition to this work, motivated by the desire to achieve picosecond pulses from a (comparative to current methods) compact system, an intra-cavity mode locked diamond Raman laser was designed and built. Difficulties arising from competition in nonlinearities, however, limited the Raman shifter output that could be achieved to 300mW.

6.1.3. Laser induced damage threshold of diamond.

In chapter 5, the surface laser induced damage threshold of diamond is studied. A laser induced damage threshold of around 25Jcm^{-2} is measured for samples with a variety of surface finishes, prepared with both mechanical polishing and chemically assisted etches. Other than the comparatively low sample prepared with a "lap" finish, no significant difference in threshold was observed between each sample. Differences in the mechanically polished and chemically assisted etched samples were observed: the former damaging on the rear surface (no matter the orientation of the sample) and the latter damaging only on the front etched surface. Field enhancement effects at the rear surface, caused by Fresnel reflections constructively interfering with the incident beam, increases the

intensity at the back surface to almost double the incident value, indicating that the absolute damage threshold may be 2 times higher than reported. Further studies into the morphology of the damage are required to confirm this hypothesis.

6.2 Future work

6.2.1 Diamond Raman lasers

The capabilities of diamond as a Raman laser material have recently been highlighted by Williams et al [4]. With >100W quasi CW Raman output demonstrated, there is scope for improvements on the systems presented in chapter 3 of this thesis. Although pump power limited, it is the author's opinion that, with further spectral control of the fundamental lasers presented, higher conversion efficiencies may be reached. Similar to work reported by Savitski [5] on a KGW Raman laser, a volume Bragg grating should be implemented in the fundamental cavity of a diamond Raman laser.

With regards to the pulsed work presented in chapter 4, the demonstration of a plane-plane monolithic diamond resonator may provoke a wide range of work. With minimal round trip loss, near quantum limited efficiencies should be attainable. Furthermore, unlike the microresonator, there is no pre-defined cavity mode, meaning the pump power and spot size can be simultaneously increased to maintain optimum pump intensities while increasing the Raman output power. It is also possible that sub-nanosecond pulses may be converted; however it is the author's opinion that a diamond of a shorter length would have to be used to allow several Raman round trips while the pump pulse is interacting with the diamond. Increasing the diamond length and decreasing the output coupling may allow the demonstration of CW conversion in a monolithic diamond Raman laser.

6.2.2 Laser induced damage threshold of diamond.

The results presented in chapter 5 indicate the surface laser induced damage threshold of diamond is significantly lower than the bulk damage threshold [6]. Further investigation should be conducted into surface finishes, in an attempt to increase the surface LIDT to values approaching that of the bulk. A more detailed study into the nature of the surface imperfections involved in initiating below bulk value surface damage needs to be conducted. This information will be crucial in the search for improved surface preparation techniques. It may be prudent to investigate the effect of laser spot size used, which may indicate surface imperfections cause the reduction in LIDT. If local imperfections are reducing the damage threshold, decreasing the spot size would be expected to increase the measured LIDT. Deposition of AR coatings on the back surface will also be implemented, in an attempt to increase the damage threshold of the rear surface by eliminating surface reflections back into the material.

Slight modifications to the experiment should be made in the future, as a single mode laser would be preferred when performing damage measurements. A study into the temporal and wavelength dependence of the LIDT may provide further interesting results.

6.3 Concluding remarks

The Raman lasers presented in this thesis have demonstrated the excellent properties of diamond, and highlighted that, at times, diamond Raman lasers can be used as more than just a frequency convertor; with 11 fold brightness enhancements achieved in intra-cavity DRL's. Additionally, the first compact, robust, monolithic diamond Raman laser has been reported with near quantum limited conversion efficiencies. Finally, the long process of fully characterising this novel material has been started, with a view to assessing and fulfilling diamond's full potential as a laser gain material.

Bibliography

[1] V. G. Savitski, I. Friel, J. E. Hastie, M. D. Dawson, D. Burns, and A. J. Kemp, "Characterization of Single-Crystal Synthetic Diamond for Multi-Watt Continuous-Wave Raman Lasers," *Quantum Electron. IEEE J.*, vol. 48, no. 3, pp. 328–337, 2012.

[2] A. Sabella, J. A. Piper, and R. P. Mildren, "1240 nm diamond Raman laser operating near the quantum limit," *Opt. Lett.*, vol. 35, no. 23, pp. 3874–3876, 2010.

[3] A. Penzkofer, A. Laubreau, and W. Kaiser, "High Intensity Raman Interactions," *Prog. Quantum Electron.*, pp. 56–140, 1979.

[4] R. J. Williams, O. Kitzler, A. Mckay, and R. P. Mildren, "Investigating diamond Raman lasers at the 100 W level using quasi-continuous-wave pumping," *Opt. Lett.*, vol. 39, no. 14, pp. 4152–4155, 2014.

[5] V. G. Savitski, "Experimental analysis of emission linewidth narrowing in a pulsed $KGd(WO_4)_2$ Raman laser," *Opt. Express*, vol. 22, no. 18, pp. 582–585, 2014.

[6] T. V. Kononenko, M. Meier, M. S. Komlenok, S. M. Pimenov, V. Romano, V. P. Pashinin, and V. I. Konov, "Microstructuring of diamond bulk by IR femtosecond laser pulses," *Appl. Phys. A*, vol. 90, no. 4, pp. 645–651, 2008.

Appendix A

Publications

Peer reviewed journal papers

[1] - V. G. Savitski, **S. Reilly**, and A. J. Kemp, "Steady-State Raman Gain in Diamond as a Function of Pump Wavelength," *IEEE J. Quantum Electron*., vol. 49, no. 2, pp. 218–223, 2013.

[2] - **S. Reilly**, V. G. Savitski, H. Liu, E. Gu, M. D. Dawson, and A. J. Kemp, "Monolithic diamond Raman laser," *Opt. Lett.*, vol. 40, no. 6, pp. 930–933, 2015.

Conference presentations

[1] - **S. Reilly**, V.G. Savitski, W. Lu, A. J. Kemp, E. Clarke, S. Calvez, "Study of bulk GaInNAs/GaAs material for application in passive Q-switching devices," in *European Material Research Society (EMRS) 2012 Spring Meeting, Physics and Applications of Novel gain materials based on Nitrogen and Bismuth containing III-V Compounds*, 2012.

[2] - V. G. Savitski, D. C. Parrotta, **S. Reilly**, P. W. Roth, M. D. Dawson, D. Burns, J. E. Hastie, and A. J. Kemp, "High-power, continuously operating diamond-based lasers: material characterisation and device demonstration", in *De Beers Diamond Conference*, 2012.

[3] - **S. Reilly**, V. G. Savitski, and A. J. Kemp, "Spectral Dependence of Raman Gain in Diamond," in *Photon 12*, 2012.

[4] - V. G. Savitski, **S. Reilly**, and A. J. Kemp, "Dependence of the Raman gain coefficient in diamond on pump wavelength", in *Europhoton*, 2012.

[5] - V. G. Savitski, **S Reilly**, W. Lubeigt and A. J. Kemp, "Absorption Coefficient and Raman Gain in CVD Diamond as Functions of Pump Wavelength: Towards Efficient Diamond Raman Lasers," in *CLEO/Europe and EQEC 2013 Conference Digest*, 2013.

[6] – H. Liu, **S. Reilly**, E. Xie, A. J. Kemp, E. Gu, M. D. Dawson, "Large radius of curvature micro-lenses on single crystal diamond and their application in monolithic diamond Raman lasers," *Semiconductor and Integrated OptoElectronics (SIOE)*, 2015

[7] – **S. Reilly**, V. G. Savitski, H. Liu, E. Gu, M. D. Dawson, A. J. Kemp, "Monolithic Diamond Raman Laser Operating at 573nm Utilizing Microlens Structures to Form a Stable Resonator" *CLEO/Europe and EQEC 2015 Conference Digest*, Accepted.

[8] – V. G. Savitski, **S. Reilly**, A. J. Kemp, "Yellow-Orange Emission from a Plane-Plane Monolithic Diamond Raman Laser," *CLEO/Europe and EQEC 2015 Conference Digest*, Accepted.

[9] - H. Liu, **S. Reilly**, E. Xie, J. Herrnsdorf, A. J. Kemp, E. Gu, M. D. Dawson, "Large radius of curvature micro-lenses on single crystal diamond and their application in monolithic diamond Raman lasers," *Conference on Diamond and Carbon Materials*, 2015 Accepted